www.gecarbon.org

BOLETIN del Grupo Español del Carbón

ISSN 2172 - 6094
nº 54/Diciembre 2019

INDICE

Editorial

It is a pleasure to act as guest editor of this special issue of Boletin del Grupo Español del Carbono (BGEC) dedicated to the recent research carried out on carbon materials in Portugal.

It is worth to point out that two special issues (nº 39 and nº 40) of BGEC were already dedicated to the carbon research in Portugal in 2016. I am thankful to the groups who participated in 2016 and agreed to contribute again, namely Prof. José L. Figueiredo (University of Porto) and Prof. Ana P. Carvalho (University of Lisboa). Naturally, I am also grateful to the other groups who also accepted my invitation to share their research in this special issue, like the group of Prof. Cristina Freire (University of Porto), Prof. Luísa Martins (University of Lisboa), Prof. Conceição Paiva (University of Minho), Prof. Florinda Costa and Prof. Rui Silva (University of Aveiro) and to Prof. Luís S. Lobo (Nova University of Lisboa).

The first contribution of this special issue deals with the news about the Carbon Group of the Portuguese Chemical Society, created in 2015. It was kindly provided by Prof. José L. Figueiredo, who is also the author of the second article, dealing with the recent research carried out by his group on carbon materials for catalysis, advanced functional carbon materials and their applications in energy, fuels and chemicals.

The third paper is from the group of Prof. Cristina Freire and it deals with hybrid/doped carbon-based (nano) materials for eco-sustainable catalysis, biomass valorization, energy and smart devices. The article of Prof. Luísa Martins deals with carbon materials as supports for iron and gold catalysts. The group Prof. Ana P. Carvalho writes about acid chars and their use in adsorption and catalysis.

The article from Prof. Conceição Paiva's group deals with the functionalization of carbon nanoparticles and their potential applications. Prof. Florinda and co-workers provide a short review on their research on hybrids of nanocrystalline diamond with carbon nanotubes, graphite or graphene and other graphene materials. Prof. Rui Silva and co-workers write on diamond growth on ceramics and synthesis of carbon nanotubes. Finally, Prof. Luís S. Lobo describes the mechanism of bamboo-like carbon fibers growth.

It is my wish that the research on carbon materials will continue to increase in Portugal and that in some years we will have another special issue, with the participation of these and other groups. I also trust that the publication of these interesting works will contribute to the establishment of new collaborations.

Sónia Carabineiro
(University of Lisboa)

El Grupo Portugués del Carbono (Grupo do Carbono @ SPQ)

The Carbon Group of the Portuguese Chemical Society (Grupo do Carbono @ SPQ)

José Luis Figueiredo

Laboratory of Separation and Reaction Engineering - Laboratory of Catalysis and Materials (LSRE-LCM), Departament of Chemical Engineering, Faculty of Engineering, University of Porto, Rua Dr. Roberto Frias, 4200-465 Porto, Portugal. jlfig@fe.up.pt

The Carbon Group of the Portuguese Chemical Society (Grupo do Carbono@SPQ) was set up in September 2015, upon the request of a number of members of Sociedade Portuguesa de Química (SPQ) from the Universities of Porto, Aveiro, Coimbra, Lisboa, Nova de Lisboa and Évora, and also from the Polytechnic Institute of Bragança, with research activities in the carbon field. An ad-hoc Steering Committee, under the leadership of the author, assumed the coordination of the starting activities of the Carbon Group.

Figure 1: Logo of the Carbon Group of the Portuguese Chemical Society (SPQ)

In 2016, the Carbon Group applied for membership to the European Carbon Association (ECA), becoming a full member in 2017.

The 1st Meeting of the Carbon Group was organized in Porto (12-13 June, 2017). The President of the Spanish Carbon Group (GEC), Prof. Maria Jesús Lázaro Elorri, was invited for the opening session. The Scientific Program included two Plenary Lectures, five Key-note Lectures, and the presentation of 90 communications (13 oral presentations and 77 posters). The meeting was attended by 102 participants, a very promising start, indeed!

The Plenary Lectures were presented by Prof. Nuno Peres (Univ. Minho), "Plasmonic Effects in Graphene", and Prof. Francisco Rodríguez Reinoso (Univ. Alicante), "The unique versatility of carbon materials". The Key-note Lectures were: "Doped graphene and composite carbon materials as electrocatalysts towards Pt-free fuel cells" (Maria Jesús Lázaro); "Nanocarbon hybrids grown by microwave plasma CVD and their applications" (Florinda Mendes da Costa); "Activation with carbon dioxide or air: Which is better?" (Peter Carrott); "Carbon based materials: applications in chemical catalysis and electrocatalysis" (Cristina Freire); and "Properties of carbon materials for catalytic wet peroxide oxidation" (Helder T. Gomes). The General Assembly of the Carbon Group was held during the meeting, and the Board for the period 2017-2018 was elected as follows: José Luís Figueiredo (President); Peter Carrott and Fernando Pereira (Vice-Presidents).

In 2018, the Portuguese Carbon Group organized the 8th International Symposium on Carbon for Catalysis, CarboCat – VIII (Porto, June 26-29), attended by 132 delegates from 18 different countries (*http://carbocatviii.eventos.chemistry.pt/*).

The Scientific Program included 3 Plenary Lectures, by Professors Graham Hutchings (Cardiff University, UK), Krijn P. de Jong (Utrecht University, The Netherlands) and Robert Schlögl (Fritz Haber Institute of the Max Planck Society and Max Planck Institute for Chemical Energy Conversion, Germany), 4 Key-Note Lectures (Siglinda Perathoner, Italy; Magdalena Titirici, UK; Magnus Ronning, Norway; and Nathalie Job, Belgium), 33 oral communications and 85 posters.

The Board of the Carbon Group for the period 2019-2020 was elected as follows: Peter Carrott (President); José Luís Figueiredo (past President); Fernando Pereira (future President). The 2nd Meeting of the Carbon Group should have taken place in Évora, in 2019, but unfortunately Peter Carrott passed away on April 1st [1], and it was decided to postpone the meeting.

The Direction of SPQ has recently appointed Dr. Anabela Valente (Univ. Aveiro) as interim President of the Carbon Group, until the next General Assembly. She will organize the 2nd Meeting, which will take place in Aveiro in 2020.

The Carbon Group of SPQ is still *under construction*, but it is hoped that it will become consolidated in the near future. The main objective is to provide a *forum* for all the researchers that work in the field of carbon in its various aspects and allotropies, including chemists, physicists and materials scientists, as well as those that use carbon materials in any of their multiple industrial applications.

Figure 2: Group photo of the CarboCat VIII participants

References

[1] J.L. Figueiredo, Química 2019; 43 (nº 153): 87 (*https://www.spq.pt/magazines/BSPQuimica/688*).

Materiales de carbono @LCM: una actualización

Carbon materials @ LCM: an update

José Luis Figueiredo

Laboratory of Separation and Reaction Engineering - Laboratory of Catalysis and Materials (LSRE-LCM), Departament of Chemical Engineering, University of Porto, Rua Dr. Roberto Frias, 4200-465 Porto, Portugal. jlfig@fe.up.pt

Abstract

LCM's main achievements towards the development of carbons for catalysis, energy and environmental applications were previously reviewed in *Boletin* nº 39 (March 2016). In the present report, we will provide an update, focusing only on our most recent work.

Resumen

Los logros más relevantes del LCM sobre el desarrollo de materiales de carbono para aplicaciones catalíticas, energéticas y medioambientales, fueron publicados en el Boletín nº 39 (marzo 2016). Por lo que la presente publicación se centra solamente en las actividades más recientes.

1. Introduction

The Laboratory of Catalysis and Materials (LCM) has been focusing its research activities on the fields of Carbon and Catalysis since 1994. In 2004, LCM together with LSRE (Laboratory of Separation and Reaction Engineering) received the status of *Associate Laboratory*. Nowadays, the former LCM team is Research Group 4, "Catalysis and Carbon Materials", and represents approximately 40% of the Associate Laboratory LSRE-LCM (*https://lsre-lcm.fe.up.pt/*). The current research activities are divided into three scientific areas, each one of them subdivided into projects and subprojects, as shown in Figure 1: 1) Nanostructured carbon materials; 2) Environmental catalysis and technologies; 3) Energy, fuels and chemicals.

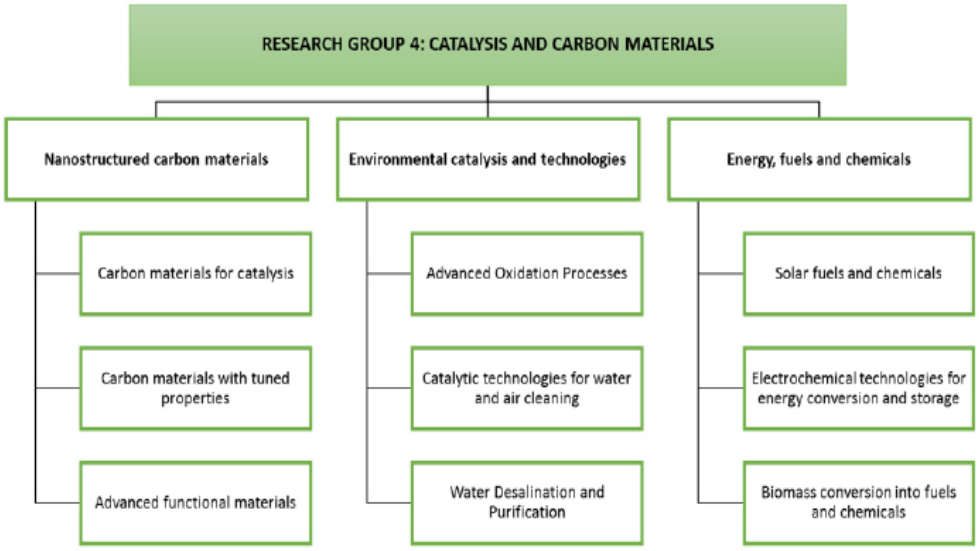

Figure 1: Scientific areas and current research projects at LCM.

Figura 1: Áreas científicas y proyectos de investigación actuales del LCM.

LCM's most relevant achievements towards the development of carbon materials for catalysis, energy and environmental applications were described three years ago in *Boletin del GEC* [1]; thus, in the present report, we will just provide an update focusing on our most recent work in each one of those research areas.

2. Nanostructured carbon materials

2.1 Carbon materials for catalysis

The application of carbon nanomaterials ("*nanocarbons*") either as catalyst supports or as catalysts on their own ("*carbocatalysis*") was recently reviewed [2], highlighting the important role of the surface chemical properties. The broad definition of *nanocarbons* includes both *nanosized* materials (carbon nanotubes/nanofibers; graphene-derived materials; nanodiamonds) and *nanostructured* materials (carbon gels and ordered mesoporous carbons).

In collaboration with the Group of Professor Armando Pombeiro, at IST (*Instituto Superior Técnico, Univ. Lisboa*), we have used carbon-supported gold nanoparticles to catalyze the carboxylation of C_n alkanes to C_{n+1} carboxylic acids, using CO, as indicated in Figure 2. The reaction is quite difficult, since C–H activation is very hard to achieve for the least reactive lower alkanes (1–6 carbon atoms). The results showed that the catalysts prepared on a properly functionalized support (oxidation with HNO_3 followed by treatment with NaOH) were stable and reusable, maintaining their initial activity and selectivity up to seven consecutive cycles [3,4]. Among the different supports tested (activated carbon, carbon nanotubes and carbon xerogels), the Au catalyst supported on carbon nanotubes (CNT) exhibited the best performance (yield > 88%) [4].

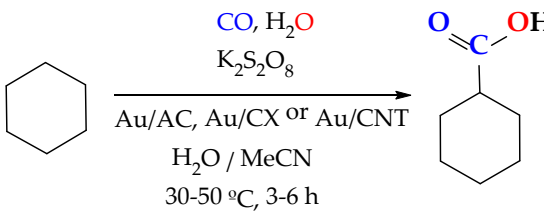

Figure 2: One-pot hydrocarboxylation of cyclohexane

Figura 2: Hydrocarboxilación de ciclohexano mediante método *one-pot*

We have also used surface functionalized carbon nanomaterials as supports for anchoring various types of C-scorpionate complexes (Au, Fe, V, Cu, Co). Figure 3 shows the immobilization protocol, using CNT as an example. These "heterogenized" complexes were efficient and recyclable catalysts for the oxidation of hydrocarbons and alcohols [5-8].

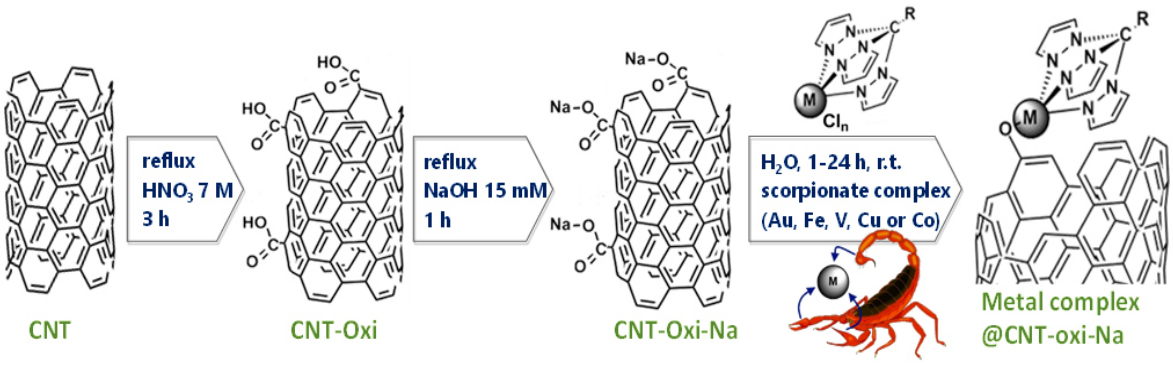

Figure 3: Immobilization of C-scorpionate complexes onto carbon nanotubes (R = H; CH_2OH).

Figura 3: Inmovilización de complejos C-escorpionato sobre CNT (R=H; CH_2OH).

These studies were then extended to the anchoring of several mononuclear Au(I) and Au(III) complexes which are commercially available [9]. In general, the complexes supported on CNT-oxi-Na yielded the best results, possibly due to the presence of more stable phenolate and carboxylate groups. In the framework of our collaboration with IST, we are currently attempting to scale-up the procedure for the production of ketones from secondary alcohols using microwave irradiation [5,8].

2.2 Carbon materials with tuned properties

Nanostructured mesoporous carbons are widely used in catalysis, adsorption and energy storage. The mesoporosity allows processing large molecules by addressing the diffusional limitations and pore blockage that may occur in purely microporous carbon materials, such as activated carbons. The different approaches that have been reported for the synthesis of mesoporous carbons, either with a disordered mesoporosity (carbon gels) or with ordered porous systems (carbons obtained by templating) were reviewed, together with the methods used for controlling their surface chemistry [10]. The design of both texture and surface chemistry allows tuning the properties, thus leading to materials that meet the requirements of the targeted applications.

The high toxicity of the reactants used in sol-gel and templating procedures justifies the search for alternative and more sustainable carbon precursors, such as biomass-derived compounds. However, the use of pure carbohydrates in sol-gel synthesis leads to carbon gels with poor mechanical and chemical resistance. More robust polymeric structures can be obtained by using graphene oxide (GO) or carbon nanotubes as condensation/polymerization promoters. The acidic sites on the surface of these nanocarbons promote dehydration/condensation reactions of the carbohydrates, whilst providing a scaffold for the growth of carbon xerogels, for example by hydrothermal carbonization (HTC). Based on these concepts, we obtained carbon xerogels from hydrothermally carbonized glucose-GO [11] (in collaboration with INCAR, CSIC, Oviedo, Spain) and glucose-CNT hybrids [12], subsequently activated with KOH (Figure 4).

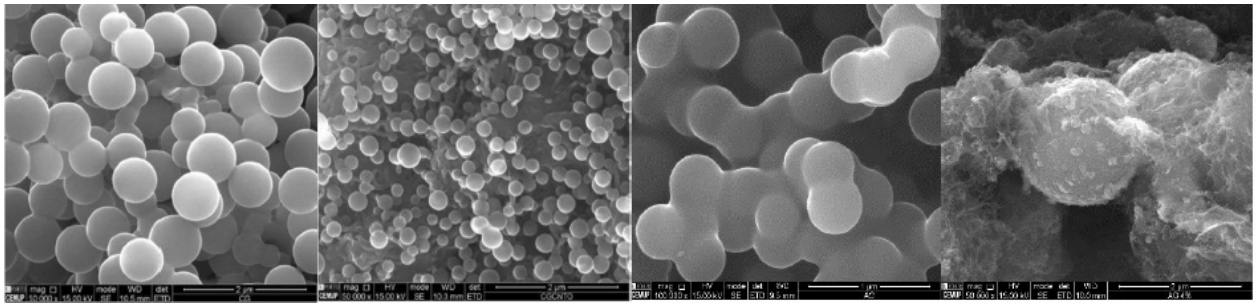

Figure 4: SEM micrographs of glucose-derived carbons: HTC Glucose; HTC Glucose-CNT_{oxid}; KOH-activated Glucose; KOH-activated Glucose-CNT (from left to right).

Figura 4: Micrografías SEM de carbones obtenidos a partir de glucosa: Glucosa carbonizada hidrotérmicamente; Glucosa-CNT_{oxid} carbonizada hidrotérmicamente; glucosa activada con KOH; glucosa-CNT activada con KOH (de izquierda a derecha).

Concerning the surface chemistry, we developed a new method for N-doping of carbon materials, which avoids the use of solvents and the production of wastes. The method consists in ball-milling the carbon material together with a suitable nitrogen precursor (such as urea or melamine), followed by thermal treatment under N_2 at 600 °C [13]. Carbon nanotubes and graphene oxide were successfully doped in this way, large amounts of nitrogen being incorporated, especially when using melamine as N-precursor. The thermal decomposition products of melamine lead to the incorporation of N-functionalities (pyridinic, N-6; pyrrolic, N-5; and quaternary nitrogen, N-Q) onto the carbon surface, as a result of the intimate mixture and the surface active sites created by ball milling (Figure 5). The method is easily scalable for practical applications, since it does not require highly specialized and expensive equipment, and has been extended to the incorporation of other heteroatoms, such as S, P and B, by using appropriate precursors [14].

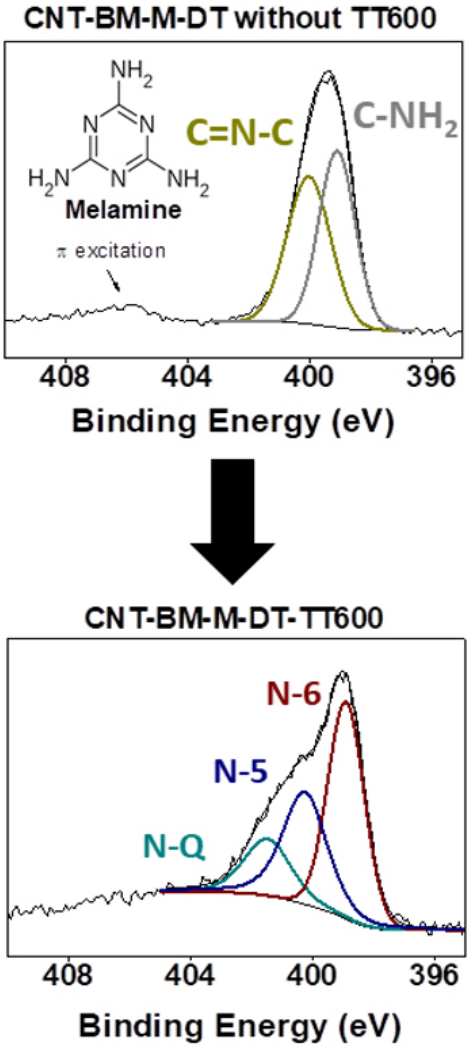

Figure 5: Changes in the N1s spectrum of ball-milled CNT with melamine upon thermal treatment (at 600 ºC, under nitrogen). Adapted from reference [13].

Figura 5: Cambios en el espectro de nitrógeno N1s de nanotubos de carbono tratados a 600 ºC en atmósfera de nitrógeno tras ser molidos en un molino de bolas en presencia de melamina. Figura adaptada de la referencia [13].

2.3 Advanced Functional Materials

Among the various activities pursued in this topic, the design and development of smart and functional textiles has been highly successful. One such example is the project "*Cork-a-Tex Yarn*" (textile yarn with high incorporation of cork) which recently received the "*Techtextil Innovation Award 2019*" in the category of "new material", one of the most important world prizes for innovation in technical textiles. The successful modification of the surface properties of cork in order to provide enhanced interaction with textile fibers and fabrics was based on our *know-how* on the surface functionalization of carbon materials. This was the subject of national and international patent applications [15]. We were also able to develop visible-light-induced self-cleaning functional textiles by coating graphene oxide and polymeric carbon nitride (g-C_3N_4) onto a cotton fabric. The coatings were efficient for the photocatalytic degradation of caffeine and rhodamine-B under LED visible light irradiation [16].

Another project concerned the development of magnetic carbon nanostructures for biomedical applications. In particular, we synthesized hydrophilic graphene-based yolk-shell magnetic nanoparticles functionalized with Pluronic F-127, for application in combined hyperthermia and dual stimuli-responsive drug delivery [17].

3. Environmental catalysis and technologies

This is a consolidated research area within the LCM Group, focusing on the development of improved technologies for the removal of pollutants from gaseous and liquid effluents and for the treatment and purification of water. Advanced oxidation processes (AOPs) are a major topic in this context, involving the development of catalysts based on nanostructured carbon materials, alone or in combination with semiconducting oxides.

In the case of water treatment, the synergies obtained by the integration of different technologies allowed the group to address the degradation of selected emergent organic micropollutants and biological contaminants. In particular, photocatalytic ozonation, photocatalysis assisted by H_2O_2, and the use of catalytic membranes, were successful approaches. Figure 6 shows the reactor used for the treatment of contaminated water by photocatalytic ozonation in continuous mode [18].

Excellent performances were achieved with nitrogen-doped carbon materials as catalysts for AOPs [19-22], and with composites of semiconducting oxides (TiO_2, ZnO) and nanosized carbons (carbon nanotubes, graphene-derived carbons, nanodiamonds) in photocatalysis [23-27]. Graphitic carbon nitride was another efficient photocatalyst for the degradation of organic pollutants [28-30].

Figure 6: Flow reactor fitted with LEDs for photocatalytic ozonation of contaminated water. The reactor is packed with glass rings coated with the TiO_2 photocatalyst

Figura 6: Reactor de flujo equipado con LEDs para la ozonización fotocatalítica de agua contaminada. El reactor funciona con un relleno de anillos de vidrio recubiertos con TiO_2.

A SolarNETmix® reactor configuration for heterogeneous Fenton/photo-Fenton processes was set-up in collaboration with Research Group 2 of LSRE-LCM [31-32].

Magnetically recoverable hybrid carbon catalysts, as well as amphiphilic carbon nanotubes for catalytic wet peroxide oxidation of aqueous solutions and oily wastewaters were developed at the LSRE-LCM branch in Bragança [33-36].

The preparation of innovative carbon-based membranes for water desalination and purification applications, eventually combined with AOPs, is a recent project with promising results [37].

4. Energy, fuels and chemicals

4.1 Solar fuels and chemicals

The use of solar light to produce renewable, sustainable and carbon-neutral fuels and chemicals, has recently emerged as an attractive alternative to traditional technologies. The concept of Solar Fuels refers mainly to the generation of hydrogen from water and products derived from CO_2 such as methanol, methane, formic acid and other chemicals. Hydrogen can be produced from water using renewable solar energy through a wide range of processes, namely, electrolysis, photo-electrochemical, photo-catalytic and thermochemical water splitting. Solar fuels derived from CO_2, water (a cheap, abundant and environmentally benign solvent) and sunlight (renewable energy source) are sustainable, produce no net CO_2 emissions and offer the advantage of leading to easily transportable liquid products, such as methanol. In addition, selective photocatalysis can provide a sustainable route to the synthesis of fine chemicals. Efficient photocatalysts are being developed in order to attain these objectives.

The photochemical generation of H_2 from water requires three components: a photosensitizer for light harvesting and electron transfer, an electron donor for the regeneration of the dye, and a catalyst for hydrogen evolution (HER). Hybrid photocatalysts consisting of g-C_3N_4 sensitized with free-base porphyrin dyes were prepared by impregnation through non-covalent interactions, and combined with Pt as co-catalyst for HER, EDTA being used as a sacrificial electron donor. With the best system, an amount of 326 mmol of H_2 was evolved in 6 hours under UV-vis light irradiation [38]. The synthesis of holey C-doped g-C_3N_4 with higher surface area and enhanced visible light absorption was also reported [39].

In the photo-reduction of CO_2 in aqueous phase, with formation of methanol and ethanol, graphene oxide-modified TiO_2 materials and derived composites loaded with Cu led to increased absorption in the visible spectral range and high photocatalytic activity [40].

We are also investigating the selective production of aromatic aldehydes from alcohols (namely anisaldehyde, benzaldehyde and vanillin, which are used as flavouring agents), under mild conditions of pH and temperature, using a benign solvent (water). The process occurs with the simultaneous production of a valuable by-product, hydrogen. Several photocatalysts were tested, including composites of ZnO with nanocarbons (carbon nanofibers; N-doped CNTs) [41,42], and g-C_3N_4 [43-45]. The best performance was achieved with carbon nitride, which offers the additional advantage of being an active photocatalyst under visible light.

4.2 Biomass conversion into fuels and chemicals

Lignocellulosic biomass is an abundant and renewable raw material composed of cellulose (40-50%), lignin (15-20%) and hemicelluloses (25-35%), and each one of these fractions can be converted into valuable products. Depolymerisation of cellulose to glucose can be combined with consecutive catalytic steps leading to valuable intermediates, thus significantly reducing the cost of biomass conversion. For example, cellulose can be converted into platform chemicals using bifunctional catalysts in one-pot tandem reactions. Following this strategy, by coupling hydrolysis of cellulose to glucose and its subsequent conversion via oxidation/hydrogenation, it is possible to obtain gluconic acid, sorbitol and many other versatile building blocks for the sustainable production of chemicals and fuels (Figure 7).

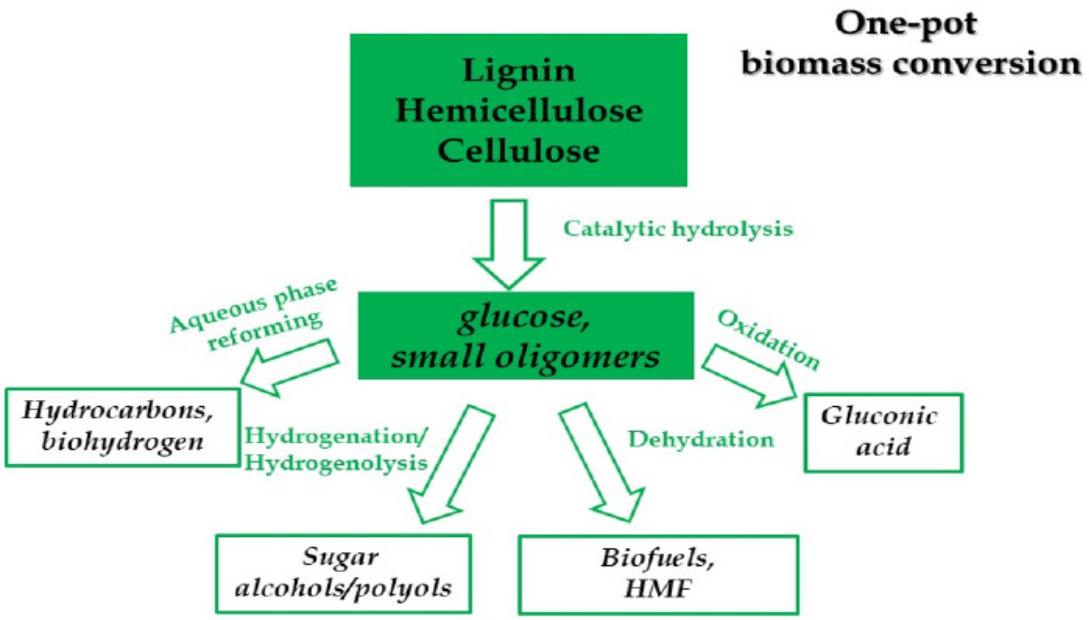

Figure 7: Alternative routes for biomass conversion.

Figura 7: Rutas alternativas para la conversión de biomasa.

Sorbitol and xylitol are two of the most important products which can be obtained from cellulose and hemicelluloses, respectively, both being in the TOP-12 biomass value-added products. We have studied the one-pot hydrolytic hydrogenation of cellulose and hemicelluloses (xylan) into these polyols using carbon-based catalysts. Ru (0.4 wt%) supported on carbon nanotubes (Ru/CNT) was found to be the most efficient of the monometallic catalysts tested for the direct conversion of cellulose [46,47]. The sorbitol yield was improved by using a Ru-Ni bimetallic catalyst [48]. The Ru/CNT catalyst was also efficient for the conversion of hemicelluloses (xylan) into xylitol. Moreover, we found that there is a synergistic effect between cellulose and xylan when converted simultaneously. Thus, yields of sorbitol and xylitol close to 80% were achieved after 6 h of reaction in the one-pot conversion of cellulose and xylan under a two-step temperature program (2 h at 170 ºC + 4 h at 205 ºC) [49]. Hydrolytic hydrogenation of cellulose on a CNT-supported Ru–W bimetallic catalyst produced ethylene glycol (40% yield after 3 h of reaction at 205 ºC) [50].

Both the monometallic Ru and the bimetallic Ru-W catalyst were later supported on glucose derived carbons (obtained by hydrothermal carbonization followed by activation), showing enhanced performances for the production of sorbitol and ethylene glycol, respectively [51,52].

The tandem oxidation of cellulose to gluconic acid requires a bifunctional catalyst with acidic sites for the hydrolysis step and metallic sites for glucose oxidation. We developed an active and selective catalyst for this process (using cellobiose as a model for cellulose), consisting of 1 wt% Au supported on functionalized carbon xerogel (Figure 8), which achieved a remarkable selectivity to gluconic acid of 80% in only 75 minutes [53].

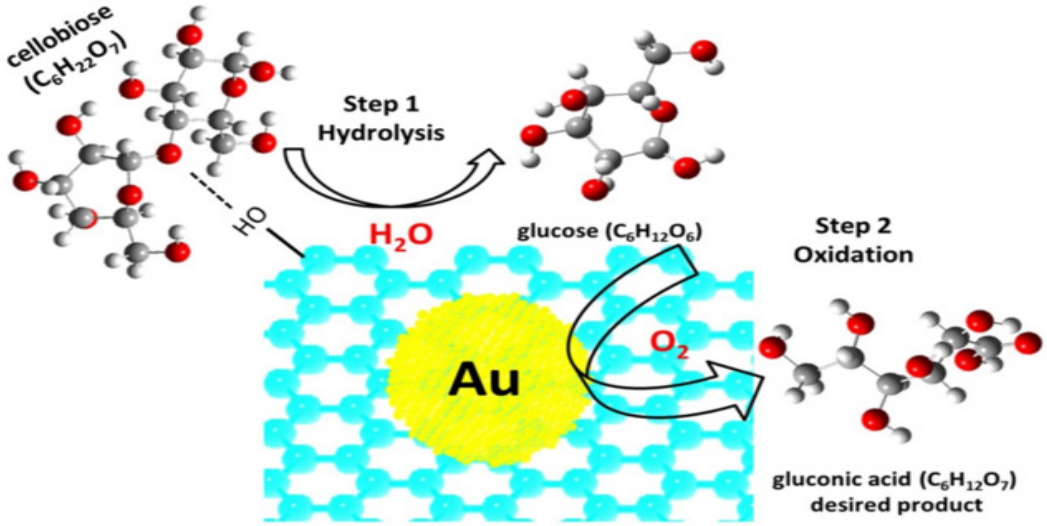

Figure 8: One-pot hydrolytic oxidation of cellobiose to gluconic acid. Reproduced from [53] with permission from Elsevier.

Figura 8: Oxidación hidrolítica de celobiosa a ácido glucónico mediante método *one-pot*. Figura reproducida de [53] con el permiso de Elsevier.

In addition, we investigated the influence of the type of surface functionalization of carbon catalysts on the hydrolysis of cellobiose. This is a key step to achieve high selectivity, since the feedstock (cellulose or cellobiose) is more stable than the product (glucose). Among the carbon xerogels (CX) prepared with different heteroatoms (S, P, N, O), CX containing 3.4 wt% of phosphorus showed the best catalytic performance, reaching 90 % cellobiose conversion with 72 % selectivity to glucose under oxidative atmosphere and in a short reaction time of only 4 h. The presence of phosphonates (-P-C-) was found to increase the selectivity to glucose up to 87 % [54].

4.3 Electrochemical energy conversion and storage

Our activities in this area include the development of hierarchical porous carbons for energy storage in supercapacitors, and carbon-based electrocatalysts for fuel cells and electrolysers.

The intrinsic principle of charge storage in supercapacitors (or electrochemical double-layer capacitors) consists on the electrostatic adsorption of electrolyte ions on the electrode surface. The energy density can be further enhanced by promoting reversible faradaic reactions between the electrode surface and the electrolyte (pseudocapacitance). Thus, hybrid supercapacitors combining both electrostatic and electrochemical storage mechanisms can be obtained by enriching porous carbon materials with heteroatoms (N, O, S, P or B), or by decorating their surface with transition metal oxides. The required properties for supercapacitor electrodes include a large micropore volume for ion storage, wide mesopores for enhanced ion diffusion, and good electrical conductivity [55]. We have investigated the electrochemical behavior of cerium oxide/multiwalled carbon nanotube composites prepared by sol-gel deposition of the oxide onto the carbon nanotubes. A new methodology was developed to identify the different charge storage mechanisms occurring on the surface of the composite [56]. In particular, square wave voltammetry (SWV) was used to separate the capacitive current from the pseudocapacitance. Further deconvolution of the SWV curves enabled the identification of the different faradaic processes occurring on the surface of the electrodes in acid, basic and neutral electrolytes [57].

Activated carbon xerogels obtained from hydrothermally carbonized glucose/graphene oxide hybrids were tested as supercapacitor electrodes, delivering a much higher specific capacitance than that of a commercial activated carbon (223 vs 153 F/g at 100 mA/g), as well as exhibiting a significantly improved retention of capacitance at high current densities [11]. Very good performances were also obtained with activated glucose-derived/CNT hybrid carbons [12], as shown in Figure 9 [55].

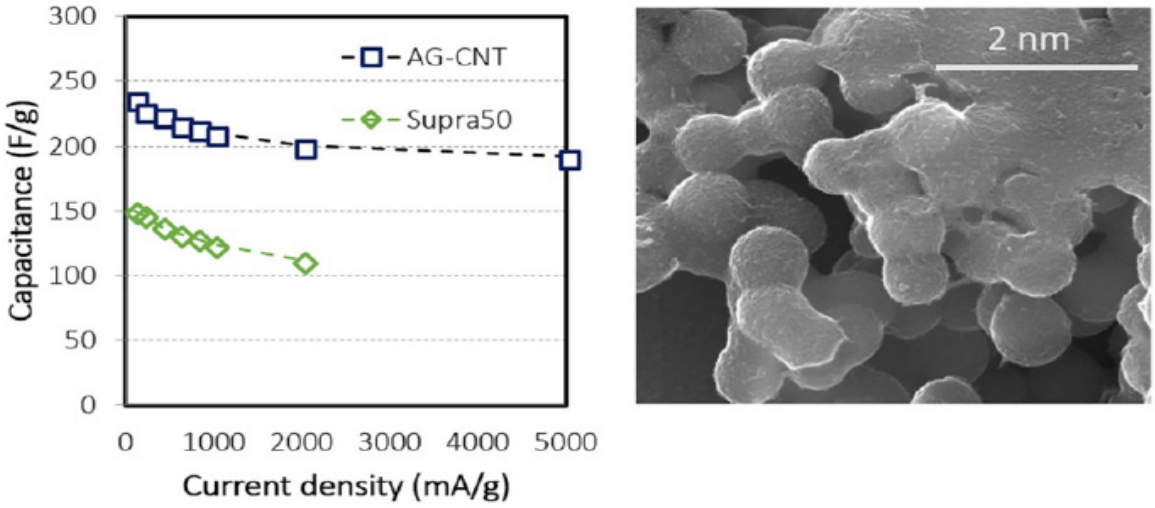

Figure 9: Electrochemical performance of a KOH activated glucose-derived/CNT hybrid carbon gel (AG-CNT), and corresponding SEM micrograph. The performance of a commercial activated carbon (Norit Supra DCL 50) is included. Reproduced from [55] with permission from Elsevier.

Figura 9: Comportamiento electroquímico de un carbón híbrido glucosa/CNT activado con KOH y micrografía SEM correspondiente (AG-CNT). La Figura incluye el comportamiento de un carbón activado comercial (Norit Supra DCL 50). Reproducida de [55] con el permiso de Elsevier.

Concerning energy conversion, our goal is to develop a new generation of carbon-based electrocatalysts without the use of precious metals. In particular, we have been focusing on N-doped CNTs for the oxygen reduction reaction (ORR) in alkaline medium. Our results highlighted the role of pyridinic and quaternary nitrogen in determining the performance of the electrocatalyst [58]. In another report, we investigated the role of the surface oxygen functional groups of CNTs on the ORR performance. Computational simulations showed that oxygen may adsorb on the quinone group without dissociation (leading to the indirect, or two-electron pathway), while adsorption can occur either associatively or dissociatively on the pyrone group, thus favoring the direct, four-electron pathway [59]. Interesting relationships between the nitrogen functionalities and the electroactivity towards the ORR were established in a study with glucose-derived carbons with tailored properties. It was found that a high pyridinic-N/quaternary-N ratio favors the

onset potential, while a low quaternary-N/pyrrolic-N ratio favors the number of electrons exchanged during ORR [60]. We have also prepared N-doped carbon xerogels with different micropore volumes and electrical conductivities for the ORR. By adding iron nanoparticles, we were able to achieve similar performances to the benchmark Pt electrocatalyst [61].

Our most recent research addresses an energy device that combines a fuel cell and an electrolyser, named "unitized regenerative fuel cell" (URFC). An URFC produces hydrogen in the electrolysis mode and delivers power in the fuel cell mode, thus overcoming the drawbacks related to the intermittent nature of renewable energies. The main challenge is to find active and stable bifunctional electrocatalysts for the direct and reverse reactions, namely the oxygen reduction and evolution reactions (ORR/OER) at the cathode, and the hydrogen oxidation and evolution reactions (HOR/HER) at the anode. We have been focusing on the oxygen reactions, which are the slowest. In particular, we have reported the synthesis of bifunctional electrocatalysts for ORR/OER derived from cobalt and manganese layered double hydroxides (LDH) compounded with carbon nanotubes [62], as well as Co_3O_4 supported on oxidized graphene flakes [63].

Acknowledgments

The work reviewed in this article was carried out at Associate Laboratory LSRE-LCM -UID/EQU/50020/2019 – financed by national funds through FCT/MCTES (PIDDAC). Additional support was provided by projects AIProcMat@N2020-Advanced Industrial Processes and Materials for a Sustainable Northern Region of Portugal 2020" (NORTE-01-0145-FEDER-000006) supported by Programme NORTE2020 under the Portugal 2020 Partnership Agreement, through the European Regional Development Fund (ERDF); and Project UNIRCELL (POCI-01-0145-FEDER-016422) funded by European Structural and Investment Funds (FEEI) through COMPETE2020 and by national funds through FCT. The LCM team is acknowledged for revising the manuscript and for assistance with some figures.

References

[1] J.L. Figueiredo. BOLETIN del Grupo Español del Carbón 2016; 39: 2-7.

[2] J.L. Figueiredo. *In:* Nanotechnology in Catalysis: Applications in the Chemical Industry, Energy Development, and Environment Protection (Marcel Van de Voorde, Bert F. Sels, editors). Wiley-VCH Verlag GmbH & Co. KGaA, Vol.1, pp. 37-55 (2017).

[3] A.P.C. Ribeiro, L.M.D.R.S. Martins, S.A.C. Carabineiro, J.L. Figueiredo, A.J.L. Pombeiro, Molecules 2017; 22: 603.

[4] A.P.C. Ribeiro, L.M.D.R.S. Martins, S.A.C. Carabineiro, J.L. Figueiredo, A.J.L. Pombeiro, Appl. Catal. A: Gen. 2017; 547: 124-131.

[5] L.M.D.R.S. Martins, A.P.C. Ribeiro, S.A.C. Carabineiro, J.L. Figueiredo, A.J.L. Pombeiro, Dalton Trans. 2016; 45: 6816-6819.

[6] J. Wang, L.M.D.R.S. Martins, A.P.C. Ribeiro, S.A.C. Carabineiro, J.L. Figueiredo, A.J.L. Pombeiro, Chem. Asian J. 2017; 12: 1915-1919.

[7] A.P.C. Ribeiro, L.M.D.R.S. Martins, S.A.C. Carabineiro, J.G. Buijnsters, J.L. Figueiredo, A.J.L. Pombeiro, ChemCatChem 2018; 10: 1821-1828.

[8] A.J.L.O. Pombeiro, L.M.D.R. Sousa Martins, A.P.C. Ribeiro, S.A.C. Carabineiro, J.L. Figueiredo. European Patent nº EP3397609 (B1), published on July 3rd, 2019.

[9] S.A.C. Carabineiro, L.M.D.R.S. Martins, A.J.L. Pombeiro, J.L. Figueiredo. ChemCatChem 2018; 10: 1804-1813.

[10] M. Enterría, J.L. Figueiredo, Carbon 2016; 108: 79-102.

[11] M. Enterria, F.J. Martin-Jimeno, F. Suarez-Garcia, J.I. Paredes, M.F.R. Pereira, J.I. Martins, A. Martinez-Alonso, J.M.D. Tascon, J.L. Figueiredo. Carbon 2016; 105: 474-483.

[12] N. Rey-Raap, M. Enterria, J.I. Martins, M.F.R. Pereira, J.L. Figueiredo. ACS Appl. Mater. Interfaces 2019; 11: 6066-6077.

[13] O.S.G.P. Soares, R.P. Rocha, A.G. Gonçalves, J.L. Figueiredo, J.J.M. Órfão, M.F.R. Pereira. Carbon, 91: 114-121 (2015).

[14] O.S.G.P. Soares, R.P. Rocha, J.J.M. Órfão, M.F.R. Pereira, J.L. Figueiredo. C 2019; 5: 30.

[15] A.F.M.F. Ramôa, M.G.C.O.B.S.M. Pizarro, J.A. Morgado, S.O. Prozil, M.F.R. Pereira, O.S.G.P. Soares, P.S.F. Ramalho, C.A.M.P. Sá, V.L.G.P. Sá, S.G.C.S. Ventura, J.S. Abreu. International Patent Application: PCT/IB2017/050485, Filling Date: January 2017. Portuguese Patent: 109121, Entry Date: January 2016.

[16] M. Pedrosa, M.J. Sampaio, T. Horvat, O.C. Nunes, G. Dražić, A.E. Rodrigues, J.L. Figueiredo, C.G. Silva, A.M.T. Silva, J.L. Faria. Appl. Surf. Sci. 2019; 497: article 143757, in press (*https://doi.org/10.1016/j.apsusc.2019.143757*).

[17] R.O. Rodrigues, G. Baldi, S. Doumett, L. Garcia-Hevia, J. Gallo, M. Banobre-Lopez, G. Drazic, R.C. Calhelha, I.C.F.R. Ferreira, R. Lima, H.T. Gomes, A.M.T. Silva. Mat. Sci. Eng. C-Mater. 2018; 93: 206-217.

[18] N.F.F. Moreira, J.M. Sousa, G. Macedo, A.R. Ribeiro, L. Barreiros, M. Pedrosa, J.L. Faria, M.F.R. Pereira, S. Castro-Silva, M.A. Segundo, C.M. Manaia, O.C. Nunes, A.M.T. Silva. Water Res. 2016; 94: 10-22.

[19] O.S.G.P. Soares, R.P. Rocha, A.G. Gonçalves, J.L. Figueiredo, J.J.M. Órfão, M.F.R. Pereira. Appl. Catal. B: Environ. 2016; 192: 296-303.

[20] 16. D.F.M. Santos, O.S.G.P. Soares, A.M.T. Silva, J.L. Figueiredo, M.F.R. Pereira. Appl. Catal. B: Environ. 2016; 199: 361-371.

[21] M. Martin-Martinez, R.S. Ribeiro, B.F. Machado, P. Serp, S. Morales-Torres, A.M.T. Silva, J.L. Figueiredo, J.L. Faria, H.T. Gomes. ChemCatChem 2016; 8: 2068-2078.

[22] R.P. Rocha, O.S.G.P. Soares, A.G. Gonçalves, J.J.M. Órfão, M.F.R. Pereira, J.L. Figueiredo. Appl. Catal. A: Gen. 2017; 548: 62-70.

[23] C.A. Orge, O.S.G.P. Soares, J.L. Faria, M.F.R. Pereira. J. Environ. Chem. Eng. 2017; 5: 5599-5607.

[24] M. Pedrosa, L.M. Pastrana-Martínez, M.F.R. Pereira, J.L. Faria, J.L. Figueiredo, A.M.T. Silva. Chem. Eng. J. 2018; 348: 888-897.

[25] C.A. Orge, O.S.G.P. Soares, J.L. Faria, M.F.R. Pereira. J. Environ. Chem. Eng. 2017; 5: 5599-5607.

[26] C.A. Orge, M.F.R. Pereira, J.L. Faria. Chem. Eng. J. 2017; 318: 247-253.

[27] C.A. Orge, J.L. Faria, M.F.R. Pereira. J. Environ. Manag. 2017; 195: 208-215.

[28] L. Svoboda, P. Praus, M.J. Lima, M.J. Sampaio, D. Matýsek, M. Ritz, R. Dvorský, J.L. Faria, C.G. Silva. Mater. Res. Bull. 2018; 100: 322-332.

[29] N.F.F. Moreira, M.J. Sampaio, A.R. Ribeiro, C.G. Silva, J.L. Faria, A.M.T. Silva. Appl. Catal. B: Environ. 2019; 248: 184-192.

[30] A. Torres-Pinto, M.J. Sampaio, C.G. Silva, J.L. Faria, A.M.T. Silva. Appl. Catal. B: Environ. 2019; 252: 128-137.

[31] M.J. Lima, C.G. Silva, A.M.T. Silva, J.C.B. Lopes, M.M. Dias, J.L. Faria. Chem. Eng. J. 2017; 310: 342–351.

[32] M.J. Lima, A.M.T. Silva, C.G. Silva, J.L. Faria, J.C.B. Lopes, M.M. Dias. Chem. Eng. J. 2016; 287: 419-424.

[33] R.S. Ribeiro, A.M.T. Silva, J.L. Figueiredo, J.L. Faria, H.T. Gomes. Appl. Catal. B: Environ. 2016; 187: 428-460.

[34] R.S. Ribeiro, A.M.T. Silva, P.B. Tavares, J.L. Figueiredo, J.L. Faria, H.T. Gomes. Catal. Today 2017; 280: 184-191.

[35] R.S. Ribeiro, R.O. Rodrigues, A.M.T. Silva, P.B. Tavares, A.M.C. Carvalho, J.L. Figueiredo, J.L. Faria, H.T. Gomes. Appl. Catal. B: Environ. 2017; 219: 645-657.

[36] J.L. Diaz de Tuesta, B.F. Machado, P. Serp, A.M.T. Silva, J.L. Faria, H.T. Gomes. Catal. Today 2019; in press (https://doi.org/10.1016/j.cattod.2019.07.012).

[37] M. Pedrosa, G. Drazic, P.B. Tavares, J.L. Figueiredo, A.M.T. Silva. Chem. Eng. J. 2019; 369: 223-232.

[38] E.S. da Silva, N.M.M. Moura, M.G.P.M.S. Neves, A. Coutinho, M. Prieto, C.G. Silva, J.L. Faria. Appl. Catal. B: Environ. 2018; 221: 56-69.

[39] E.S. da Silva, N.M.M. Moura, A. Coutinho, G. Dražić, B.M.S. Teixeira, N.A. Sobolev, C.G. Silva, M. Graça, P.M.S. Neves, M. Prieto, J.L. Faria. ChemSusChem 2018; 11: 2681-2694.

[40] L.M. Pastrana-Martínez, A.M.T. Silva, N.N.C. Fonseca, J.R. Vaz, J.L. Figueiredo, J.L. Faria. Top. Catal. 2016; 59: 1279-1291.

[41] M.J. Sampaio, A. Benyounes, P. Serp, J.L. Faria, C.G. Silva. Appl. Catal. A: Gen. 2018; 551: 71-78.

[42] R.A. Fernandes, M.J. Sampaio, E.S. da Silva, P. Serp, J.L. Faria, C.G. Silva. Catal. Today 2019; 328: 286-292.

[43] M.J. Lima, A.M.T. Silva, C.G. Silva, J.L. Faria. J. Catal. 2017; 353: 44-53.

[44] M.J. Lima, M.J. Sampaio, C.G. Silva, A.M.T. Silva, J.L. Faria. Catal. Today 2019; 328: 293-299.

[45] J.C. Lopes, M.J. Sampaio, R.A. Fernandes, M.J. Lima, J.L. Faria, C.G. Silva. Catal. Today 2019; in press. (*https://doi.org/10.1016/j.cattod.2019.03.050*).

[46] L.S. Ribeiro, J.J. Delgado, J.J.M. Órfão, M.F.R. Pereira. Catal. Today 2017; 279: 244-251.

[47] L.S. Ribeiro, J.J. Delgado, J.J.M. Órfão, M.F.R. Pereira. ChemCatChem 2017; 9: 888-896.

[48] L.S. Ribeiro, J.J. Delgado, J.J.M. Órfão, M.F.R. Pereira. Appl. Catal. B: Environ. 2017; 217: 265-274.

[49] L.S. Ribeiro, J.J.M. Órfão, M.F.R. Pereira. Bioresource Technol. 2017; 244: 1173-1177.

[50] L.S. Ribeiro, J. Órfão, J.J.M. Órfão, M.F.R. Pereira. Cellulose 2018; 25: 2259-2272.

[51] N. Rey-Raap, L.S. Ribeiro, J.J.M. Órfão, J.L. Figueiredo, M.F.R. Pereira. Appl. Catal. B: Environ. 2019; 256: in press (*https://doi.org/10.1016/j.apcatb.2019.117826*).

[52] L.S. Ribeiro, N. Rey-Raap, J.L. Figueiredo, J.J.M. Órfão, M.F.R. Pereira. Cellulose 2019; 26: 7337-7353.

[53] K.M. Eblagon, M.F.R. Pereira, J.L. Figueiredo. Appl. Catal. B: Environ. 2016; 184: 381-396.

[54] K.M. Eblagon, A. Malaika, M.F.R. Pereira, J.L. Figueiredo. ChemCatChem 2018; 10: 4934-4946.

[55] J.L. Figueiredo. Surface and Coatings Technology 2018; 350: 307-312.

[56] M. Enterría, A.G. Gonçalves, M.F.R. Pereira, J.I. Martins, J.L. Figueiredo. Electrochim. Acta 2016; 209: 25-35.

[57] M. Enterría, A.G. Gonçalves, M.F.R. Pereira, J.I. Martins, J.L. Figueiredo. J. Electroanal. Chem. 2019; 847: in press (*https://doi.org/10.1016/j.jelechem.2019.113269*).

[58] I.M. Rocha, O.S.G.P. Soares, I.M. Fernandes, C. Freire, J.L. Figueiredo, M.F.R. Pereira. ChemistrySelect 2016; 1: 2522-2530.

[59] I.M. Rocha, O.S.G.P. Soares, J.L. Figueiredo, C. Freire, M.F.R. Pereira. Catal. Sci. Technol. 2017; 7: 1868-1879.

[60] R.G. Morais, N. Rey-Raap, J.L. Figueiredo, M.F.R. Pereira. Beilstein J. Nanotech. 2019; 10: 1089-1102.

[61] M. Canal-Rodríguez, N. Rey-Raap, J.A. Menéndez, M.A. Montes-Morán, J.L. Figueiredo, M.F.R. Pereira, A. Arenillas. Micropor. Mesopor. Mat., in press. *https://doi.org/10.1016/j.micromeso.2019.109811*.

[62] M.F.P. Duarte, I.M. Rocha, J.L. Figueiredo, C. Freire, M.F.R. Pereira. Catal. Today 2018; 301: 17-24.

[63] M.P. Araujo, M. Nunes, I.M. Rocha, M.F.R. Pereira, C. Freire. ChemistrySelect 2018; 3: 10064-10076.

Hybrid/Doped Carbon-Based (Nano)materials for Advanced Applications: Eco-Sustainable Catalysis, Biomass Valorization, Energy Technologies & Smart Devices

Cristina Freire*, Clara Pereira*, Andreia F. Peixoto, Diana M. Fernandes, Bruno Jarrais, Marta Nunes and Ruben Ramos

REQUIMTE/LAQV, Departamento de Química e Bioquímica, Faculdade de Ciências, Universidade do Porto, Rua do Campo Alegre s/n, 4169-007 Porto, Portugal
** Corresponding authors: acfreire@fc.up.pt; clara.pereira@fc.up.pt*

Abstract

Carbon-based (nano)materials are remarkable building blocks that have been boosting innovation in a multitude of advanced applications, ranging from Catalysis and Environment to Energy and Smart Technologies.

Our research group from the Associated Laboratory for Green Chemistry REQUIMTE/LAQV, at the Chemistry and Biochemistry Department of Faculty of Sciences of Porto University, Portugal, has been developing research work within the context of R&TD projects in the areas of hybrid and doped carbon-based (nano)materials for eco-sustainable catalysis, biomass valorization, energy technologies and smart devices. In this article, the main achievements and progress in these fields are reviewed.

1. Introduction

The Associated Laboratory REQUIMTE/LAQV is the largest Chemistry Network in Portugal, being recognized as a Research Centre of Excellence, covering Chemistry, Chemical Engineering and Biotechnology areas. Among the different thematic lines of LAQV, our research group – *Catalysis and Functional and Smart (Nano)materials* – which is located at the Chemistry and Biochemistry Department of the Faculty of Sciences of Porto University (LAQV@FCUP), is integrated in the thematic line of *Functional Materials*, and in the research group of *Materials for Sustainability and Wellbeing*. It is devoted to the production of advanced multifuncional (nano) materials with unique/enhanced properties through eco-friendly routes to address the 21st Century Grand Challenges, boosting innovation on for core scientific areas: (i) Catalysis for a Sustainable Environment, (ii) Renewable Energy and Climate Change Mitigation, (iii) Environmental Protection and Remediation, and (iv) Wearable Technologies and Devices.

Among the landscape of engineered (nano)materials developed by our group and used as building blocks for the aforementioned applications, carbon (nano) materials occupy a pivotal position, owing to their remarkable physicochemical properties and wide versatility in terms of doping, functionalization and composite fabrication/hybridization with other components (*e.g.*, transition metal complexes, noble and earth abundant metals, metal oxides, polyoxometalates, etc.).

In this article, the different R&TD activities that are being carried out at LAQV@FCUP in the field of hybrid and doped carbon-based (nano)materials for advanced applications are reviewed, with special highlight to four key applications: eco-sustainable catalysis, biomass valorization, energy production and storage technologies & smart electrochromic devices. The article starts by reviewing the works developed in the areas of recyclable heterogeneous carbon-based catalysts for oxidation and reduction reactions, namely hybrid carbon-metal complex heterogeneous catalysts, carbon supported gold(0) catalysts and the new generations of metal-free carbocatalysts and graphene-based photo(electro) catalysts for emerging pollutants removal. Afterwards, the development of biochar-based catalysts for biomass valorization is presented. Subsequently, the fabrication of hybrid/doped carbon-based (nano) materials for energy applications, namely fuel cells and electrochemical energy storage devices, including energy storage textiles and flexible devices, is described. Finally, the last section is devoted to the development of smart electrochromic devices based on carbon-poly(nickel complex) nanocomposites.

2. Eco-Sustainable Catalytic Systems Based on Carbon (Nano)Materials

2.1 Hybrid Carbon-Metal Complex Heterogeneous Catalysts for the Epoxidation of Alkenes and Allylic Alcohols

Transition metal complexes are ubiquitous catalysts in several important chemical transformations for the synthesis of valuable fine and bulk chemicals and chemical intermediates, through oxidation, addition or reduction reactions [1,2]. The heterogenization of such metal complexes on solid supports allows the combination of the catalytic properties of the homogeneous complexes with the advantages of heterogeneous catalysts, namely the ease of separation from the reaction medium, shape selectivity and reusability [3–7]. Our group has developed several anchoring procedures to immobilize Schiff-base transition metal complexes onto activated carbons (ACs) in collaboration with Professors J. L. Figueiredo and M. F. R. Pereira from the Associate Laboratory LSRE-LCM (Laboratory of Separation and Reaction Engineering and Laboratory of Catalysis and Materials), at the Chemical Engineering Department of Faculty of Engineering of University of Porto (FEUP) [8–12].

In one of those works, oxidovanadium(IV) acetylacetonate ([$VO(acac)_2$]) was anchored onto two oxidized activated carbons (ACs) previously functionalized with 3-aminopropyl)triethoxysilane

or with bis(3-aminopropyl)amine (methods A and B, respectively), through Schiff-base condensation between the free amine groups covalently attached to the AC surface and the oxygen atoms of the acetylacetonate ligand, as shown in Figure 1 [13].

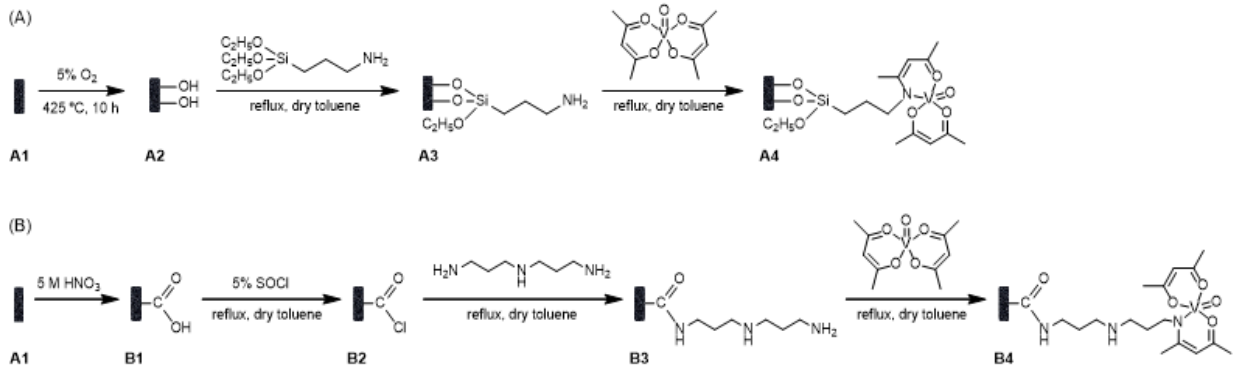

Figure 1. Proposed routes for the immobilization of $[VO(acac)_2]$ onto amine-functionalized ACs by methods A and B. Reproduced from ref. [13]which possesses carboxylic surface groups, was treated with thionyl chloride to give surface acyl chloride groups (132 by permission of John Wiley and Sons.

The catalytic activity of the two novel AC-based $[VO(acac)_2]$ heterogeneous catalysts, A4 and B4, was tested in the epoxidation of an allylic alcohol (3-buten-2-ol) at 0 °C in dichloromethane, using *tert*-butyl hydroperoxide as the oxygen source. Both catalysts showed high catalytic activity (A4: substrate conversion, %C = 100% after 144 h; B4: %C = 100% after 192 h), with the A4 catalyst being more active than B4 (0.4 *vs* 0.3 h^{-1} turnover frequencies, respectively). Moreover, both materials were reused with no significant loss of activity, indicating that the metal complexes were irreversibly anchored to the carbon surface, which prevented the leaching of the active phase and possible catalyst deactivation.

In another work, the *Jacobsen* catalyst, [(*R,R*)-(-)-*N,N'*-Bis(3,5-di-*tert*-butylsalicylidene)-1,2-cyclohexanediaminomanganese(III) chloride], was immobilized onto four ACs with different average pore sizes prepared by a gasification process with CO_2 during four exposure times (X = 0, 60, 180, 300 min) followed by thermal treatment with O_2 [14]. An increase of the specific surface area of the ACs was observed upon the increase of the gasification time, as well as of other textural parameters, such as the mesopore area, micropore volume and average pore size. Afterwards, the materials were treated with NaOH to facilitate the subsequent *Jacobsen* complex immobilization through axial coordination, as shown in Figure 2.

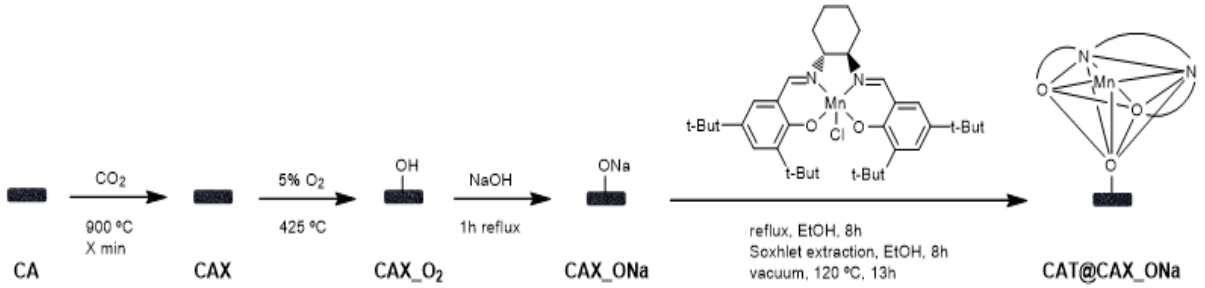

Figure 2. Anchoring procedure for the immobilization of the *Jacobsen* catalyst onto modified ACs. Reproduced from ref. [14] by permission of Elsevier.

The heterogeneous catalysts were tested in three systems: (i) epoxidation of styrene using *m*-chloroperoxybenzoic acid as oxidant and 4-methylmorpholine *N*-oxide as co-oxidant (–5 ºC, in CH_2Cl_2); (ii) epoxidation of 6-cyano-2,2-dimethylchromene using NaOCl as oxidant (0 ºC, in CH_2Cl_2) and (iii) epoxidation of 6-cyano-2,2-dimethylchromene using iodosylbenzene as oxidant (at room temperature, in CH_3CN). The catalysts were found to be active and enantioselective in the three systems, as summarized in Table 1.

The activity of the heterogeneous catalysts in the epoxidation of both substrates generally increased with the increase of the porosity of the AC support. In parallel, the total Mn(III) loading in the heterogeneous catalysts increased with the AC support pore size, as well as the metal complex distribution within the carbon porous matrix, which could account for the increased catalytic activity. Concerning the enantioselectivity, in the case of the epoxidation of styrene (system i), the increase of the AC porosity also led to an increase of the enantiomeric excess values (%ee). Moreover, when that particular reaction was catalyzed by CAT@CA180_ONa and CAT@CA300_ONa, the obtained %ee values were higher than those achieved with the homogeneous counterpart (43% *vs.* 40% in both cases). In the case of the epoxidation of 6-cyano-2,2-dimethylchromene, systems ii and iii, similar enantioselectivity trends were observed, except when using CAT@CA180_ONa as catalyst.

Catalyst	System	*t* (h)	C (%)	S (%)	ee (%)
CAT@CA_ONa	(i)	4	19	76	30
CAT@CA60_ONa		4	34	86	36
CAT@CA180_ONa		4	67	95	43
CAT@CA300_ONa		4	74	96	43
CAT@CA_ONa	(ii)	48	5	89	82
CAT@CA60_ONa		48	8	95	84
CAT@CA180_ONa		48	20	98	80
CAT@CA300_ONa		48	22	84	85
CAT@CA_ONa	(iii)	72	30	32	64
CAT@CA60_ONa		72	36	88	71
CAT@CA180_ONa		72	50	96	70
CAT@CA300_ONa		72	46	98	73

[a] C – substrate conversion; S – epoxide selectivity; ee – enantiomeric excess.

Table 1. Asymmetric epoxidation of alkenes catalyzed by heterogeneous AC-supported *Jacobsen* catalysts[a]

The activity of the heterogeneous catalysts in the epoxidation of both substrates generally increased with the increase of the porosity of the AC support. In parallel, the total Mn(III) loading in the heterogeneous catalysts increased with the AC support pore size, as well as the metal complex distribution within the carbon porous matrix, which could account for the increased catalytic activity. Concerning the enantioselectivity, in the case of the epoxidation of styrene (system i), the increase of the AC porosity also led to an increase of the enantiomeric excess values (%ee). Moreover, when that particular reaction was catalyzed by CAT@CA180_ONa and CAT@CA300_ONa, the obtained %ee values were higher than those achieved with the homogeneous counterpart (43% *vs.* 40% in both cases). In the case of the epoxidation of 6-cyano-2,2-dimethylchromene, systems ii and iii, similar enantioselectivity trends were observed, except when using CAT@CA180_ONa as catalyst.

Reusability experiments revealed a general decrease of the catalytic performance of the AC-based catalysts. Nevertheless, CAT@CA180_ONa and CAT@CA300_ONa materials still led to turnover numbers (TONs) higher than those obtained in the homogeneous phase for the epoxidation of 6-cyano-2,2-dimethylchromene with iodosylbenzene (CAT@CA180_ONa: TON = 17 *vs.* 16; CAT@CA300_ONa: 12 *vs.* 9).

2.2 Activated Carbon Supported Gold(0) Catalysts for the Oxidation of Glycerol

In the midst of our studies on the immobilization of metal complexes onto ACs, we made a serendipitous discovery. We found that these ACs could reduce Au(III) ions in solution to metallic Au(0), in the absence of any reductant. Hence, we prepared novel Au(0)-based heterogeneous catalysts by direct reduction of Au(III) ions onto different AC materials, namely a non-functionalized AC (A1, Figure 1) and an oxidized AC (A2, Figure 1), using ethanol (Au@A1, Au@A2) or water (Au@A1', Au@A2') as solvent [15]. Geometrical shaped and amorphous gold was formed at the surface of the carbon materials (Figure 3). Smaller Au particles were detected in Au@AC1 and Au@AC2 materials, as well as geometric shaped particles, while only gold aggregates could be observed in Au@A1' and Au@A2'. These results suggested that the reduction of gold in water was significantly faster than in ethanol.

Liquid-phase catalytic oxidation is a promising route

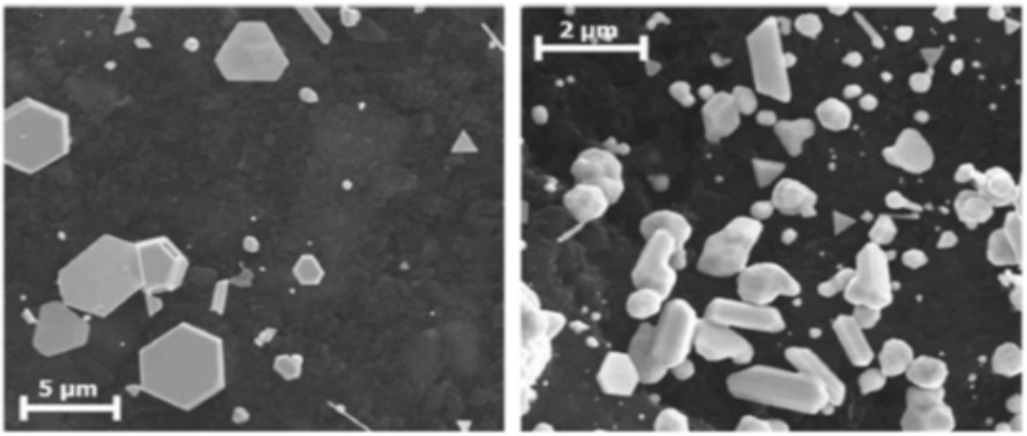

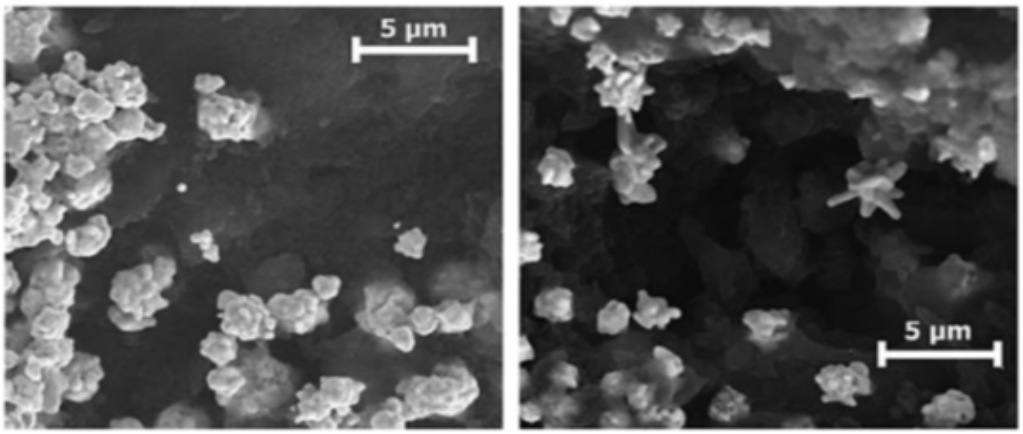

Figure 3. SEM micrographs of Au@A1 (top left), Au@A2 (top right), Au@A1' (bottom left) and Au@A2' materials (bottom right). Reproduced from ref. [15] by permission of Elsevier.

for the valorization of glycerol by conversion into useful products, provided that the used catalysts are sufficiently active and selective for the formation of compounds, such as glyceric acid. Specifically, for gold species to be active, the presence of small metallic Au(0) species is required. In this context, the new Au(0)-based heterogeneous catalysts were tested in the oxidation of glycerol (60 ºC, in NaOH/glycerol, using 3 bar of O_2). Catalyst Au@A2 showed the best performance (%C = 90% after 7 h), with high and constant selectivity towards the compound of commercial interest, glyceric acid (%S = 58% after 7 h), which could be explained by the higher amount of smaller gold particles in that material.

2.3 Metal-Free Carbocatalysts

Carbon materials have been extensively used as catalyst supports for many years. However, certain carbon materials have recently demonstrated to be promising metal-free alternatives for low-cost catalytic processes owing to their wide availability, environmental acceptability, corrosion resistance, and unique surface properties [16]. Despite the few examples of reactivity of pristine carbon materials, their catalytic activity can be greatly enhanced upon introduction of new active sites, either through functionalization with oxygen groups or through doping with heteroatoms.

In this sense, modified multi-walled carbon nanotubes (MWCNTs) and graphene flakes (GFs) were prepared by three different oxidation procedures: (i) nitric acid treatment, (ii) nitric acid followed by thermal treatment at 400 ºC, and (iii) gas phase oxidation with O_2, as illustrated in Figure 4 [17].

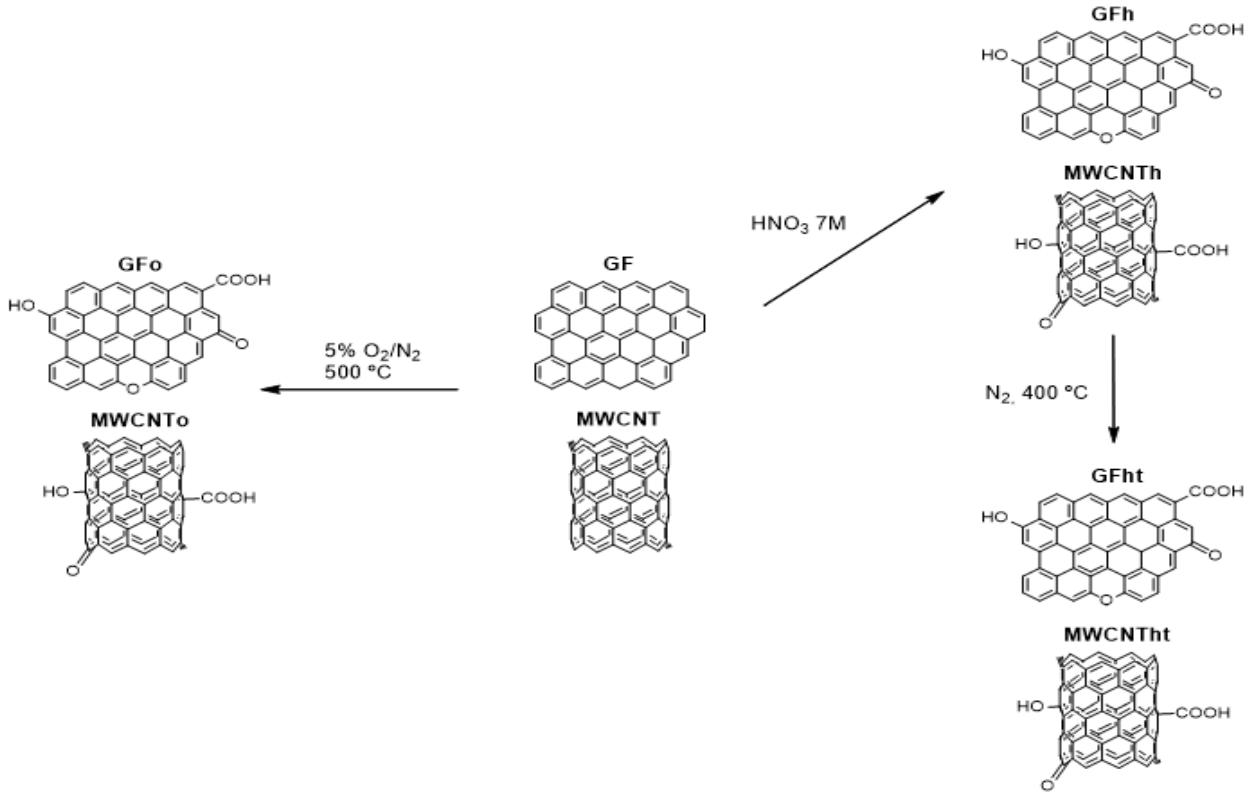

Figure 4. Schematic representation of the procedures for the oxidation of MWCNTs and GFs. Reproduced from ref. [17] by permission of The Royal Society of Chemistry (RSC) on behalf of the Centre National de la Recherche Scientifique (CNRS) and the RSC.

All the oxidized materials showed an overall increase of the oxygen content relative to the parent counterparts. Moreover, the different oxidation procedures induced different surface chemical compositions, namely: (i) nitric acid treated materials MWCNTh and GFh presented increased amounts of carboxylic acids, anhydrides and phenols; (ii) nitric acid followed by thermal treatment at 400 ºC induced the removal of carboxylic acids and an increase of the anhydrides content; (iii) gas phase oxidation promoted the introduction of phenols, carbonyls/ quinones, and lactones.

The catalytic oxidation of *cis*-cyclooctene with 30% H_2O_2 at 80 ºC in acetonitrile was studied in heterogeneous phase, using the pristine and modified carbon nanomaterials as catalysts. All nanomaterials were active and selective towards epoxycyclooctane and the modifications introduced in the MWCNTs and GFs through nitric acid followed by thermal treatment at 400 ºC (procedure ii), originated catalysts with superior activity and selectivity when compared with their pristine counterparts (MWCNTht: %C = 47% *vs.* 43% and %S = 79% *vs.* 81%; GFht: %C = 57% *vs.* 25 and %S = 85% *vs.* 76%), as shown in Figure 5.

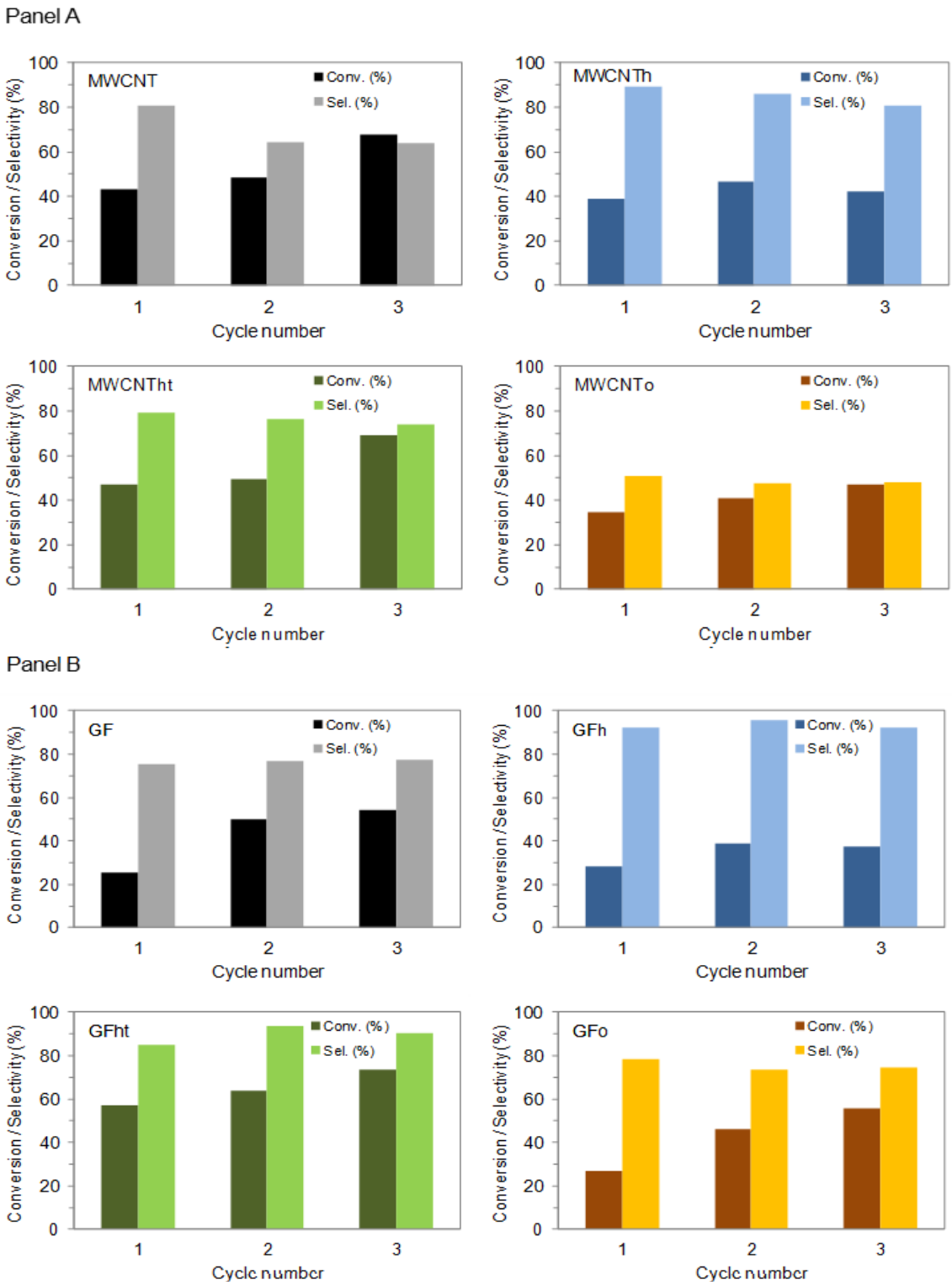

Figure 5. Substrate conversion and epoxycyclooctane selectivity evolution in the oxidation of *cis*-cyclooctene catalyzed by MWCNT-based materials (panel A) and GF-based materials (panel B) for up to three cycles. Reproduced from ref. [17] by permission of RSC on behalf of CNRS and the RSC.

Reusability experiments revealed a slight increase of the catalytic activity of the carbocatalysts for up to three cycles: this was tentatively attributed to the use of H_2O_2 as oxidant, which could be responsible for the oxidation of the nanomaterials surface, enhancing their catalytic performance. These results indicated that the fine-tuning of the morphology and surface chemistry of carbon materials, concerning the amount of defects and type and amount of oxygen surface groups, respectively, is of high importance to pursue the fabrication of metal-free carbocatalysts with superior performance and selectivity.

In another work, MWCNTs and GFs doped with heteroatoms, namely N, P, B, and S, were prepared through a simple ball milling procedure using adequate precursors, followed by thermal treatment in an inert atmosphere, as depicted in Figure 6 [18].

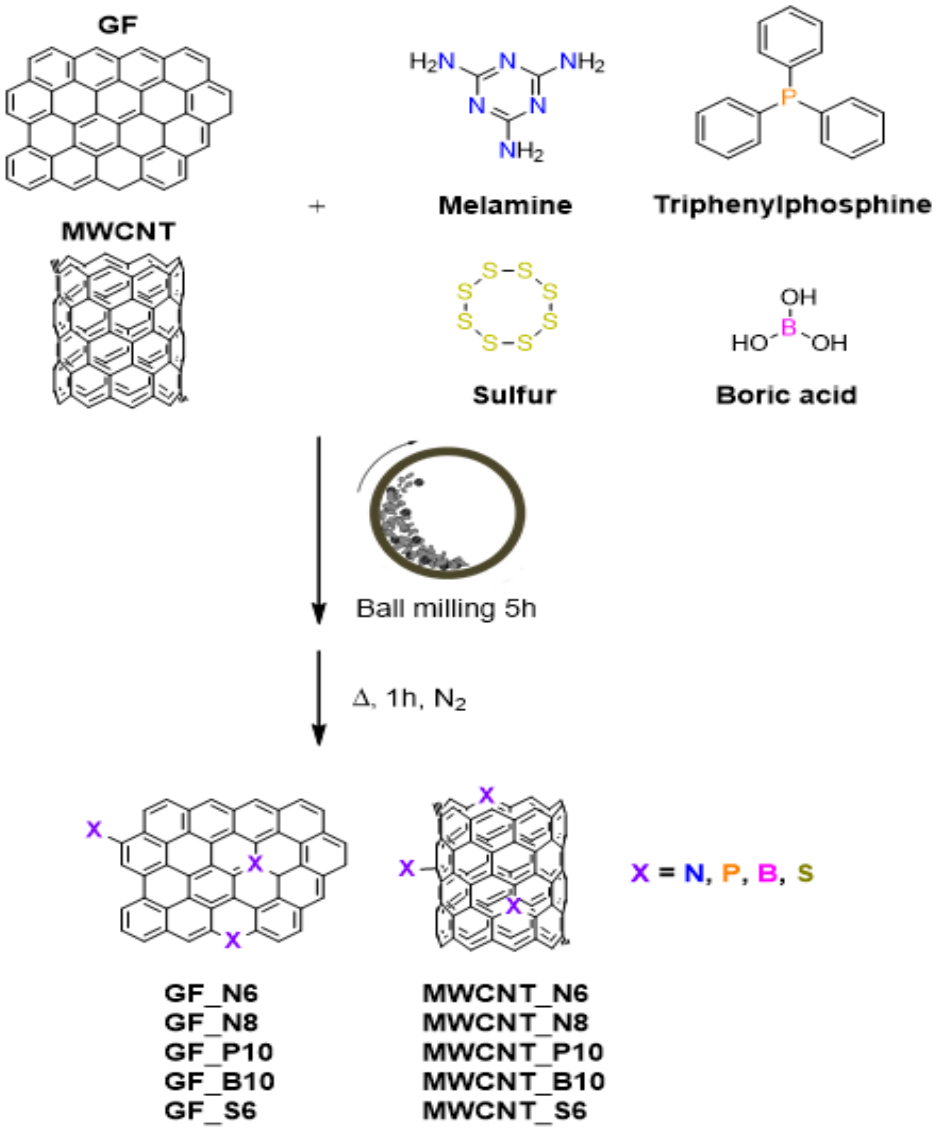

Figure 6. Schematic representation of the procedures for heteroatom doping of MWCNTs and GFs (MWCNT_XY and GF_XY, where X = doping element and Y = ºC of thermal treatment/100).

The catalytic performance of the pristine and heteratom-doped carbon nanomaterials was evaluated in the reduction of 4-nitrophenol (4-NP) in water, at room temperature, in the presence of $NaBH_4$, and duly corrected for adsorption phenomena. Remarkably, the modifications introduced by doping MWCNTs and GFs with heteroatoms overall yielded catalysts with superior activity in regard to their pristine counterparts (MWCNT-based catalysts: %C = 59–80% *vs.* 19%; GF-based catalysts: %C = 63–84% *vs.* 50%), as shown in Figure 7. The only exceptions were P-doped MWCNTs and N-doped GFs, which presented inferior catalytic performance (%C = 9% and 27%, respectively). Reusability experiments revealed no loss of catalytic activity of the doped MWCNTs for up to three catalytic cycles, whereas the GF-based materials showed some deterioration of the catalytic performance due to ineffective washing between catalytic runs. These results indicated that the doping of the carbon materials with heteroatoms (N, P, B and S) is a convenient and facile way to obtain metal-free carbocatalysts with superior performance in the reduction of 4-NP.

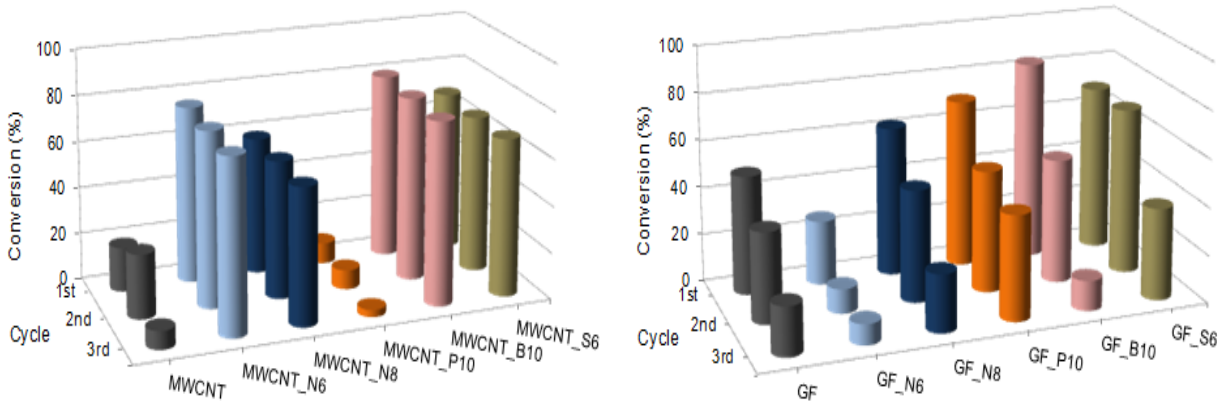

Figure 7. Catalytic results for the MWCNT and GF-based carbocatalysts in the reduction of 4-NP. Reproduced from ref. [18] by permission of John Wiley and Sons.

2.4 Graphene-Based Photo(Electro)Catalysts for Clean Water

In the last decades, the growth of population and worldwide industry processes is having a tremendous impact on the environment. New emerging pollutants are being detected in water and wastewater, such as pharmaceuticals, hormones and their metabolites, which can cause adverse effects on fauna, flora and human health [19–21]. In this context, the quest for new advanced technologies to ensure a safe and sustainable water supply is growing at an accelerating pace, being one of the major global challenges of the 21st century [19]. Nanotechnology-enabled photocatalytic water treatment processes are recently emerging as new opportunities to develop the next-generation of water supply and wastewater treatment systems to produce higher quality water using less energy and with lower treatment costs. Graphene-based nanosystems based on the assembly of graphene flakes and semiconductor nanoparticles stand out as new advanced photocatalytic solutions for the efficient and sustainable removal of water pollutants, with a triple role as photocatalysts, adsorbents and antimicrobial agents. In the project FOTOCATGRAF – Graphene-based semiconductor photocatalysis for a safe and sustainable water supply: an advanced technology for emerging pollutants removal (UTAP-ICDT/CTM-NAN/0025/2014), coordinated by LAQV@FCUP, and where LAQV at Instituto Superior de Engenharia of Instituto Politécnico do Porto (ISEP), CICECO at University of Aveiro, INESC-TEC@FCUP, University of Texas at Austin (UT-Austin) and the Wastewater Treatment Plant Águas do Centro Litoral teams participated as partners, the goal was the design and production of a new generation of high-performance graphene-based photocatalysts for the removal of emerging pollutants, namely pharmaceuticals from the wastewater treatment stations of the north and centre regions of Portugal (Figure 8).

To achieve that goal, LAQV@FCUP and CICECO@UA teams initially focused on the preparation of individual components: a) large-scale production of graphene flakes by cost-effective top-down approaches, (b) POMs and other metal oxides based on abundant metals and (c) metal sulphides; the UT-Austin team participated on the advanced materials characterization. At the same time, while the LAQV@ISEP team together with **Águas** do Centro Litoral were developing analytical tools to detect and quantify the envisaged pollutants, their metabolites and transformation products in wastewaters, the INESC-TEC@FCUP team was designing and building a prototype of an electrochemical sensor capable of measuring the concentration of a specific pharmaceutical in loco.

The new generation of graphene-based nanocomposites produced were efficiently applied as electrocatalysts for the determination of several pharmaceuticals and as photocatalysts on the degradation of the envisaged emerging pollutants.

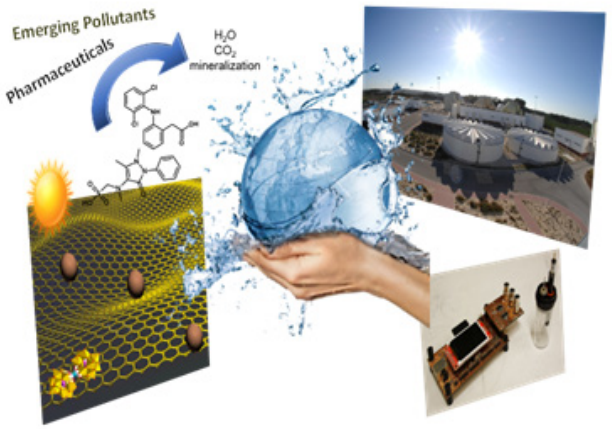

Figure 8. FOTOCATGRAF project concept.

3. Development of Biochar-Based Catalysts for Biomass Valorization

Emerging environmental concerns and declining availability of petroleum reserves have promoted worldwide interest in developing alternative technologies to convert sustainable biomass resources into value-added chemicals. Thermochemical processes have been used to obtain biomass degradation to produce biofuels, biochemicals and biomaterials, such as bio-oils, platform chemicals, biochars, etc. [22].

Biochar is a solid residual byproduct of these processes. As compared to other carbonaceous materials, biochar is an inexpensive, environmentally friendly and easily-produced charcoal [23,24]. The

properties of biochar are affected by the composition and morphology of biomass feedstock, as well as by the production process. However, the utilization of as-prepared biochar as catalyst is not ideal because of its poor physicochemical properties, including low specific surface area and poor porosity [25]. These characteristics can be improved through various activation and functionalization approaches aiming at enhancing the biochar´s catalytic properties. The surface area and porosity of biochar can be increased *via* physical activation or chemical activation. The biochar surface can be functionalized by surface sulfonation, surface amination or surface oxidation. The physicochemical properties can be also finely tuned by *in situ* heteroatom doping. In addition, the preparation of composites with other materials, such as metals, metal carbides, and nanostructured carbon materials, is also a common method to make use of biochar as a catalyst material. Thus, sulfonated biochar has shown favourable activity for various acid-catalyzed chemical reactions, including esterification of organic acids in aqueous media, acylation of alcohols and amines, alkylation of aromatics and biomass hydrolysis. On the other hand, biochar-supported metal nanoparticles exhibit high performance for the catalysis of many organic reactions, including oxygen reduction reactions in fuel cells, hydrogenation and dehydrogenation, and thermal decomposition by pyrolysis or gasification [26]. The described biochar activation/ functionalization approach offers a great opportunity that can be readily incorporated into future biorefinery schemes.

Within this context, since 2018 three teams from REQUIMTE/LAQV are conducting the project *BioreVinery – A biorefinery approach to valorize vineyard pruning waste using sustainable extraction and catalytic processes* (PTDC/BII-BIO/30884/2017; Figure 9), coordinated by LAQV@FCUP. The *BioreVinery* project is based on a biorefinery concept, which aims on producing bioproducts with added-value from vineyard pruning waste (VPW), an abundant lignocellulosic agriculture waste generated in winemaking industry one of the main economic agro-food activities in the world with a special incidence in Mediterranean countries. Vine shoots are generated during vine pruning process and have extremely rich chemical constituents. However, their valorization is practically unexplored and the search for innovative uses to consider them as a resource rather than a waste is mandatory in the context of circular economy.

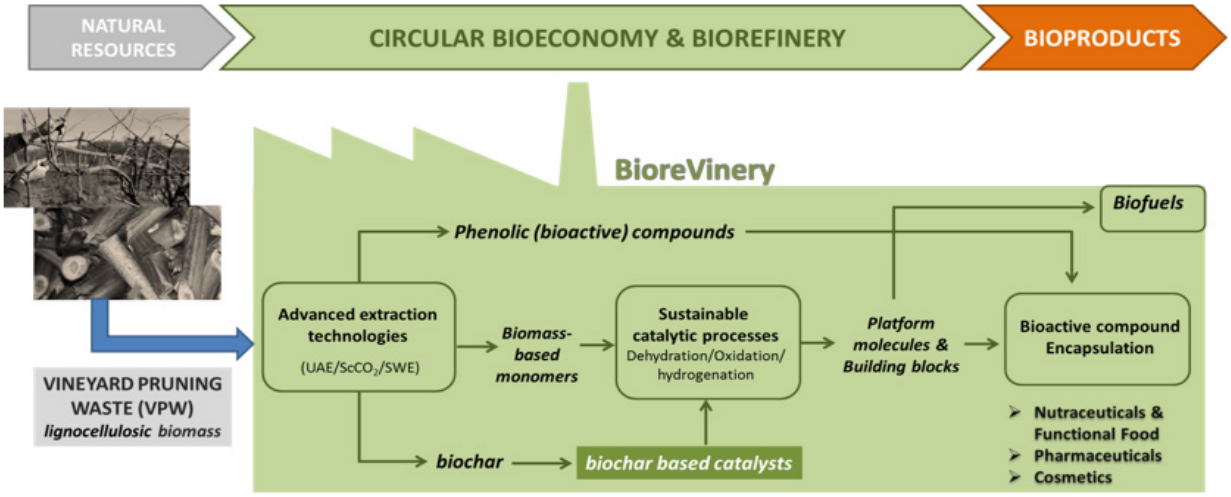

Figure 9. *BioreVinery* project representation.

The first steps of the project research work are focused on the development of advanced extraction technologies to extract phenolic compounds and to obtain biomass-derived monomers. Different extraction methodologies have been employed, including ultrasound-assisted extraction (UAE), supercritical CO2 extraction (ScCO2) and hydrothermal extraction under subcritical conditions (SWE). The anti-oxidant activity of the extracts obtained from these advanced extraction technologies has been also evaluated. As a byproduct of these processes, a solid fraction of biochar is obtained, which is being used for the preparation of novel catalysts to convert the produced biomass-derived monomers into the targeted bioproducts. In light of the great potential of biochar-based catalysts for catalytic biomass upgrading [27], our research is devoted to investigate their versatile applications for the upgrading of biomass-derived VPW, including the biochar activation through different procedures (hydro treatment, CO2 gasification) and biochar functionalization by sulfonation, incorporation of heteroatoms, metal oxides and/ or metallic nanoparticles. The efficiency of the resulting catalysts will be tested in the dehydration of C5/C6 sugars to platform molecules (e.g., furfural, 5-hydroxymethylfurfural), and upgrading of platform molecules to valuable bioproducts by hydrogenation, oxidation and hydrogenolysis reaction pathways.

Until now, the biochar directly obtained by the SWE was used to prepared sulfonic acid functionalized catalysts using two different methodologies: a) direct sulfonation with chlorosulfonic acid and b) direct organosilylation using the 2-(4-chlorosulfonylphenyl) ethyltrimethoxysilane (CSPTMS). The as-prepared

catalysts have been efficiently used in the production of levulinate esters from levulinic acid (LA) as an excellent alternative to the homogeneous catalysts conventionally used in industry. Very promising catalytic results were obtained in LA esterification at 120 ºC in butanol using the biochar-based catalysts, with almost 100% conversion and selectivity for butyl levulinate after 1 h. The evaluation of the catalysts stability revealed excellent reusability, without significant loss of activity for up to 5 cycles. Recently, and in collaboration with Professor C. A. M. Afonso [28] from Research Institute for Medicines (iMed.ULisboa), Faculty of Pharmacy, University of Lisbon, the biochar functionalized with the CSPTMS organosilane (BIO_CSP) was used as solid catalyst on the efficient production of a biofuel additive 5-(t-butoxymethyl)furfural from 5-hydroxymethylfurfural at 120 ºC in t-butanol, leading to similar yield (41%) to that obtained with MWCNTs (43 %) after long reaction times (7 h).

Furthermore, the prepared biochar-derived materials (functionalized by the incorporation of Ni, Co and Cu metal phases *via* incipient wetness impregnation) have been tested on the catalytic transfer hydrogenation of furfural, using a batch stirred reactor and 2-propanol as solvent and hydrogen donor. The observed remarkable activity (>70%) and selectivity (>90%) towards the formation of furfuryl alcohol (industrially-valuable biomass-derived intermediate) using these catalysts established a promising catalytic route to valorize a biomass platform molecule, such as furfural, using 3*d* transition metal-based catalysts and without any external hydrogen supply.

4. Hybrid/Doped Carbon-Based (Nano)materials for Energy Technologies

4.1 Unitized Regenerative Fuel Cell for Efficient Renewable Energy Supply

The current global energy crisis reflected in the depletion of fossil fuels and growth of the environmental pollution, which has stimulated the development of novel renewable energy storage and conversion technologies [29,30]. Hydrogen energy storage is a crucial issue for a fully sustainable energy paradigm. H2 produced by water electrolysis during base load moments, stored and converted back to electricity through the inverse reaction is a promising solution. The possibility of large-scale use of H2 as a transport fuel massively increases the potential renewables and base-load electricity supply. The Unitized Regenerative Fuel Cell (URFC), which includes in the same device an electrolyzer (EL) that converts electricity in H2, and a Fuel Cell (FC) which produces electricity using the stored H2, has great potential [31]. The cost, weight and volume of an URFC are potentially lower than the combination of separate FC and EL units, but the materials and the device critical function requirements are severe.

Within this context, the project *UniRCell – Unitised regenerative fuel cell for efficient renewable energy supply: from materials to device* (SAICTPAC/0032/2015) is being developed, coordinated by CICECO@University of Aveiro, and where LAQV@FCUP participates as team member along with other institutions: LSRE-LCM@FEUP, Transport Phenomena Research Center (CEFT)@FEUP and University of Trás-os-Montes and Alto Douro. *UniRCell* aims to develop a new generation of environmentally sustainable, high-performance and cost-effective materials for application in an URFC prototype. The project is organized in several tasks ranging from electrocatalysts design to membrane electrode assemblies (MEA) fabrication. The first stages of the project research work are focused on the design and preparation of novel noble metal-free composites with enhanced electrocatalytic properties for oxygen evolution and reduction reactions (OER/ORR) and hydrogen evolution and reduction reactions (HER/HOR), through eco-sustainable protocols. Our contribution is mainly focused on the synthesis and physicochemical characterization of electrocatalysts involving polyoxometalates (POMs), metal-organic frameworks (MOFs) and carbon materials (doped or non-doped), as well as on the electrochemical characterization of electrolytes and electrocatalysts.

So far, several hybrid bi- or tri-component nanomaterials based on metal oxides, POMs, MOFs and carbon materials (doped or non-doped) have been prepared and successfully applied to one or more of the reactions mentioned above. Very promising results were obtained with POM@carbon materials for HER (overpotentials of 0.033–0.044 V *vs.* 0.024 V for Pt/C) and ORR (higher diffusion-limiting current densities j_L = −168.3 mA cm^2 mg^{-1} *vs.* −130.0 mA cm^2 mg^{-1} for Pt/C), showing activities comparable to that of noble metal state-of-the-art Pt/C electrocatalyst and excellent stabilities. MOF-derived carbons have been synthesized at room temperature, avoiding hard condition solvothermal processes and, contrary to the more extended pyrolysis treatments, these were carbonized at relatively lower temperature, 500 °C. Their electrocatalytic properties were evaluated towards OER, exhibiting remarkable results with overpotentials as low as 0.41 V *vs.* RHE.

Currently, some of these novel carbon-based electrocatalysts are being incorporated onto an electrolyte membrane for future assembly and testing of MEAs.

4.2 Smart Textiles and Flexible Devices for Energy Storage

The development of clean and sustainable energy technologies has been one of the Grand Challenges of the 21st Century. Energy storage technologies became a major target to address the ever-increasing energy demand and depletion of non-renewable energy sources [32]. The fast proliferation of wearable and smart portable electronics opened new market opportunities for energy storage systems, especially for batteries and supercapacitors, with a vast scope of applications, ranging from medicine, sports, healthcare and fashion to military and the

consumer in general (Figure 10) [33]. High efficiency, durability, safety, flexibility and lightness became key requirements on the quest for wearable and flexible energy storage technologies [32,33]. Within this framework, the self-powered smart garments and portable devices currently available in the market rely on Li-ion batteries. Although displaying high energy density, they present limitations concerning their toxicity, safety, limited cycle life and high (re) charging time. Supercapacitors (SCs) emerged as an eco-sustainable and safer technology for energy storage, due to their higher power density, faster charging, longer cycle life (up to 106 cycles), stability and lower maintenance cost. Nevertheless, they still present lower energy density and faster discharging than batteries [32–34].

Nanotechnology opened new horizons in the field of smart textiles to confer new functionalities to the fabrics, while at the same time preserving their intrinsic features, namely the comfort to the user. Carbon (nano)materials are promising building blocks for the design of high-performance flexible and wearable energy storage technologies (*e.g.*, textile/fabric/fiber SCs, plastic electronics) [34,35] we will start by providing a brief introduction to the main principles of supercapacitors, followed by the importance of carbon (nano. In particular, carbon nanotubes and graphene are among the top choices as electrode materials for the fabrication of this type of devices due to their excellent mechanical properties, lightness, high electrical conductivity, large specific surface area and high chemical and thermal stability, leading to SCs with high power density, low charging times and high cycling stability. Typically, the intrinsic energy storage mechanism of carbon-based SCs is non-Faradaic, with the charge being stored electrostatically at the electrode/electrolyte interfaces – the so-called *electrical double-layer capacitors* (EDLCs). As a result, carbon-based SCs still possess low specific capacitance and, consequently, low energy density.

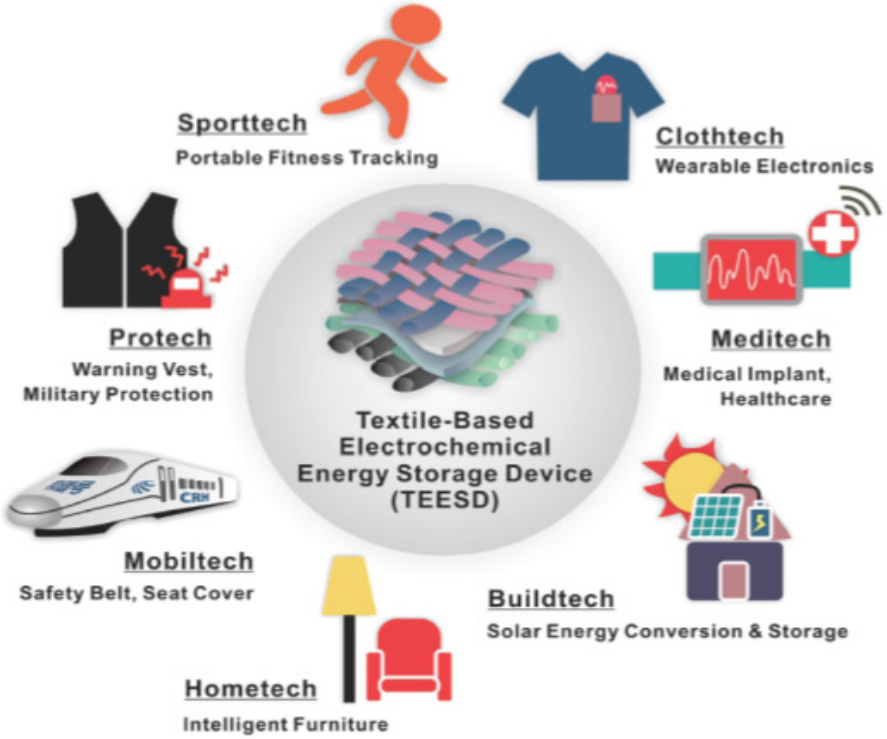

Figure 10. Applications of textile-based energy storage devices. Reproduced from ref. [33] by permission of John Wiley and Sons.

The doping of carbon (nano)materials with heteroatoms (*e.g.*, N, O, S, B, P) and/or their hybridization with transition metal oxides and/or conductive polymers constitute potential strategies to enhance the energy density properties of SCs, while preserving their power density [32,34]we review the state-of-the-art advancements in FSSCs to provide new insights on mechanisms, emerging electrode materials, flexible gel electrolytes and novel cell designs. The review begins with a brief introduction on the fundamental understanding of charge storage mechanisms based on the structural properties of electrode materials. The next sections briefly summarise the latest progress in flexible electrodes (i.e., freestanding and substrate-supported, including textile, paper, metal foil/wire and polymer-based substrates. This improvement arises from the occurrence of an additional pseudocapacitive energy storage mechanism in the devices (Faradaic mechanism), *i.e.*, involving the charge transfer between the electrode and the electrolyte through reduction-oxidation reactions, ion intercalation/ deintercalation and electrosorption at the surface or in the bulk near the surface of the electrodes.

In this sense, a new generation of *hybrid capacitors* emerged which can be classified in three different classes, according to the nature of the electrodes [36]: (i) *composite or symmetric hybrid capacitors* – bearing two electrodes composed of hybrid or composite materials with similar composition,

both containing an EDLC-type component and a pseudocapacitive component; (ii) *asymmetric hybrid capacitors* – composed of two electrodes with different charge storage mechanisms, with an EDLC-type mechanism occurring on one electrode and a pseudocapacitive or a combination of EDLC-type and pseudocapacitive mechanisms occurring on the other electrode; (iii) *battery-type hybrid capacitors* – with one of the electrodes being a Li^+-ion containing material to allow the occurrence of Li^+ intercalation/deintercalation.

Another R&TD area of our research group is related with the design of high-performance all-solid-state smart textiles and flexible devices for energy storage based on hybrid carbon nanomaterials. To achieve that goal we have been fabricating novel hybrid carbon-based nanomaterials with enhanced electrochemical properties to be used as SC electrode materials through the immobilization of transition metal oxides onto oxidized/doped carbon nanomaterials. We have developed a straightforward eco-sustainable and less time-consuming one-pot coprecipitation route that promoted the controlled nucleation/growth of transition metal ferrite nanoparticles (MFe_2O_4, M(II) = Mn, Fe, Co) with sizes in the range of 3.2–5.4 nm on the surface of conductive N-doped carbon nanotubes and their subsequent immobilization through covalent bonding (Figure 11A) [37]. The N-doped carbon nanotubes (CNT-N) were provided by the group of Prof. Antonio Guerrero-Ruiz, Instituto de Catálisis y Petroleoquímica, CSIC, Madrid, Spain. The resulting nanohybrids (CNT-N@X, where X = $MnFe_2O_4$, Fe_3O_4 or $CoFe_2O_4$) were then tested as electrode active nanomaterials in all-solid-state asymmetric paper SCs, leading to synergistically enhanced energy storage properties due to the simultaneous occurrence of EDLC-type and pseudocapacitive charge storage mechanisms. In particular, an improvement of the energy density to up to 6.0× and of the power density to up to 4.3× were achieved relatively to the symmetric CNT-N based paper SC (Figure 11B). Additionally, when compared with solid-state hybrid paper SCs based on carbon materials reported in the literature, they afforded up to 11.1× higher volumetric energy density and up to 5.2× higher volumetric power density. The paper SC that led to the highest energy density was the fully asymmetric hybrid CNT-N@Fe//CNT-N@Mn device, whereas the device that maximized the power density output was the CNT-N//CNT-N@Co system. Finally, all asymmetric SCs presented high cycling stability, preserving >90% of the initial capacitance after 1500 charge/discharge cycles.

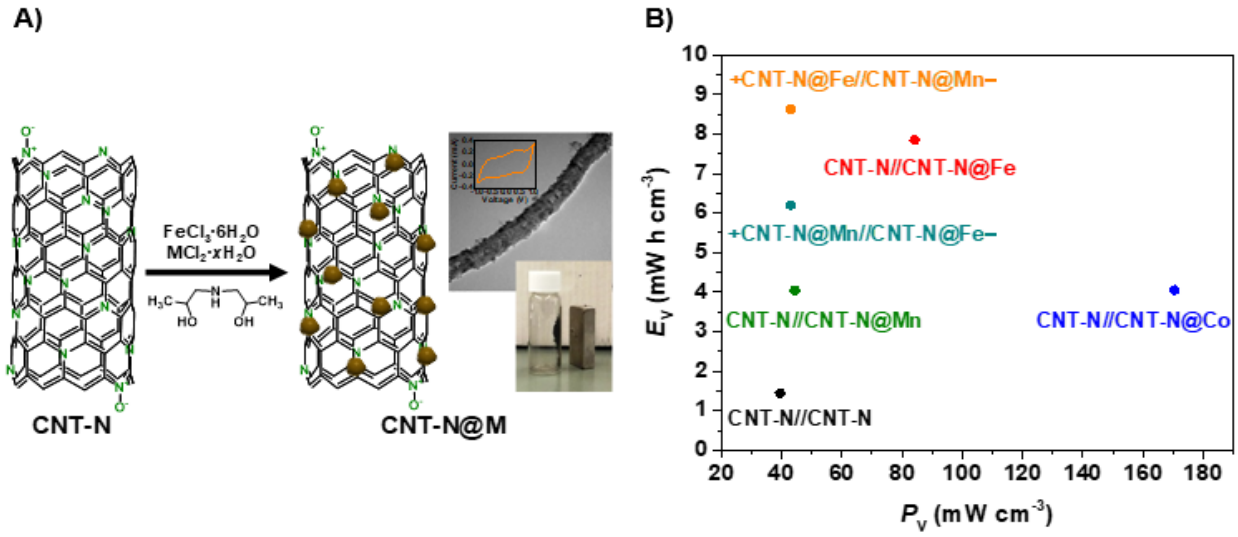

Figure 11. A) Schematic representation of the immobilization of MFe_2O_4 onto CNT-N by one-pot *in situ* coprecipitation. B) Ragone plot of energy density *vs.* power density of the all-solid-state CNT-N based paper SCs. Adapted from ref. [37] by permission of RSC.

Since 2018, a multidisciplinary R&TD project is being developed in this area, entitled *SmarText4EStore – Smart Textiles for Energy Storage: From New Scalable Fabrication Processes to Wearable Supercapacitor Clothing* (PTDC/CTM-TEX/31271/2017), coordinated by LAQV@FCUP, in collaboration with two research units – IFIMUP, Institute of Physics for Advanced Materials, Nanotechnology and Photonics at FCUP, and LSRE-LCM@FEUP – and the Technological Centre for the Textile and Clothing Industry of Portugal, CITEVE. *SmarText4EStore* project envisages the production of a new generation of hybrid textile SCs based on hybrid carbon nanomaterials featuring enhanced electrochemical performance, long lifetime, flexibility, lightness and safety through scalable eco-friendly fabrication processes, to meet the energy/power density demands of wearable electronic devices.

In parallel, an entrepreneurship startup project is being developed – WEStoreOnTEX – involving members from LAQV@FCUP and IFIMUP@FCUP, aiming to boost the technological transfer of wearable energy storage technologies towards marketable products. WEStoreOnTEX is focused on the creation of innovative technological solutions for energy storage on garments or accessories to power portable devices and sensors integrated on clothes. Textile SCs with small dimensions (14 cm^2) were directly integrated on clothing and, when charged for 5 min, were able to power sensor devices and lightning systems during up to 50 min (Figure 12).

Figure 12. Digital thermometer/hygrometer sensor and LED lightning system powered by textile SCs produced by WEStoreOnTEX.

4.3 Development of Cobalt Oxide Nanofoam-Based Electrocatalysts for Energy Storage

Electrochemical energy storage devices have become key players on the development of efficient solutions for energy management [38]. Asymmetric SCs pave the way to boost electrical mobility and efficiency of storage systems, combining the "best of a battery" with the "best of a SC" to deliver enhanced energy and high power density. However, they still require important electrode material developments to increase charge storage capacity and long-term stability [39]. Zn-air batteries have raised interest due to their low price and high energy density, but face important challenges that prevent their widespread application and require more efficient air electrode electrocatalysts, namely bifunctional electrodes for both oxygen reduction (ORR) and oxygen evolution (OER) reactions. Novel functional materials are the key to enable these two storage technologies.

In this context, the project *Foam4Ener – Multifunctional cobalt oxide nanofoams: novel electrode materials for supercapacitors and electrocatalytic oxygen reactions* (PTDC/QUI-ELT/28299/2017) is being developed, coordinated by Associação do Instituto Superior Técnico para a Investigação e o Desenvolvimento (IST-ID), and involving LAQV@ FCUP and Instituto Superior de Engenharia de Lisboa (ISEL) as team members. *Foam4Ener* project aims at designing and preparing a new generation of highly porous 3D Co-nanofoams (CoNFs) and Co-graphene nanofoams that, after functionalization with polyoxometalates (POMs) and graphene derivatives, can serve as high-performance electrodes for energy storage in asymmetric SCs and as bifunctional electrocatalysts for ORR and OER in rechargeable metal-air batteries. The IST-ID and ISEL teams have been conducting, since September 2018, work on the optimization of CoNFs preparation, while LAQV@ FCUP team is focused on the production of different POM families and the preparation of doped-graphene derivatives by scalable and green synthesis routes. A set of transition metal-based POMs has already been selected for near future doping of the already optimized Co-NFs. Then, LAQV@FCUP team will be responsible for testing the most promising candidates as ORR and OER electrocatalysts, while IST-ID team will test them on asymmetric SCs.

At the end of the project, the researchers hope to deliver novel solutions for energy storage namely, high capacity electrodes for electric mobility for asymmetric SCs, and high efficiency O_2 reaction electrocatalysts, which are crucial for the large-scale implementation of rechargeable metal-air batteries.

5. Smart Electrochromic Devices Based on Carbon-Poly(Nickel Complex) Nanocomposites

Electrochromic materials, which present reversible color changes upon the occurrence of electrochemical oxidation-reduction reactions, are a family of materials with remarkable interest for several smart applications, including energy-saving smart windows, smart optical displays and rear-view mirrors for the automotive industry [40,41]. They are typically composed of redox-active species, namely conducting polymers. The main challenge nowadays for their implementation is ensuring high optical contrast, high color switching rates, high electrochemical stability and long cycle life (reversibility of the color changes over multiple cycles) [42]. To achieve these goals, conductive polymers can be combined with nanomaterials, namely carbon-based nanomaterials, to potentiate synergistic effects [43].

Our group has been working in this field, namely through the use of graphene as electroactive nanomaterial. In particular, a new electrochromic nanocomposite based on [Ni(*salen*)] polymeric film was prepared through the incorporation of N-doped few-layered graphene (N-FLG) onto the electroactive poly[Ni(3-Me*salen*)] film (where Me*salen* = *N*,*N'*-bis(3-methylsalicylideneiminate)), by *in situ* electropolymerization (Figure 13) [42]. The resulting nanocomposite exhibited multi-electrochromic properties, with the color changing from yellow (reduced state) to green/russet (oxidized state). Moreover, it presented enhanced electrochromic performance when compared with the parent poly[Ni(3-Me*salen*)] film (Figure 13),

with 71% increase of the electrochemical stability (decrease of 2.7% of charge after 10000 switching cycles), lower switching time for oxidation and reduction (9 and 11 s, respectively), improved optical contrast (38% increase; ΔT = 35.9%) and coloration efficiency (12% increase; η = 108.9 cm^2 C^{-1}). More remarkably, the electronic structure of the polymer was preserved upon the incorporation of N-FLG, with an improvement of its robustness to degradation phenomena. These achievements were assigned to morphological changes and alternative conducting pathways promoted by N-FLG.

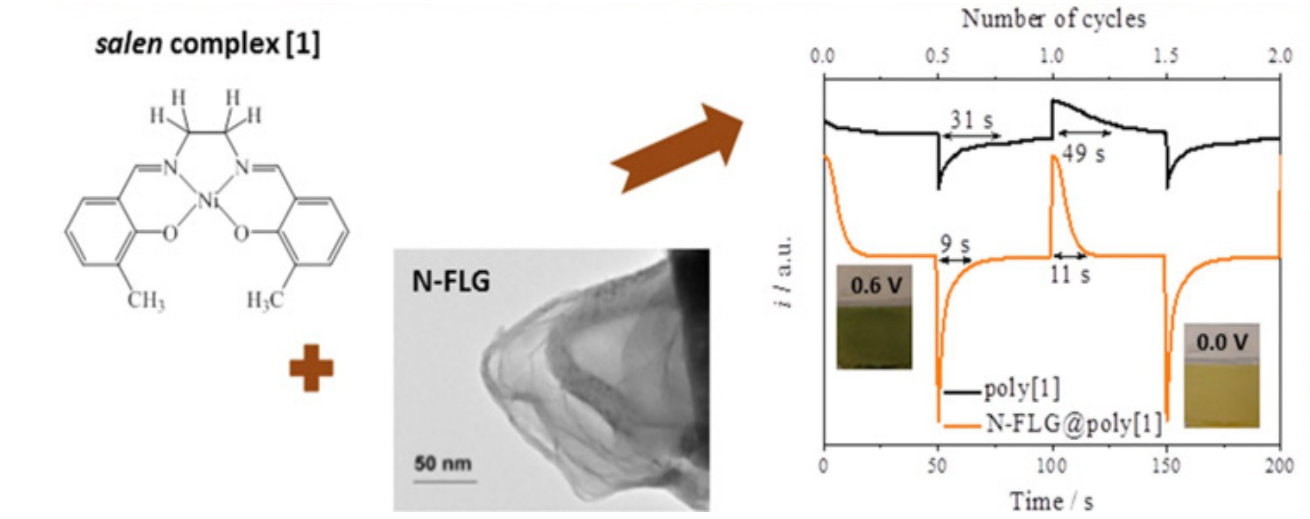

Figure 13. Chemical structure of [Ni(3-Mesalen)] complex, morphology of N-FLG and electrochemical stability of N-FLG@poly[Ni(3-Me*salen*)] and pristine poly[Ni(3-Me*salen*)] films evaluated by chronoamperometry. Reproduced from ref. [42] by permission of Elsevier.

In another work, graphene nanoplatelets (GFNP) were incorporated onto the same type of polymeric film [44]. The resulting GFNP@poly[Ni(3-Me*salen*)] nanocomposite also presented multi-electrochromic behavior, with the color changing between yellow (reduced state) and green (oxidized state). Additionally, its switching time responses were significantly lower than those of the parent poly[Ni(3-Me*salen*)] film, with 50.7% decrease in the response time for green coloration and 60.0% decrease for yellow coloration. GFNP@poly[Ni(3-Me*salen*)] film also presented enhanced electrochemical stability, with only a slight loss of charge (7%) after 10000 electrochemical cycles. Finally, a flexible solid-state electrochromic device was assemble based on GFNP@poly[Ni(3-Me*salen*)] and using flexible indium tin oxide/polyethylene terephthalate (ITO/PET) as substrate (Figure 14). The device presented remarkable electrochemical stability during an extended switching test, with only 3% of charge loss after 15 days of continuous activity, highlighting the potentialities of the film for electrochromic applications, namely on optical/electronic displays and electrochromic paper.

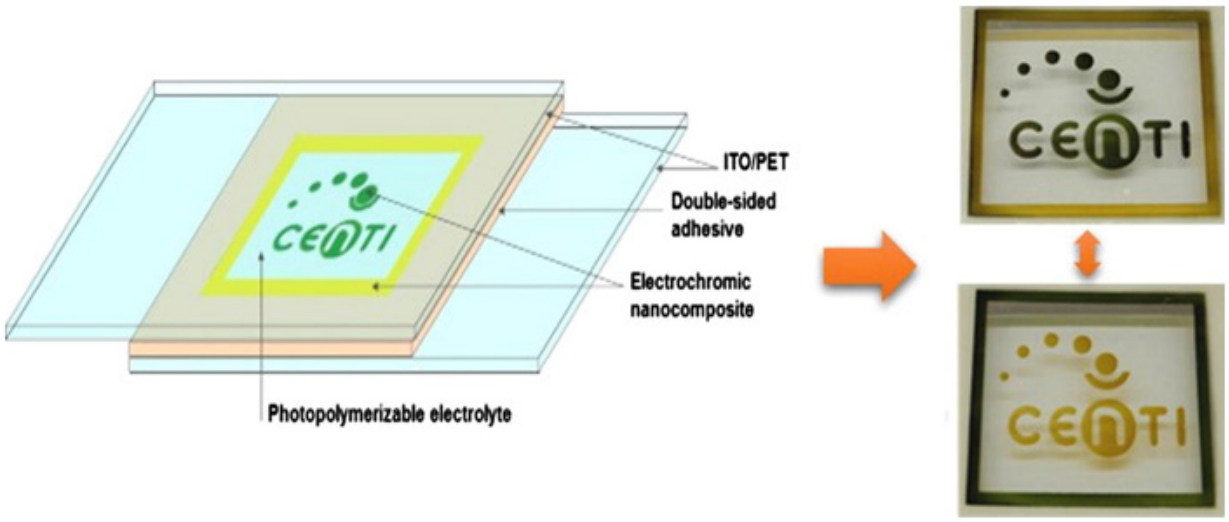

Figure 14. Schematic representation of the structure of the flexible solid-state electrochromic device based on GFNP@poly[Ni(3-Me*salen*)] and pictures showing the device color change upon the application of a potential (redox process). Reproduced from ref. [44] by permission of Elsevier.

In another work, graphene nanoplatelets (GFNP) were incorporated onto the same type of polymeric film [44]. The resulting GFNP@poly[Ni(3-Me*salen*)] nanocomposite also presented multi-electrochromic behavior, with the color changing between yellow (reduced state) and green (oxidized state). Additionally, its switching time responses were significantly lower than those of the parent poly[Ni(3-Me*salen*)] film, with 50.7% decrease in the response time for green coloration and 60.0% decrease for yellow coloration. GFNP@poly[Ni(3-Me*salen*)] film also presented enhanced electrochemical stability, with only a slight loss of charge (7%) after 10000 electrochemical cycles. Finally, a flexible solid-state electrochromic device was assemble based on GFNP@poly[Ni(3-Me*salen*)] and using flexible indium tin oxide/polyethylene terephthalate (ITO/PET) as substrate (Figure 14). The device presented remarkable electrochemical stability during an extended switching test, with only 3% of charge loss after 15 days of continuous activity, highlighting the potentialities of the film for electrochromic applications, namely on optical/electronic displays and electrochromic paper.

Acknowledgements

This work was funded by FEDER - European Regional Development Fund through COMPETE 2020 - Operacional Programme for Competitiveness and Internationalization (POCI) and by Portuguese funds through FCT/MCTES under Program PT2020 in the framework of the projects PTDC/BII-BIO/30884/2017, PTDC/CTM-TEX/31271/2017, PTDC/QUI-ELT/28299/2017, SAICTPAC/0032/2015 and UID/QUI/50006/2019. CP thanks FCT for the FCT Investigator contract IF/01080/2015. AFP and DF acknowledge FCT/MCTES for their work contracts (in the scope of the framework contract foreseen in the numbers 4, 5 and 6 of the article 23, of the Decree-Law 57/2016, of August 29, changed by Law 57/2017, of July 19) supported by national funds (OE). MN and RR thank the SAICTPAC/0032/2015 and PTDC/QUI-QIN/30649/2017 project contracts, respectively, based on DL57/2016, funded by FCT/MCTES through national funds.

References

[1] Shaw S, D. White J. Asymmetric Catalysis Using Chiral Salen–Metal Complexes: Recent Advances. Chem Rev 2019; 119: 9381–9426.

[2] Gupta KC, Sutar AK. Catalytic activities of Schiff base transition metal complexes. Coord Chem Rev 2008; 252: 1420–1450.

[3] Freire C, Nunes M, Pereira C, Fernandes DM, Peixoto AF, Rocha M. Metallo(salen) complexes as versatile building blocks for the fabrication of molecular materials and devices with tuned properties. Coord Chem Rev 2019; 394: 104–134.

[4] Freire C, Pereira C, Rebelo S. Green oxidation catalysis with metal complexes: From bulk to nano recyclable hybrid catalysts. In: Catalysis, Volume 24. Spivey J and Gupta M (Eds.), Royal Society of Chemistry, UK, 2012, pp. 116–203.

[5] Gupta KC, Kumar Sutar A, Lin C-C. Polymer-supported Schiff base complexes in oxidation reactions. Coord Chem Rev 2009; 253: 1926–1946.

[6] Xia Q-H, Ge H-Q, Ye C-P, Liu Z-M, Su K-X. Advances in Homogeneous and Heterogeneous Catalytic Asymmetric Epoxidation. Chem Rev 2005; 105: 1603–1662.

[7] Fan QH, Li YM, Chan ASC. Recoverable catalysts for asymmetric organic synthesis. Chem Rev 2002; 102: 3385–3466.

[8] Silva AR, Freitas MMA, Freire C, De Castro B, Figueiredo JL. Heterogenization of a functionalized copper(II) Schiff base complex by direct immobilization onto an oxidized activated carbon. Langmuir 2002; 18: 8017–8024.

[9] Silva AR, Figueiredo JL, Freire C, de Castro B. Manganese(III) salen complexes anchored onto activated carbon as heterogeneous catalysts for the epoxidation of olefins. Microporous Mesoporous Mater 2004; 68: 83–89.

[10] Silva AR, Martins M, Freitas MMA, Valente A, Freire C, De Castro B, Figueiredo JL. Immobilisation of amine-functionalised nickel(II) Schiff base complexes onto activated carbon treated with thionyl chloride. Microporous Mesoporous Mater 2002; 55: 275–284.

[11] Silva AR, Freire C, De Castro B, Freitas MMA, Figueiredo JL. Anchoring of a nickel(II) Schiff base complex onto activated carbon mediated by cyanuric chloride. Microporous Mesoporous Mater 2001; 46: 211–221.

[12] Silva AR, Martins M, Freitas MMA, Figueiredo JL, Freire C, De Castro B. Anchoring of copper(II) acetylacetonate onto an activated carbon functionalised with a triamine. Eur J Inorg Chem 2004: 2027–2035.

[13] Jarrais B, Silva AR, Freire C. Anchoring of vanadyl acetylacetonate onto amine-functionalised activated carbons: Catalytic activity in the epoxidation of an allylic alcohol. Eur J Inorg Chem 2005: 4582–4589.

[14] Maia F, Silva R, Jarrais B, Silva AR, Freire C, Pereira MFR, Figueiredo JL. Pore tuned activated carbons as supports for an enantioselective molecular catalyst. J Colloid Interface Sci 2008; 328: 314–323.

[15] Jarrais B, Silva AR, Ribeiro LS, Rodrigues EG, Órfão JJM, Pereira MFR, Figueiredo JL, Freire, C. Spontaneous gold decoration of activated carbons. Inorganica Chim Acta 2013; 408: 235–239.

[16] Serp P, Figueiredo JL. Carbon Materials for Catalysis. John Wiley & Sons, New Jersey, USA, 2009.

[17] Jarrais B, Guedes A, Freire C. Selectively oxidized carbon nanocatalysts for the oxidation of cis -cyclooctene. New J Chem 2018; 42: 2306–2319.

[18] Jarrais B, Guedes A, Freire C. Heteroatom-Doped Carbon Nanomaterials as Metal-Free Catalysts for the Reduction of 4-Nitrophenol. ChemistrySelect 2018; 3: 1737–1748.

[19] Qu X, Alvarez PJJ. Applications of nanotechnology in water and wastewater treatment. Water Res 2013; 47: 3931–3946.

[20] Li WC. Occurrence, sources, and fate of pharmaceuticals in aquatic environment and soil. Environ Pollut 2014; 187: 193–201.

[21] Rivera-Utrilla J, Sánchez-Polo M, Ferro-García MÁ, Prados-Joya G, Ocampo-Pérez R. Pharmaceuticals as emerging contaminants and their removal from water. A

review. Chemosphere 2013; 93: 1268–1287.

[22] Zhou C-H, Xia X, Lin C-X, Tong D-S, Beltramini J. Catalytic conversion of lignocellulosic biomass to fine chemicals and fuels. Chem Soc Rev 2011; 40: 5588–5617.

[23] Downie A, Crosky A, Munroe P, Physical properties of biochar. In: Biochar for environmental management. Lehmann J, Joseph S (Eds.), Routledge, London, UK, 2012, pp. 45-64.

[24] Liu W-J, Jiang H, Yu H-Q. Development of Biochar-Based Functional Materials: Toward a Sustainable Platform Carbon Material. Chem Rev 2015; 115: 12251–12285.

[25] Lee J, Kim K-H, Kwon EE. Biochar as a Catalyst. Renew Sustain Energy Rev 2017; 77: 70–79.

[26] Cheng F, Li X. Preparation and application of biochar-based catalysts for biofuel production. Catalysts 2018; 8: 346.

[27] Cao X, Sun S, Sun R. Application of biochar-based catalysts in biomass upgrading: a review. RSC Adv 2017; 7: 48793–48805.

[28] Cuervo OHP, Simeonov SP, Peixoto AF, Popova MD, Lazarova HI, Romanelli GP, Martínez, JJ, Freire, C, Afonso, CAM. Efficient Continuous Production of the Biofuel Additive 5-(t-Butoxymethyl) Furfural from 5-Hydroxymethylfurfural. Energy Technol 2019; 7: 1900780.

[29] Seh ZW, Kibsgaard J, Dickens CF, Chorkendorff I, Nørskov JK, Jaramillo TF. Combining theory and experiment in electrocatalysis: Insights into materials design. Science 2017; 355: eaad4998.

[30] Jiao Y, Zheng Y, Jaroniec MT, Qiao SZ. Design of electrocatalysts for oxygen- and hydrogen-involving energy conversion reactions. Chem Soc Rev 2015; 44: 2060–2086.

[31] Pettersson J, Ramsey B, Harrison D. A review of the latest developments in electrodes for unitised regenerative polymer electrolyte fuel cells. J Power Sources 2006; 157: 28–34.

[32] Dubal DP, Chodankar NR, Kim D-H, Gomez-Romero P. Towards flexible solid-state supercapacitors for smart and wearable electronics. Chem Soc Rev 2018; 47: 2065–2129.

[33] Huang Q, Wang D, Zheng Z. Textile-Based Electrochemical Energy Storage Devices. Adv Energy Mater 2016; 6: 1600783–1600811.

[34] Pereira C, Pereira AM. Functional Carbon-Based Nanomaterials for Energy Storage: Towards Smart Textile Supercapacitors. Boletín Del Grup Español Del Carbón 2016: 40: 42–48.

[35] Yao F, Pham DT, Lee YH. Carbon-Based Materials for Lithium-Ion Batteries, Electrochemical Capacitors, and Their Hybrid Devices. ChemSusChem 2015; 8: 2284–2311.

[36] Beguin F, Frackowiak E. Supercapacitors: Materials Systems and Applications, 1st Edition. Wiley-VCH, Weinheim, Germany, 2013.

[37] Pereira C, Costa RS, Lopes L, Bachiller-Baeza B, Rodríguez-Ramos I, Guerrero-Ruiz A, Tavares PB, Freire C, Pereira, AM. Multifunctional mixed valence N-doped CNT@MFe_2O_4 hybrid nanomaterials: from engineered one-pot coprecipitation to application in energy storage paper supercapacitors. Nanoscale 2018; 10: 12820–12840.

[38] Aricò AS, Bruce P, Scrosati B, Tarascon J-M, van Schalkwijk W. Nanostructured materials for advanced energy conversion and storage devices. Nat Mater 2005; 4: 366–377.

[39] Béguin F, Presser V, Balducci A, Frackowiak E. Carbons and Electrolytes for Advanced Supercapacitors. Adv Mater 2014; 26: 2219–2251.

[40] Mortimer RJ. Electrochromic Materials. Annu Rev Mater Res 2011; 41: 241–268.

[41] Rosseinsky DR, Mortimer RJ. Electrochromic Systems and the Prospects for Devices. Adv Mater 2001; 13: 783–793.

[42] Nunes M, Araújo M, Bacsa R, Ferreira RV, Castillejos E, Serp P, Hillman AR, Freire, C. N-doped few-layered graphene-polyNi complex nanocomposite with excellent electrochromic properties. Carbon 2017; 120: 32–43.

[43] Kuilla T, Bhadra S, Yao D, Kim NH, Bose S, Lee JH. Recent advances in graphene based polymer composites. Prog Polym Sci 2010; 35: 1350–1375.

[44] Araújo MP, Nunes M, Fonseca J, Moura C, Hillman R, Freire C. Graphene-poly(nickel complex) as novel electrochromic nanocomposite for the fabrication of a robust solid-state device. J Colloid Interface Sci 2017; 504: 790–799.

The role of carbon materials as supports for transition metal-based catalysts

Luísa M.D.R.S. Martins

Centro de Química Estructural, Instituto Superior Técnico, Universidade de Lisboa, Portugal - luisammartins@tecnico.ulisboa.pt

Abstract

In this communication, a brief overview of the studies developed by the Coordination Chemistry and Catalysis (CCC) Group of Centro de Química Estrutural (Instituto Superior Técnico, Universidade de Lisboa) related to the use of carbon materials as catalysts supports is presented. CCC recent and relevant achievements in the field of carbon supported catalysis are highlighted, focusing on oxidative catalytic reactions.

Resumen

En esta comunicación se divulga una visión general de los estudios que se realizan en el Grupo de Química de Coordenação e Catálise (CCC) del Centro de Química Estrutural (Instituto Superior Técnico, Universidade de Lisboa) correspondiente a el uso de materiales de carbono como soporte de catalizadores. Se destacan los logros más relevantes y recientes del CCC centrados en el campo de la catálisis soportada, en particular en reacciones catalíticas oxidativas.

1. Introduction

The interest on carbon materials to be used as supports for catalysts, pioneered at CCC by Luísa Martins, emerged in 2010 when she met Sónia Carabineiro, from the University of Porto, at the *XVI Encontro Luso-Galego de Química* held in Aveiro, Portugal.

Luísa Martins was working in homogeneous catalysis mainly for alkane and alcohol selective oxidations, one of the most important processes to produce useful value-added chemical compounds from petroleum-based materials. She designed C-scorpionate tris(pyrazol-1-yl)methane complexes (Figure 1) of several transition metals (*e.g.*, V, Fe, Cu, Ru or Re) [1-17] to act as efficient catalysts for the above reactions. They have been studied with great success and interesting results have been achieved, leading, in most of the cases, to the award of Portuguese patents [13-17] and articles [1-12]. In fact, the facile interchange between bi- and tridentate coordination modes of the poly(pyrazolyl) moieties (Figure 1), changing their denticity during the catalytic reaction, is at the core of the structural and chemical versatility of C-scorpionate complexes and was essential for their catalytic applications. Moreover, the presence of N- and O- donor atoms in C-scorpionate ligands allow their complexes to assist proton-transfer steps, which are believed to be involved in key processes of the oxidation reactions such as the metal-promoted radical generation [18,19].

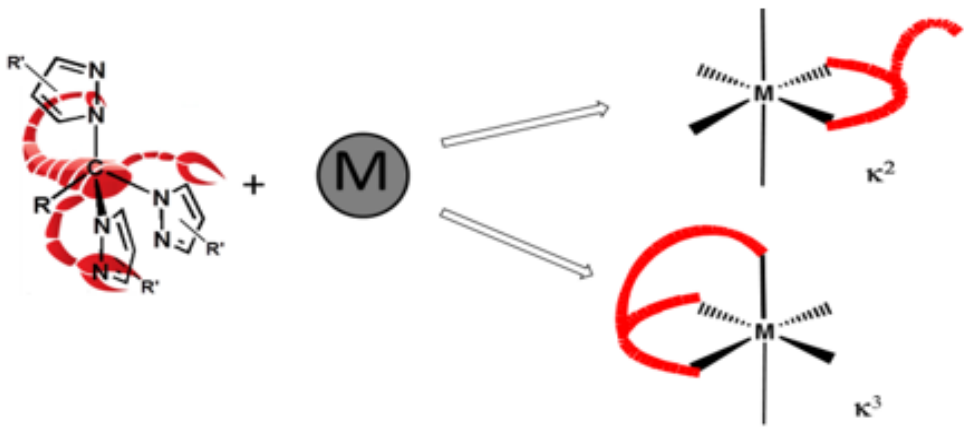

Figure 1. Schematic structure of a tris(pyrazolyl) type scorpionate [R = H, Me, CH_2OH, CH_2NH_2, COOH, $CH_2O(CH_2)_nY$ (Y = SO_3, Ph, Py), $P(O)(OR)_2$, etc.; R' = H, Me, Ph ^{i}Pr, ^{t}Bu, etc.], its common coordination modes to a metal centre (M), and analogy with a scorpion and its attack on a prey. Adapted from [18].

However, although active and selective, the above homogeneous catalysts lack in reusability. The immobilization of a molecular catalyst in an inert support could improve its catalytic activity and allow its easier separation and recycling, which are required conditions in sustainable processes. In particular, the use of carbons as catalyst supports provides unparalleled flexibility in tailoring their physical (surface area and porosity) and chemical (surface functional groups) properties. Therefore, the combination of the properties of homogeneous complexes with the advantages of heterogeneous systems would be obtained.

By that time, Sónia Carabineiro had already a long experience in the production of various types of carbon materials and in the modification of the nature and concentration of surface functional groups [20-22], which can be used to anchor metal complexes.

She also had also acquired expertise in anchoring procedures [23]. Thus, a collaboration started aiming at producing hybrid materials based on C-scorpionate complexes and testing them as catalysts for important industrial oxidation reactions.

The first supported materials prepared were C-scorpionate iron(II) and gold(III) complexes immobilized in functionalized carbon materials such as activated carbon, carbon xerogel or multiwalled carbon nanotubes, to be applied as catalysts for the peroxidative oxidation of cyclohexane [24,25]. Then, these studies were extended to *i*) other metal complexes, not exclusively C-scorpionates [26-30]; *ii*) other catalytic reactions [26-31]; *iii*) gold nanoparticles [32-35], and *iv*) different nanostructured carbon materials (*e.g.*, graphene oxide, reduced graphene oxide, graphene nanoplatelets, nanodiamonds and nanohorns) [35-37].

In the last approach, in collaboration with Ana Paula Carvalho from Centro de Química e Bioquímica of Faculty of Sciences of Universidade de Lisboa, biomass-derived carbons, obtained from lignocellulosic wastes, were successfully used [30,37]. Recently, in collaboration with José Virgílio Prata from the Chemical Engineering Department of Instituto Superior de Engenharia de Lisboa, C-dots prepared from industrial wastes have been tested, in particular, for the oxidation reaction of primary alcohols.

Thus, the above collaborations, with the Laboratory of Catalysis and Materials of Faculty of Engineering of University of Porto (FEUP), Centro de Química e Bioquímica of Faculty of Sciences of Universidade de Lisboa and Instituto Superior de Engenharia de Lisboa research groups, were fundamental to prepare the materials used in the catalytic applications, being the developed works listed in section 8 of this communication. It must also be mentioned that this interest on the field of transition metal-based catalysts supported at carbon materials gave rise to several M.Sc. and Ph.D. theses and, as a natural consequence, allowed numerous oral and panel presentations in international conferences, namely at *Carbon* and *CarboCat* congresses.

2. Oxidation of alkanes

As mentioned above, the immobilization of homogeneous catalysts on carbon supports, thus rendering the systems heterogeneous in order to facilitate the separation and catalyst recycle, to simplify other reaction procedures and/or to increase the stability or the selectivity of the catalyst has been applied to metal C-scorpionate complexes in the field of alkane oxidation [18,19]. As model reaction, the cyclohexane oxidation to cyclohexanol and cyclohexanone (Figure 2), important reagents for the production of adipic acid and caprolactam used for the manufacture of nylon, was chosen.

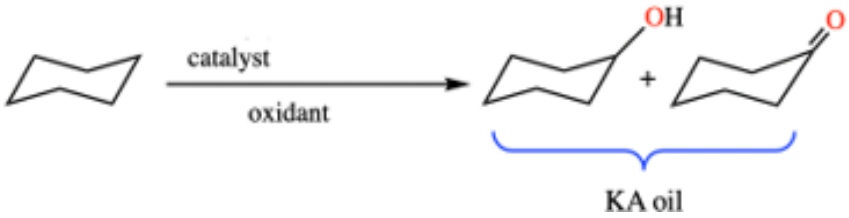

Figure 2. Catalytic oxidation of cyclohexane to cyclohexanol and cyclohexanone.

The iron(II) [$FeCl_2\{\kappa^3$-$HC(pz)_3\}$] (pz = pyrazolyl) complex was anchored on three different carbon materials [activated carbon (AC), carbon xerogel (CX) and multi-walled carbon nanotubes (CNT)] in the original form or upon surface treatment (with nitric acid or with nitric acid followed by sodium hydroxide), being the heterogenisation at multi-walled carbon nanotubes treated with nitric acid and sodium hydroxide (CNT-Oxi-Na), the most efficient process. This hybrid material, in particular, led to an outstanding improved catalytic performance of the complex [$FeCl_2\{\kappa^3$-$HC(pz)_3\}$] upon heterogenisation (TON up to 5.6 x 10^3 and overall yield of 21% [24]) relative to the homogeneous system.

Simultaneously, interesting results were obtained with the heterogenised C-scorpionate gold(III) catalysts [$AuCl\{\kappa^2$-$RC(R'pz)_3\}$]Cl (R = H or CH_2OH, R′ = H or 3,5-Me_2 pz = pyrazol-1-yl) for the above reaction [25]. Much higher turnover numbers and yield values with lower loading of oxidant were obtained with the hybrid catalysts than with the homogeneous counterparts.

The heterogenised iron(II) and gold(III) systems also offered practical advantages of recycling (by the facile separation from products), allowing successive cycles to be performed without significant loss of activity and with a rather high selectivity to the desired cyclohexanol and cyclohexanone mixture. The possibility of applying such complexes as catalyst precursors for the single-pot peroxidative cyclohexane oxidation to cyclohexanol and cyclohexanone, at room temperature, was considered much more attractive and environmentally friendly than the current industrial process.

To note that the hybrid metal complexes-based catalysts showed much higher catalytic activity than gold nanoparticles supported on the same carbon materials [32].

Then, the scope of carbon materials used to anchorage [$FeCl_2\{\kappa^3$-$HC(pz)_3\}$] was extended to other nanostructured carbon materials showing a high surface area such as graphene oxide, reduced graphene oxide, graphene nanoplatelets, nanodiamonds and nanohorns (these chosen for the first time as a metal complex support) (Figure 3) [36]. The highly selective heterogenized systems exhibited good activity in producing cyclohexanol and

cyclohexanone with co-catalyst pyrazine carboxylic acid (Hpca) by microwave-promoted oxidation of cyclohexane (yields up to 29%; again, higher values than in homogeneous conditions). Moreover, they were easily recovered and reused for five consecutive cycles maintaining *ca.* 90% of their initial activity. The oxidized supports (oxidized nanodiamonds, graphene oxide and oxidized single-walled carbon nanohorns) [36] led to the highest yields of desired oxygenated products, highlighting the importance of the presence of oxygen groups at the materials surface as anchorage sites for the complex [$FeCl_2\{\kappa^3$-$HC(pz)_3\}$].

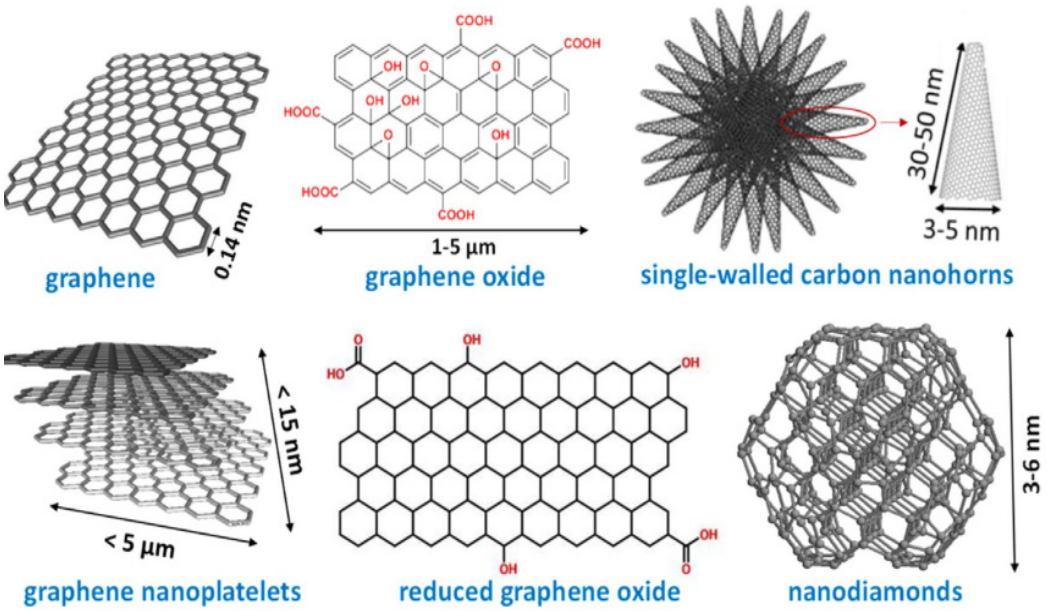

Figure 3. Nanostructured carbon materials used as supports. Reproduced with permission of ref. [36] Copyright, 2018, Wiley-VCH.

Recently, the influence of porous carbon supports on the performance of the heterogenized [$FeCl_2\{\kappa^3$-$HC(pz)_3\}$] catalyst was investigated [37] using materials with distinct porosity: microporous (GL50-ox, wet oxidized GL50 Norit sample and S, sisal-derived activated carbon prepared by chemical activation) and mesoporous (CMK-3) materials. The heterogenized systems exhibited good activity and rather high selectivity to the formation of cyclohexanol and cyclohexanone mixture from microwave-assisted oxidation of cyclohexane, and allowed their easy recovery and reuse, at least for four consecutive cycles.

3. Oxidation of xylenes

Catalytic oxidation of other hydrocarbons, besides alkanes, was essayed, in particular the oxidation of xylenes (Figure 4), in view of the industrial significance of terephthalic acid production (manly used in polyethylene terephthalate (PET) manufacturing) from the oxidation of *p*-xylene, and of the limitations of the current Amoco process.

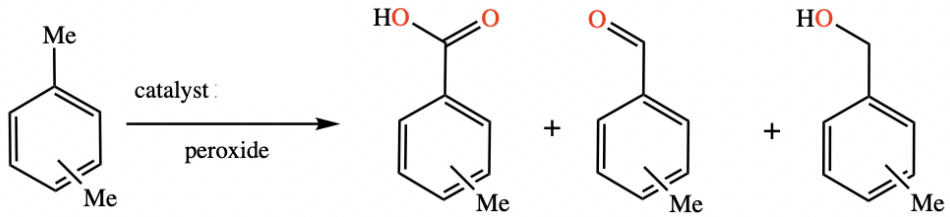

Figure 4. Catalytic oxidation of xylene to methylbenzyl alcohol, tolualdehyde and toluic acid.

C-scorpionate vanadium(IV) complexes, [$VO_xCl_{3-x}\{\kappa^3$-$RC(pz)_3\}$] (x = 0 or 1, R = SO_3, CH_2OH or CH_2OSO_2Me) [26] heterogenized on oxido-functionalized multiwalled carbon nanotubes (CNT), combined with microwave irradiation, improve the formation of toluic acid: *e.g.,* a *p*-toluic acid yield of 43% (73% selectivity, TON = 1.34×10^3) was achieved using TBHP (70% aq. solution) and a very low loading of [$VOCl_2\{\kappa^3$-$HOCH_2C(pz)_3\}$] (3.2×10^{-2} mol% *vs*. substrate) at O-functionalized CNT [26].

The anchorage of the C-homoscorpionate V-complexes on the CNT is believed to occur by formation of a covalent V-O bond with the CNT surface carboxylate or phenolate groups, displacing a chloride or replacing one pyrazolyl ring of the C-scorpionate, which would behave as a bi-dentate ligand (a well-known feature of these ligands [18,19]). The stability of the supported V-catalysts allowed their reuse with preservation of their activity for six consecutive cycles. After the 6th cycle, vanadium leaching is observed, and activity starts to decrease [26].

4. Oxidation of styrene

C-scorpionate Cu(II) complexes such as [$CuCl_2${κ^3-$RC(R'pz)_3$}] (R = H or CH_2OH, R' = H or 3,5-Me_2) [30] were immobilized (up to a Cu loading of 2%) on sucrose derived hydrochars, *i.e.,* carbon materials synthetized by hydrothermal carbonization (HTC) of different types of biomass (*e.g.*, glucose, sucrose, fructose or their derivatives, as furfural or hydroxymethyl furfural). The choice (not reported before) of using hydrochars as supports for the C-scorpionate complexes arose from their easy surface chemistry tuning during the elegant synthetic procedure (HTC) avoiding the usual oxidation (*e.g.*, with HNO_3) treatments. Moreover, the carboxylic groups functionalization obtained by such procedure significantly enhanced the direct immobilization of the C-scorpionate copper(II) complexes, leading to the first recyclable C-scorpionate catalysts used so far for the selective oxidation of styrene to benzaldehyde (Figure 5).

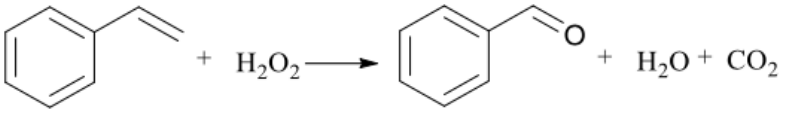

Figure 5. Catalytic selective oxidation of styrene to benzaldehyde.

5. Oxidation of alcohols

In 2016, the highly efficient eco-friendly synthesis of ketones (yields over 99%) from secondary alcohols was achieved by combination of [$FeCl_2${κ^3-$HC(pz)_3$}] supported on functionalized multi-walled carbon nanotubes and microwave irradiation, in a solvent-free medium [31]. This C-scorpionate iron(II) complex was the first one of his class to be used as catalyst for the oxidation of alcohols and the developed work led to the award of a WO patent [38]. This catalytic system is currently under scale-up attempts to produce ketones from secondary alcohols using microwave irradiation (Figure 6).

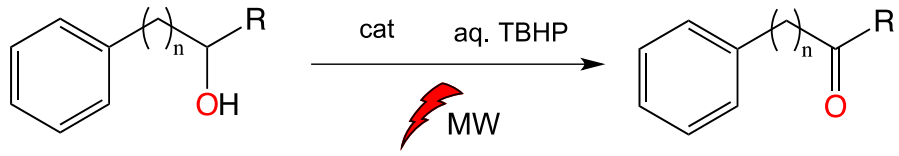

n = 0, R = Me; n = 1, R = H

Figure 6. Catalytic selective oxidation of alcohols to ketones.

More recently [36], [$FeCl_2${κ^3-$HC(pz)_3$}] immobilized at functionalized nanodiamonds support (used for the first time as supports for iron complexes) was also able to effectively (yields up to 97%) catalyze the MW-induced oxidation of 1- and 2-phenylethanol to acetophenone and 2-phenylacetaldehyde, respectively, and be reused for seven consecutive cycles without losing catalytic activity.

Other types of complexes as oxidovanadium(V) aroylhydrazone complexes derived from (3,5-di-*tert*-butyl-2-hydroxybenzylidene)-2-hydroxybenzohydrazide (H_2L^1) and (3,5-di-*tert*-butyl-2-hydroxybenzylidene)-2-aminobenzohydrazide (H_2L^2), *viz.* [$VOL^1(OEt)$]·[$VOL^1(OEt)$ (EtOH)], [$VOL^2(OEt)$], [Et_3NH][VO_2L^1], [$VO_2(HL^2)$]·2EtOH, [$(VOL^1)_2$(μ-O)] or [$(VOL^2)_2$(μ-O)] [28], have also been immobilized on oxidised carbon materials and tested as catalysts for the microwave-assisted solvent-free peroxidative oxidation of 1-phenylethanol to acetophenone by *t*-BuOOH. The immobilization of the above oxidovanadium complexes improved the oxidation efficiency and allowed catalyst reuse preserving their activity.

These studies were then extended to the assessment of the catalytic activity of Au nanoparticles deposited on different types of carbon materials, namely, polymer based carbon xerogel, activated carbon, microdiamonds, nanodiamonds, graphite and silicon carbide by double impregnation and sol immobilisation, which were used as catalysts for the microwave-assisted solvent-free oxidation of 1-phenylethanol, under different conditions [35]. The results showed that the catalytic activity was influenced by several factors, namely, the nature of the support, reaction time and temperature, amount of catalyst, presence of additives, among others. The best values for acetophenone yield (99.9%) were obtained with Au deposited on microdiamonds by the colloidal method. Catalyst recyclability was tested up to six consecutive cycles at the optimized conditions for each catalyst, and it was found that Au on microdiamonds, prepared by the colloidal method, also maintained higher activity after several reaction cycles as compared to the other carbon supports.

6. Carboxylation of alkanes

The carboxylation of C_n alkanes to C_{n+1} carboxylic acids, using CO, is an attractive process for alkane functionalization that might have important applications in industry and surpass the disadvantages of the present synthesis procedures. Therefore, the cyclohexane hydrocarboxylation to cyclohexanecarboxylic acid with CO, water and

peroxodisulfate (Figure 7) [33,34], was attempted in the presence of gold nanoparticles deposited by a colloidal method on carbon nanotubes and activated carbon with three different surface chemistries: in their original forms (CNT or AC, respectively), oxidized with HNO_3 (-ox) or oxidized with HNO_3 and subsequently treated with NaOH (-ox-Na).

Figure 7. Catalytic hydrocarboxylation of cyclohexane.

Au/CNT-ox-Na was the best catalyst, yielding cyclohexanecarboxylic acid up to 88.2% yield, with excellent recyclability (97.5% of the initial activity was maintained after five consecutive catalytic cycles) [33,34].

7. Conclusions

In general, the immobilization of the catalysts (in particular C-scorpionate complexes) on functionalized carbon materials revealed to be a good strategy to improve their catalytic activity (remarkable increase of product yields) for alkane, alkene or alcohol oxidations, and to facilitate the catalyst separation and recycling. Moreover, the use of unconventional conditions such as microwave heating proved to be promising toward the promotion of activity, tuning of selectivity, catalyst recycling [19], etc., although remaining virtually unexplored.

Acknowledgements

The work reported here was supported by the Fundação para a Ciência e a Tecnologia (FCT) through the financial to the Centro de Química Estrutural (UID/QUI/00100/2013-2019), the projects PTDC/EQU-EQU/122025/2010, PTDC/QEQ-ERQ/1648/2014 and PTDC/QEQ-QIN/3967/2014 and the CATSUS PhD Program. CRUP - Ação n.º13/16 is also acknowledged.

References

[1] E.C.B.A. Alegria, L.M.D.R.S. Martins, M. Haukka, A.J.L. Pombeiro, Rhenium Complexes of Tris(pyrazolyl)methanes and Sulfonate Derivative, *Dalton Trans.,* 2006, 4954-4961.

[2] E.C.B.A. Alegria, M.V. Kirillova, L.M.D.R.S. Martins, A.J.L. Pombeiro, Pyrazole and tris(pyrazolyl)methane rhenium complexes as catalysts for ethane and cyclohexane oxidations, *Appl. Catal. A-Gen.,* 2007, 317, 43-52.

[3] G.S. Mishra, E.C.B.A. Alegria, L.M.D.R.S. Martins, J.J.R. Fraústo da Silva, A.J.L. Pombeiro, Cyclohexane oxidation with dioxygen catalyzed by supported pyrazole rhenium complexes, *J. Mol. Cat. A: Chem*, 2008, 285, 92-100

[4] T.F.S. Silva, E.C.B.A. Alegria, L.M.D.R.S. Martins, A.J.L. Pombeiro, scorpionate vanadium, Iron and Copper complexes as selective catalysts for the peroxydative oxidation of cyclohexane under mild conditions, *Adv., Synth. Cat.*, 2008, 350, 706-716.

[5] R. Wanke, P. Smoleński, M.F.C. Guedes da Silva, L.M.D.R.S. Martins, A.J.L. Pombeiro, Cu(I) complexes bearing the new sterically hindered and coordination flexible tris(3-phenyl-1-pyrazolyl)methanesulfonate (TpmsPh) ligand and the water-soluble phosphine 1,3,5-triaza-7-phosphaadamantane (PTA) or related ligands, *Inorg. Chem.*, 2008, 47, 10158-10168.

[6] G.S. Mishra, T.F.S. Silva, L.M.D.R.S. Martins, A.J.L. Pombeiro, Scorpionate V(III-V) complexes as catalyst precursors for solvent-free cyclohexane oxidation with dioxygen, *Pure Appl. Chem.*, 2009, 81(7), 1217-1227.

[7] T.F.S. Silva, G.S. Mishra, M.F.G. Silva, R. Wanke, L.M.D.R.S. Martins, A.J.L. Pombeiro, CuII complexes bearing the 2,2,2-tris(1-pyrazolyl)ethanol or 2,2,2-tris(1-pyrazolyl)ethyl methanesulfonate scorpionates. X-ray structural characterization and application in the mild catalytic peroxidative oxidation of cyclohexane, *Dalton Trans.*, 2009, 42, 9207-9215.

[8] R. Wanke, M.F.C.G. Silva, S. Lancianesi, T.F.S. Silva, L.M.D.R.S. Martins, C. Pettinari, A.J.L. Pombeiro, Synthesis and Coordination Chemistry of a New N4-Polydentate class of pyridyl-functionalized scorpionate ligands: complexes of FeII, ZnII, NiII, VIV, PdII and use for heterobimetallic systems, *Inorg. Chem.,* 2010, 49, 7941-7952.

[9] T.F.S. Silva, K.V. Luzyanin, M.V. Kirilova, M.F.C.G Silva, L.M.D.R.S. Martins, A.J.L. Pombeiro, Novel scorpionate and pyrazole dioxovanadium complexes, catalysts for carboxylation and peroxidative oxidation of alkanes, *Adv., Synth. Cat.,* 2010, 352, 171–187.

[10] F. Marchetti, C. Pettinari, R. Pettinari, A. Cerquetella, L.M.D.R.S. Martins, M.F. Guedes da Silva, T.F.S. Silva, A.J.L. Pombeiro, Ru(II) arene complexes bearing tris(pyrazolyl)methanesulfonate capping ligands. Electrochemistry, spectroscopic and X-ray structural characterization**,** *Organometallics,* 2011, 30, 6180-6188.

[11] C. Pettinari, F. Marchetti, G. Lupidi, L. Quassinti, M. Bramucci, D. Petrelli, L.A. Vitali, M.F.C. Guedes da Silva, L.M.D.R.S. Martins, P. Smoleński, A.J.L. Pombeiro, Synthesis, Antimicrobial and antiproliferative activity of novel silver(i) tris(pyrazolyl)methanesulfonate and 1,3,5-triaza-7-phosphadamantane complexes, *Inorg. Chem.*, 2011, 50, 11173-11183.

[12] T.F.S. Silva, M.F.C.G. Silva, G.S. Mishra, L.M.D.R.S. Martins, A.J.L. Pombeiro, Synthesis and structural characterization of iron complexes with 2,2,2-tris(1-pyrazolyl)ethanol ligands: application in the peroxidative oxidation of cyclohexane under mild conditions, *J. Organomet. Chem.,* 2011, 696, 1310-1318.

[13] A.J.L. Pombeiro, L.M.D.R.S. Martins, E.C.B.A. Alegria, M.V. Kirillova, **PT103735**, 2008.

[14] A.J.L. Pombeiro, L.M.D.R.S. Martins, T.F.S. Silva, G.S. Mishra, PT104447, 2009.

[15] A.J.L. Pombeiro, L.M.D.R.S. Martins, E.C.B.A. Alegria, T.F.S. Silva, PT104153, 2009.

[16] A.J.L. Pombeiro, L.M.D.R.S. Martins, E.C.B.A. Alegria, G.S. Mishra, J.J.R. Fraústo da Silva, **PT104197,** 2009.

[17] A.J.L. Pombeiro, L.M.D.R.S. Martins, M.F.C. G. Silva, G.S. Mishra T.F.S. Silva, R. Wanke, PT104713, 2010.

[18] L.M.D.R.S. Martins, A.J.L. Pombeiro, Tris(pyrazol-1yl) methane metal complexes for catalytic mild oxidative functionalizations of alkanes, alkenes and ketones, *Coord. Chem. Rev.,* 2014, 265, 74-88.

[19] L.M.D.R.S. Martins, C-scorpionate complexes: ever young catalytic tools, *Coord. Chem. Rev*. 2019, 396, 89-102.

[20] S.A.C. Carabineiro, M.F.R. Pereira, J.J.M. Órfão, J.L. Figueiredo, Surface Chemistry of Activated Carbons, In: Activated Carbon: Classifications, Properties and Applications, Eds. J.F. Kwiatkowski, Nova Science Pub Inc., New York, 2011, Chapter 4, pp. 125-168 (ISBN-978-1-61209-684-1).

[21] S.A.C. Carabineiro, T. Thavorn-amornsri, M.F.R. Pereira, J.L. Figueiredo, Adsorption of ciprofloxacin on surface modified carbon materials, *Water Res.* 2011, 45 (15) 4583-4591.

[22] S.A.C. Carabineiro, T. Thavorn-amornsri, M.F.R. Pereira, P. Serp, J.L. Figueiredo, Comparison between activated carbon, carbon xerogel and carbon nanotubes for the adsorption of the antibiotic ciprofloxacin, *Catal. Today* 2012, 186 (1) 29-34.

[23] C.J.P. Monteiro, S.A.C. Carabineiro, T. Lauterbach, C. Hubbert, A.S.K. Hashmi, J.L. Figueiredo, M.M. Pereira, (S)-BINOL immobilized onto MWCNT through covalent linkage: New chiral carbon material, *ChemNanoMat* 2015, 1, 178-187.

[24] L.M.D.R.S. Martins, M. Peixoto de Almeida, S.A.C. Carabineiro, J.L. Figueiredo, A.J.L. Pombeiro, Heterogenisation of a C-scorpionate Fe(II) complex in carbon materials for cyclohexane oxidation with hydrogen peroxide*, ChemCatChem*, 2013, *5*, 3847–3856.

[25] M. Peixoto de Almeida, L.M.D.R.S. Martins, S.A.C. Carabineiro, T. Lauterbach, F. Rominger, A.S.K. Hashmi, A.J.L. Pombeiro, J.L. Figueiredo, Homogeneous and heterogenised new gold C-scorpionate complexes as catalysts for cyclohexane oxidation, *Catal. Sci. Technol.,* 2013, *3*, 3056-3069.

[26] J. Wang, L.M.D.R.S. Martins, A.P.C. Ribeiro, S.A.C. Carabineiro, J.L. Figueiredo, A.J.L. Pombeiro, Supported C-scorpionate vanadium(IV) complexes as reusable catalysts for xylene oxidation, *Chem. Asian J.,* 2017, 12, 1915-1919.

[27] S.A.C. Carabineiro, L.M.D.R.S. Martins, A.J.L. Pombeiro, J.L. Figueiredo, Commercial gold(I) and gold(III) compounds supported on carbon materials as greener catalysts for the oxidation of alkanes and alcohols, *ChemCatChem*, 2018, 10, 1804-1813.

[28] M. Sutradhar, L.M.D.R.S. Martins, S.A.C. Carabineiro, M.F.C. Guedes da Silva, J.G. Buijnsters, J.L. Figueiredo, A.J.L. Pombeiro, Oxidovanadium(V) complexes anchored on carbon materials as catalysts for the oxidation of 1-phenylethanol, *ChemCatChem*, 2016, 8, 2254-2266.

[29] E. Pakrieva, A.P.C. Ribeiro, L.M.D.R.S. Martins, I.A.S. Matias, S.A.C. Carabineiro, E. Kolobova, A.J.L. Pombeiro, J.L. Figueiredo, A. Pestryakov, Commercial gold(III) complex supported on functionalized carbon materials as catalyst for cyclohexane hydrocarboxylation*, Catal. Today*, 2019 (*in press, doi: 10.1016/j.cattod.2019.05.050*).

[30] T.A.G. Duarte, A.P. Carvalho, L.M.D.R.S. Martins, Styrene oxidation catalyzed by copper(II) C-scorpionates in homogenous medium and immobilized on sucrose derived hydrochars, *Catal. Today.*, 2019 (*in press, doi: 10.1016/j.cattod.2019.04.044*).

[31] L.M.D.R.S. Martins, A.P.C. Ribeiro, S.A.C. Carabineiro, J.L. Figueiredo, A.J.L. Pombeiro, Highly efficient and reusable CNT supported iron(II) catalyst for microwave assisted alcohol oxidation, *Dalton Trans*., 2016, 45, 6816-6819.

[32] S.A.C. Carabineiro, L.M.D.R.S. Martins, M. Avalos-Borja, J.G. Buijnsters, A.J.L. Pombeiro, J.L. Figueiredo, Gold nanoparticles supported on carbon materials for cyclohexane oxidation with hydrogen peroxide, *Appl. Catal. A-Gen.,* 2013, *467*, 279-290.

[33] A.P.C. Ribeiro, L.M.D.R.S. Martins, S.A.C. Carabineiro, J.L. Figueiredo, A.J.L. Pombeiro, Gold nanoparticles deposited on surface modified carbon materials as reusable catalysts for hydrocarboxylation of cyclohexane*, Appl. Cat. A: Gen.,* 2017, 547C, 124-131.

[34] A.P.C. Ribeiro, L.M.D.R.S. Martins, S.A.C. Carabineiro, J.L. Figueiredo, A.J.L. Pombeiro, Gold nanoparticles deposited on surface modified carbon xerogels as reusable catalysts for cyclohexane C-H activation towards CO and water, *Molecules*, 2017, 22, 603.

[35] S.A.C. Carabineiro, A.P.C. Ribeiro, J.G. Buijnsters, M. Avalos-Borja, A.J.L. Pombeiro, J.L. Figueiredo, L.M.D.R.S. Martins, Solvent-free oxidation of 1-phenylethanol catalysed by gold nanoparticles supported on carbon powder materials, *Catal. Today*, 2019 (*in press, doi: j.cattod.2019.06.041*).

[36] A.P.C. Ribeiro, L.M.D.R.S. Martins, S.A.C. Carabineiro, J.G. Buijnsters, J.L. Figueiredo, A.J.L. Pombeiro, Heterogenised C-scorpionate iron(II) complex on nanostructured carbon materials as catalysts for microwave-assisted oxidation reactions, *ChemCatChem*, 2018, 10, 1821-1828.

[37] M.A. Andrade, A.S. Mestre, A.P. Carvalho, A.J.L. Pombeiro, L.M.D.R.S. Martins, The role of nanoporous carbon materials in catalytic cyclohexane oxidation, *Catal. Today*, 2019 (*in press, doi: 10.1016/j.cattod.2019.07.036*).

[38] A.J.L. Pombeiro, L.M.D.R.S. Martins, A.P.C. Ribeiro, S.A.C. Carabineiro, J.L. Figueiredo, WO 2017/116253, 2017.

Acid-chars - versatile materials for adsorption and catalysis

Ana Paula Carvalho* and Ana Sofia Mestre

Centro de Química e Bioquímica e Centro de Química Estructural, Faculdade de Ciências, Universidade de Lisboa, 1749-016 Lisboa, Portugal - ana.carvalho@fc.ul.pt

Abstract

In this communication an overview of the most recent studies developed in the Adsorption and Adsorbent Materials Group related with the use of acid mediated carbonization (AMC) to prepare carbon materials is presented. The chars obtained by this methodology – acid-chars – have been explored for different purposes; so far the application studied in more detail is their use as precursors of activated carbons with tuned textural properties. In this particular application both literature studies from other researchers and our contributions are reviewed. It must be highlighted that we proved that AMC is able to transform a low density biomass, as is the case of sisal fibers, in high density acid-chars and activated carbons with tailored features. The use of as-synthesized acid-chars as supports for catalysts immobilization and, even though still in a preliminary stage, also as catalysts or adsorbents were also assessed in our group with very promising results. The overall data herein discussed points out the versatility of acid-chars as a precursor of activated carbons with controlled features but also as a self-standing carbon material for adsorption, catalysis and catalysts support.

1. Introduction

The research for new synthesis strategies to prepare carbon materials based on renewable biomass sources has been addressed by several groups and, in the last years, it has also been an important research topic of the Adsorption and Adsorbent Materials Group (AAM) of Centro de Química e Bioquímica and Centro de Química Estrutural – Pólo Ciências of Faculdade de Ciências da Universidade de Lisboa. As reviewed in a previous issue of this bulletin the carbon precursors explored by the AAM group cover several renewable residues from national industries, namely, cork powder, granules of expanded corkboard, sisal fibers, fly ash from pine wood gasification, and rapeseed waste from biodiesel production [1].

The synthesis of porous carbon materials usually consists in two thermochemical processes – carbonization and activation. The carbonization (or pyrolysis) under an inert atmosphere allows to remove most of the heteroatoms and to obtain a carbon-rich material usually called char (or charcoal if prepared from a coal precursor). Hydrothermal carbonization (HTC) is a promising alternative route to conventional carbonization. HTC is inspired in the natural process of coal formation and has received great attention from the scientific community due to the sustainability of the process. (*i.e.* water as solvent, mild temperatures, self-generated pressure, occurs in hours, and no CO_2 emissions) and interesting properties of the obtained solid products – hydrochars [2,3]. The AAM group developed sucrose-derived hydrochars that were further chemically activated and the resulting activated carbon were successfully applied in adsorption and catalysis [4-6].

Among the processes available to obtain carbon functionalized materials, acid-mediated carbonization (AMC) has been far less explored than conventional thermal or HTC processes, but the resulting solid materials, named acid-chars, plenty of oxygen reactive functional groups, can compete with hydrochars or chars in several processes [3]. In the present communication literature studies reporting the synthesis of acid-chars through AMC is reviewed and recent data obtained in our research group on the synthesis and application of acid-chars from various biomass precursors in adsorption and catalytic processes (Fig. 1) will be presented.

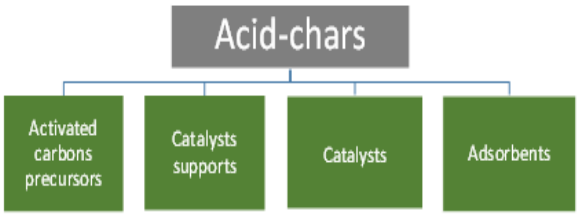

Figure 1. Application fields of acid-chars explored in the studies developed by AAM group.

2. Acid-chars synthesis and properties

Acid-chars are synthesized by acid-mediated carbonization (AMC) of solid or liquid carbon precursors at atmospheric pressure, being a valuable approach to maximize the carbon content of precursors with high inorganic content (*e.g.* rice husk) or with considerable amounts of water. The few literature studies exploring this approach report the synthesis of acid-chars at distinct temperatures: lower than 100 °C for rice husk and sisal [7-9] but at temperatures between 400 and 800 °C when using glycerol as carbon source [10]. Both H_2SO_4 and H_3PO_4 can be used as effective acid catalysts in this process but the majority of the works only tested the stronger H_2SO_4, with some of them evaluating the effect of the acid concentration. Depending on the acid used, the structure of the acid-char will contain sulfur or phosphorus groups besides the oxygen rich functionalities, which can be valuable when envisaging, for example, catalysts immobilization or higher reactivity towards activation.

The AAM group explored the AMC of sisal residues which, due to the high percentage of carbohydrate-containing polymers (65.8 % cellulose and 12 % hemicellulose [11]) and low amount of lignin (9.9 % [11]), that is more resistant to decomposition, can be successfully digested with acid and further

carbonized to yield versatile acid-chars. H_2SO_4 was selected as acid catalyst and we explored the influence of the acid concentration in both digestion and carbonization step on the properties of the final acid-char [9]. The AMC consisted in the digestion of sisal fibers with H_2SO_4 at concentration of 12 M or 13.5 M during 15 min at 50 °C and at concentration 9 M during 30 min at the same temperature (10 mL of H_2SO_4 solution per gram of sisal fibers), followed by the polycondensation during 6 h at 90 °C under reflux [9]. Although less extensively, besides sisal we have also explored other biomasses – pine sawdust, cork powder, corn stalk, and carbohydrates – proving that a large range of carbon precursors can successfully yield acid-chars. More recently we are exploring the influence of other experimental conditions on the acid-chars properties (*e.g.* duration of polycondensation step and higher H_2SO_4 concentration).

The thermogravimetric profiles of the sisal-derived acid-chars (Fig. 2(b)) confirmed the polycondensation of cellulose and hemicellulose since the decomposition peaks of these polymers in the raw sisal are not observed in the derived acid-chars [9]. All the acid-chars presented incipient porosity, amorphous-like carbon structures (Fig. 2(d)) and surfaces decorated with acidic oxygen and sulfur functionalities as proved by the DRIFT spectra (Fig. 2(c)) and also quantified by elemental analysis, and very low pH at the point of zero charge (pH_{PZC} around 2). Even though the just mentioned properties of the acid-chars are almost independent on the concentration of the acid during the synthesis, the morphology (see Fig 2(e) and (f)) and density (Fig.2 (a)) of these materials are highly dependent on the acid concentration during the digestion and carbonization steps. While for example the samples prepared with 13.5 M and 12 M H_2SO_4 in both steps are composed of particles with a compact and rough surface and with high apparent density (> 500 kg m^{-3}), those obtained with lower acidic concentration (*e.g.* S9/9) present an aerogel-like structure composed by interconnected spheres with apparent densities between 100 kg $m^{-3}$and 200 kg m^{-3}. The polycondensation yield is also dependent on the acid concentration since acid-chars synthesized with 13.5 M and 12 M during digestion step allow to attain yields between 30 and 35 %, while those obtained after digestion with H_2SO_4 9 M present and yield around 15 %.

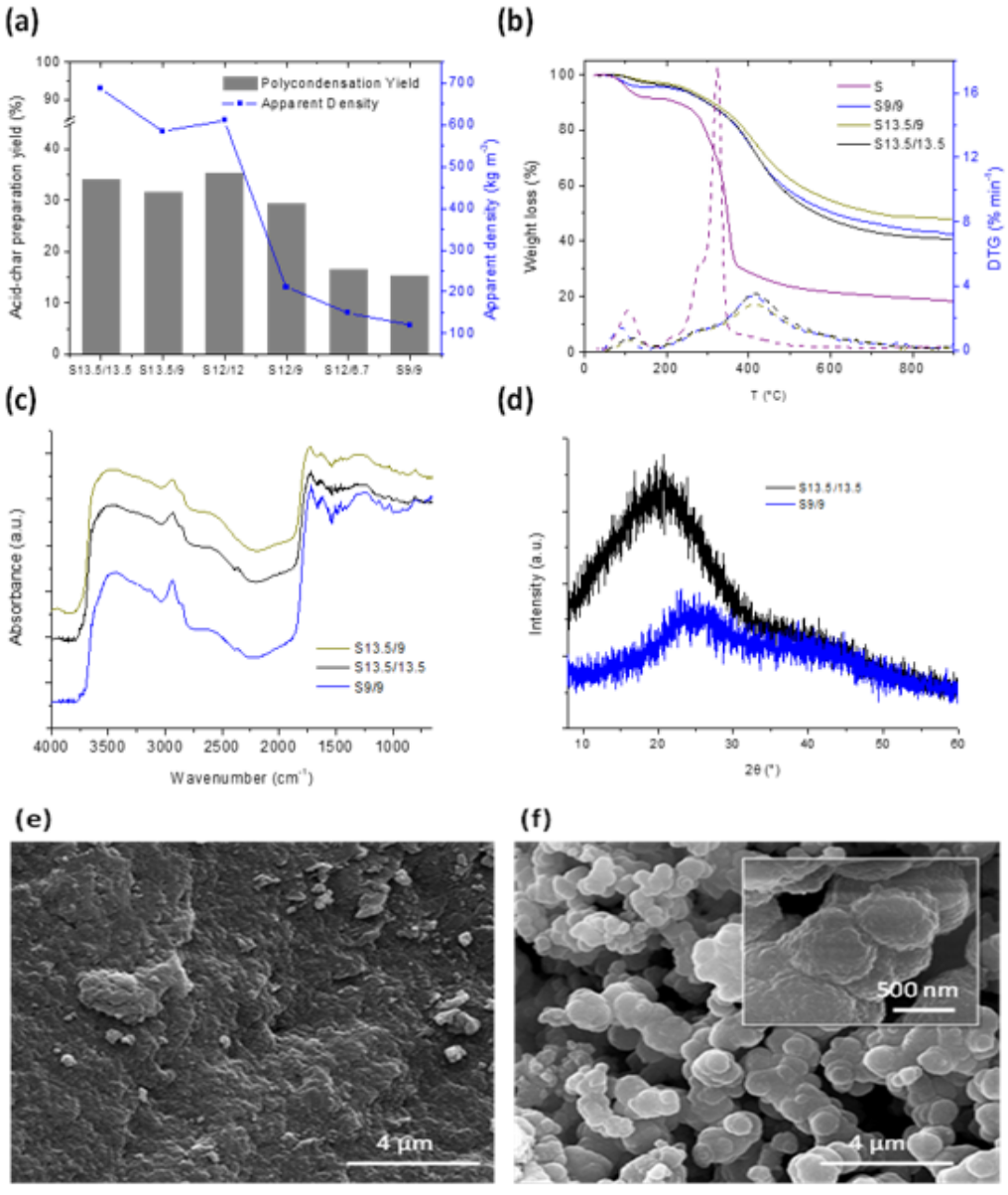

Figure 2.

(a) Effect of H_2SO_4 concentration on the digestion steps on the yields and tapped densities of the acid-chars;

(b) thermogravimetric profiles (TG) and derivative (DTG) curves of selected samples;

(c) DRIFT spectra and

(d) XRD patterns of selected acid-chars. SEM images of samples (e) S13.5/13.5 and S9/9 (S[H_2SO_4]digestion/[H_2SO_4]polycondensation). Reproduced from [9] with permission of Elsevier.

3. Acid chars as activated carbon precursor

To the best of our knowledge the published works reporting acid-chars obtained by AMC were focused on the development of the pore structure to obtain nanoporous carbon materials. Wang et al. [7,8] used H_2SO_4 to synthesize acid-chars from rice husk, which were further chemically activated with H_3PO_4 or KOH. The acid-char derived activated carbons obtained by KOH activation attained BET areas of 2500 m^2g^{-1} and microporous structure [8], while those activated with H_3PO_4 were micro and mesoporous solids and presented a wider range of BET area values (750 to 2700 $m^2\,g^{-1}$) [7]. The activated carbons prepared from rice husk-derived acid-chars presented good electrochemical performances comparing favorable with commercial counterparts, attaining specific capacitances of 130 Fg^{-1} in the case of activation with H_3PO_4 and superior than 220 Fg^{-1} when KOH activated [7,8]. In another study Wang et al. also report the carbonization of acid-chars prepared from rice husk to synthesize carbon materials with BET areas up to 1034 m^2g^{-1} [12]. These materials present electrical conductivity reaching 156 $\Omega^{-1}m^{-1}$ at 900 kPa, that is, close to the performance of a commercial carbon black.

Cui and Atkinson [10] explored several acid catalysts (H_2SO_4, H_3PO_4, HCl and CH_3COOH) for the synthesis of acid-chars from glycerol at mild to high carbonization temperatures, and used physical activation (steam or CO_2) to develop the pore networks. Depending on the acid (H_2SO_4 and/or H_3PO_4), the obtained oxygen-rich chars contain sulfur (0.43-4.20 wt.%) or phosphorus (6.32-16.31 wt.%) groups, which enhance the reactivity for subsequent activation and allow joining a well-developed pore network with heteroatom doping. Independently of the acid catalyst and activating agent all the acid-char derived activated carbons presented a micro and mesopore network with BET areas between 1000 $m^2\,g^{-1}$and 2400 $m^2\,g^{-1}$. These activated carbons were tested for the removal of toluene and hexane (volatile organic compounds, VOCs) in gas phase, and also for the removal of Cr(VI) in aqueous solution, outperforming commercial activated carbons. The authors propose that the best activated carbon material for an industrial application in the removal of VOCs is that prepared with H_2SO_4 and further steam activated, since it presents high adsorption capacity at low pressure due to the high micropore volume allied with hydrophobic properties [10]. In what concerns Cr(VI) removal the materials prepared with H_3PO_4 are preferred since their hydrophilic character, high mesopore volumes and higher amount of oxygen surface functionalities favor the adsorption of this cation [10].

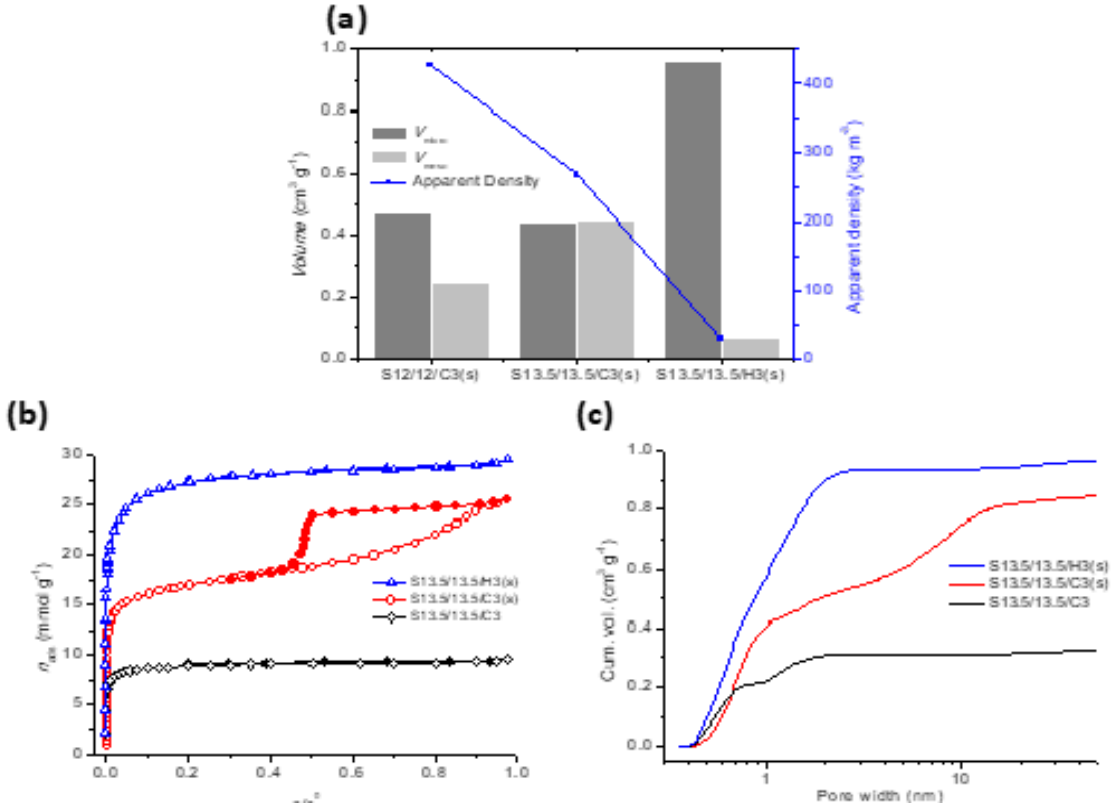

Figure 3.

(a). Micro and mesopore volumes of the activated carbons prepared by solution impregnation of acid-chars S12/12 and S13.5/13.5 with K_2CO_3 or KOH (3g of activating agent per gram of acid-char) followed by activation at 800 °C during 1h. The influence of acid-char precursor in apparent density of the activated carbon is also displayed;

(b) N_2 adsorption isotherms of activated carbons prepared from acid-char S13.5/13.5;

(c) Cumulative pore size distributions obtained from the 2D-NLDFT-HS method applied to the N_2 adsorption isotherms. For chars designation see caption of Figure 2. Reproduced from [9] with permission of Elsevier.

The sisal-derived acid-chars prepared in the AAM group were chemically activated with K_2CO_3 and KOH aiming to understand the influence of the acid-char properties on the final characteristics of the activated carbons [9]. Figure 3 clearly illustrates the distinct pore structures of some of the activated carbon materials synthetized. While K_2CO_3 solution impregnation and further activation of acid-chars obtained with H_2SO_3 12 M and 13.5 M yields activated carbons (S12/12/C3(s) and S13.5/13.5/C3(s)) with high apparent densities and pore networks composed of micro and mesopores, the solution impregnation of the same acid-char with KOH (S13.5/13.5/H3(s)) originated a microporous solid with a density lower than 50 kg m^{-3} (Figure 3(a)). The N_2 adsorption isotherms (Figure 3(b)) and pore size distributions (Figure 3(c)) reveal that by changing the contacting method of K_2CO_3 and acid-char (S13.5/13.5/C3(s) – solution impregnation and S13.5/13.5/C3 – physical mixing) we can also tune the porosity of the resulting activated carbon without significant changes in the apparent density and morphology of the samples (for more details see [9]). The overall data collected proved that by controlling the synthesis conditions of the acid-chars (*i.e.* acid concentration during digestion and polycondensation), the chemical activating agent and the contacting method between the acid-char and the activating agent it is possible to obtain activated carbons with very distinct properties (*i.e.* BET areas from 600 m^2 g^{-1} to 2400 m^2 g^{-1}, apparent densities from < 50 kg m^{-3} to 600 kg m^{-3} and exclusively micropore structures or micro and mesopore networks). Moreover, it is important to highlight that although sisal is a low density biomass, the control of AMC condition allows to tailor the density of the acid-chars and control the features of the derived activated carbons thus proving the versatility of this less explored carbonization route.

Materials S13.5/13.5/H3(s) and S13.5/13.5/C3(s) were assayed as adsorbents of two pharmaceutical compounds – ibuprofen and iopamidol – with the sample obtained by KOH activation attaining the double of the adsorption capacity of a high performing commercial product from Cabot-Norit certainly due to the presence of a large amount of supermicropores. A large set of these materials was successfully tested for the oxygen reduction reaction (ORR) in alkaline medium, presenting tolerance to methanol when compared with commercial Pt/C and long-term electrochemical stability [13]. The material S13.5/13.5/C3(s), with micro and mesopore structure associated with the presence of nitrogen and sulfur, showed the most promising electrocatalytic performance for ORR, with onset potential of 0.84 V vs. RHE, diffusion-limiting current density (0.26V, 1600 rpm) of -3.12 mA cm^{-2} and with the mechanism closest to the direct 4-electron reaction (n_{O2} = 3.6).

4. Acid chars as catalysts supports

The immobilization of homogeneous catalysts onto solids has been explored by the scientific community for quite some time. This has been also one of our research interests and, in the frame of collaborations with Inorganic Chemistry Groups of our Faculty, of Instituto Superior Técnico (IST), and of Faculty of Sciences from University of Porto (FCUP), several studies were made to test different porous solids, namely modified zeolite structures [14-16] and obviously also carbon materials [17-21]. The studies developed with carbon materials have in common the fact that in all cases the synthesis procedure used gave rise to acid supports (*e.g.* CMK-3) thus preventing the need of an oxidation post-synthesis treatment generally reported when carbon materials are used as supports for immobilization of homogeneous catalysts [22].

Therefore, attending to the acid surface chemistry of the acid-chars, it was evident that they would be a good option to anchor catalytic active metal complexes. To evaluate this hypothesis we carried out a study where complex $[MoI_2(CO)_3(MeCN)_2]$ was immobilized on sisal-derived acid-char S13.5 (Fig. 4) [19].

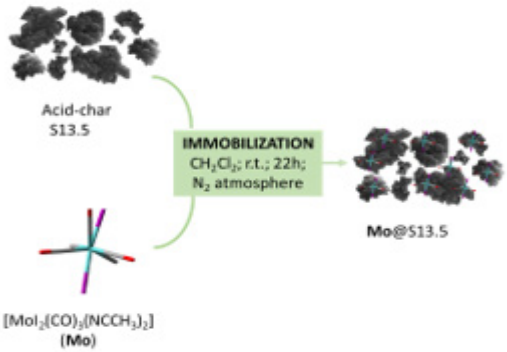

Figure 4. Simplified scheme of immobilization procedure.

The procedure allowed the incorporation of 2.98 (wt.%) of Mo, and the analysis of the FITR spectra (Fig. 5) allowed to concluded out immobilization of the complex occurred by the displacement of the labile acetonitrile ligands. In fact, bands at 2276 and 2303 cm^{-1} assigned to stretching of C=N group from the acetonitrile ligands are almost undetectable in Mo@biochar. These very low intensity bands must correspond to complex that was not coordinated with the acid-char being adsorbed.

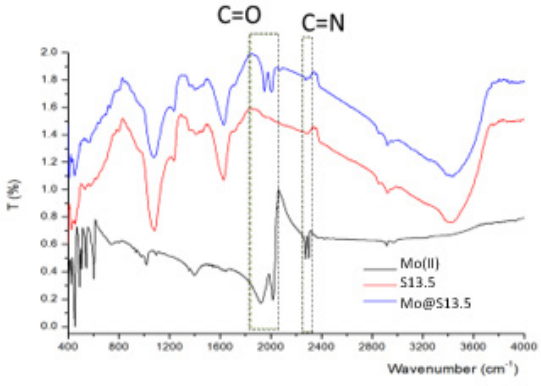

Figure 5. FTIR spectra of molybdenum complex (Mo(II)), acid-char S13.5, and immobilized catalyst *Mo@S13.5*.

Oxidation of *cis*-cyclooctene (Cy8) with *tert*-butyl hydroperoxide was the model reaction selected to assess the catalytic properties of Mo@S13.5 sample. Data presented in Table 1 exemplify the most relevant results obtained in one of the solvents tested (CH_2Cl_2) and in solventless conditions. In both cases the acid-char is practically inactive so it is only acting as host of the complex. Concerning the catalytic behaviour of Mo@13.5 the results could not be better as under solvent conditions the Cy8 conversion after 24 h is higher than its homogeneous counterpart. However the most important results were those obtained in solventless conditions since a complete convention of the reagent was achieved maintaining the 100 % selectivity to the epoxide.

Catalyst	Conversion at 24h (%)	
	Solvent: CH_2Cl_2	No solvent
S13.5	1	1
$MoI_2(CO)_3(MeCN)_2$	81*	100
Mo@S13.5	93	100

All reaction were made at 55 °C using 150 mg catalyst (0.31 mmol Mo g^{-1}) and oxidant: *cis*-cyclooctene =2:1 (molar). *Data from ref. [23]

Table 1. Results of catalytic oxidation of *cis*-cyclooctene with *tert*-butyl hydroperoxide.

As the final goal of this type of studies is to prove that the immobilized catalyst is, in fact, a reusable catalyst Mo@S13.5 was tested in four re-use cycles in optimized experimental conditions (Fig. 6). No changes in selectivity was observed and only a quite small decrease of conversion was observed, especially between the first and the second cycles. This decrease was attributed to the leaching of the species that were not effectively linked to the acid-char, most probably those that were detected in the very low intensity bands assigned to the acetonitrile in the FTIR spectrum oh Mo@S13.5. In accordance a decrease of Mo content in the sample to 2.76 (wt.%) was found. No important further leaching was proved stopping the reacting after 2h and, after recover the catalyst, no substrate conversion was observed up to 24 h.

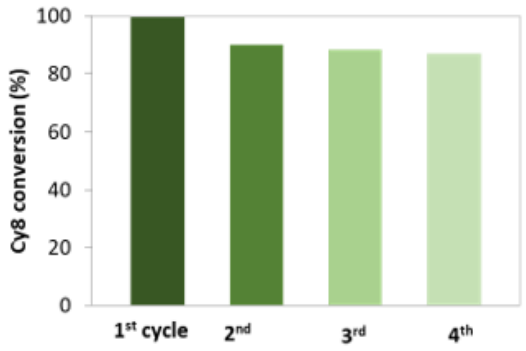

Figure 6. Re-use tests results. Reaction condition: 55 °C; 150 mg catalyst (0.31 mmol Mo g-1) and oxidant: *cis*-cyclooctene =2:1 (molar); solventless.

So, the results obtained with the sisal derived acid-char loaded with the complex $[MoI_2(CO)_3(MeCN)_2]$ proved that acid-chars can compete with more conventional carbon materials to prepare reusable catalysts that retain almost unchanged their catalytic properties in several successive.

5. Acid chars as catalysts and adsorbents

Recently we started to explore the potentialities of acid-chars as catalysts and also as adsorbents for the removal of heavy metals from water.

Regarding the use as catalysts, sawdust derived acid-chars obtained with different H_2SO_4 concentration (13.5 M and 18 M) are being tested in the esterification reaction of acetic acid with butanol. The results obtained so far show that the materials are active for this transformation, achieving reaction yields of 64 %. Moreover, a direct dependence of the reaction yield with the number of the total acid functionalities, consequently with the acid concentration used to prepare the samples was observed. Reusability tests are being made.

To evaluate the potential of acid-chars as adsorbents for the removal of heavy metals from water, sisal was also selected as starting biomass and, to evaluate the influence of the polycondensation step duration on the samples properties, 6h, 3h and 1.5h treatments were made. Somewhat unexpected, the results reveal that the synthesis yield, and the density of the samples are practically independent on the polycondensation step duration. Likewise, the preliminary data for the removal of Pb^{2+} after 24h of contact time do not evidence significant differences between the samples. On the other hand, in comparison with literature [24,25] the removal achieved show that these are very promising materials for this purpose and so, the study will be extended to other cations, namely Cd^{2+}.

Acknowledgements

The work reported was supported by Fundação para a Ciência e Tecnologia (FCT) through the financial to the Centro de Química e Bioquímica (UID/MULTI//00612/2013) and Centro de Química Estrutural (Pluriannual funding 2020-2023). ASM acknowledges FCT for the financial support to the EMBRACE project (CEECIND/01371/2017) and post-doc grant (SFRH/BPD/86693/2012). Cordex is also acknowledged for providing the sisal residues.

References

[1] A.P. Carvalho, M. Galhetas, M.A. Andrade, M.K. Batista, A.S. Mestre, Synthesis of biomass-derived activated carbons for liquid phase application, Boletin do Grupo Español del Carbón 39 (2016) 13-18 (ISSN: 2171 - 6094)

[2] A. Marinovic, F.D. Pileidis, M.M. Titirici, Chapter5. HydrothermalCarbonisation(HTC): History, State-of-the-Art and Chemistry. Porous Carbon Materials from Sustainable Precursors. The Royal Society of Chemistry; 2015.

[3] A.S. Mestre, A.P. Carvalho, Nanoporous carbons synthesis: an old story with exciting new chapters, in Porosity, T. Ghrib (Ed.) IntechOpen, Londres, 2018, p. 37-68 (ISBN 978-1-78923-043-7)

[4] A.S. Mestre, C. Freire, J. Pires, A.P. Carvalho, M.L. Pinto, High performance microspherical activated carbons for methane storage and landfill gas or biogas upgrade, Journal of Materials Chemistry A, 2 (2014) 15337-15344 (DOI: 10.1039/C4TA03242J)

[5] A.S. Mestre, E. Tyszko, M.A. Andrade, M. Galhetas, C. Freire, A.P. Carvalho, Sustainable activated carbons prepared from a sucrose derived hydrochar: remarkable adsorbents for pharmaceutical compounds, RSC Advances, 5 (2015) 19696-19707 (DOI: 10.1039/C4RA14495C)

[6] M. Nunes, I. Rocha, D. Fernandes, A.S. Mestre, A.P. Carvalho, M.F.R. Pereira, C. Freire, Sucrose-derived activated carbons: electron transfer properties and application as oxygen reduction electrocatalyst, RCS Advances, 5 (2015) 102919–102931 (DOI: 10.1039/c5ra20874b)

[7] L. Wang, Y. Guo, B. Zou, C. Rong, X. Ma, Y. Qu, Y. Li, Z.Wang, H igh surface area porous carbons prepared from hydrochars by phosphoric acid activation, Bioresource Technology, 102 (2011) 1947-1950 (DOI: 10.1016/j.biortech.2010.08.100)

[8] L. Wang, Y. Guo, Y. Zhu, Y. Li, Y. Qu, C. Rong, X. Ma, Z. Wang, A new route for preparation of hydrochars from rice husk. Bioresource Technology, 101 (2010) 9807-9810 (DOI:10.1016/j.biortech.2010.07.031)

[9] A.S. Mestre, F. Hesse, C. Freire, C.O. Ania, A.P. Carvalho, Chemically activated high grade nanoporous carbons from low density renewable biomass (Agave sisalana) for the removal of pharmaceuticals, Journal of Colloid and Interface Science, 536 (2019) 681–693 (DOI: 10.1016/j.jcis.2018.10.081)

[10] Y. Cui, J.D. Atkinson Tailored activated carbon from glycerol: Role of acid dehydrator on physiochemical characteristics and adsorption performance. Journal of Materials Chemistry A., 5 (2017) 16812-16821 (DOI: 10.1039/C7TA02898A)

[11] M. Andrade, J.B. Parra, M. Haro, A.S. Mestre, A.P. Carvalho, C.O. Ania, Characterization of the different fractions obtained from the pyrolysis of rope industry waste, Journal of Analytical and Applied Pyrolysis, 95 (2012) 31-37 (DOI: 10.1016/j.jaap.2012.01.002)

[12] L. Wang, X. Wang, B. Zou, X. Ma, Y. Qu, C. Rong, Y. Li, Y. Su, Z. Wang, Preparation of carbon black from rice husk by hydrolysis, carbonization and pyrolysis, Bioresource technology, 102 (2011) 8220-8224 (DOI: 10.1016/j.biortech.2011.05.079)

[13] D.M. Fernandes, A.S. Mestre, A. Martins, N. Nunes, A.P. Carvalho, C. Freire, *Biomass-derived nanoporous carbons as electrocatalysts for oxygen reduction reaction,* Catalysis Today, (2019) (DOI:10.1016/j.cattod.2019.02.048)

[14] L.M.D.R.S. Martins, A. Martins, E.C.B.A. Alegria, A.P. Carvalho, M. Andrade, A.J.L. Pombeiro, Efficient cyclohexane oxidation with hydrogen peroxide catalysed by a c-scorpionate iron(II) complex immobilized on desilicated MOR zeolite, Applied Catalysis A: General, 464– 465 (2013) 43-50 (*DOI: 10.1016/j.apcata.2013.05.022)*

[15] V. Van-Dúnem, A.P. Carvalho, L.M.D.R.S. Martins, A. Martins, Improved cyclohexane oxidation catalyzed by a heterogenised iron(II) complex on hierarchical Y zeolite through surfactant mediated technology, ChemCatChem, 10 (2018) 4058-4066 (DOI: 10.1002/cctc.201800921)

[16] D. Ottaviani, V.Van-Dúnem, A.P. Carvalho, A. Martins, L.M.D.R.S. Martins, Eco-friendly cyclohexane oxidation by a V-scorpionate complex immobilized at a hierarchical MOR zeolite, Catalysis Today, 2019 (DOI: 10.1016/j.cattod.2019.09.034)

[17] S. Dorbes, C. Pereira, M. Andrade, D. Barros, A.M. Pereira, S.L.H. Rebelo, J.P. Araújo, J. Pires, A.P. Carvalho, C. Freire, Oxidovanadium(IV) acetylacetonate immobilized onto CMK-3 for heterogeneous epoxidation of geraniol, Microporous and Mesoporous Materials, 160 (2012) 67-74 (DOI: 10.1016/j.micromeso.2012.03.041)

[18] H. Gaspar, M.Andrade, C. Pereira, A. M. Pereira, S. L. H. Rebelo, J. P. Araújo, J. Pires, A.P. Carvalho, C. Freire, Alkene epoxidation by manganese(III) complexes immobilized onto nanostructured carbon CMK-3, Catalysis Today, 203 (2013) 103-110 (DOI: 10.1016/j.cattod.2012.04.018)

[19] C. Petit, M.V. Silva, A.S. Mestre, P. Vaz, A.P. Carvalho, C.D. Nunes, Solventless olefin epoxidation using a Mo-loaded@sisal derived acid-char catalyst, Chemistry Select, 3 (2018) 10357-10363 (DOI: 10.1002/slct.201802055)

[20] T.A.G. Duarte, A.P. Carvalho, L.M.D.R.S. Martins, Styrene oxidation catalyzed by copper(II) C-scorpionates in homogenous medium and immobilized on sucrose derived hydrochars, Catalysis Today, 2019 (DOI: 10.1016/j.cattod.2019.04.044)

[21] M.A. Andrade, A.S. Mestre, A.P. Carvalho, A.J.L. Pombeiro, L.M.D.R.S. Martins, The role of nanoporous carbon materials in catalytic cyclohexane oxidation, Catalysis Today, 2019 (DOI: 10.1016/j.cattod.2019.07.036)

[22] M. Sutradhar, L.M.D.R.S. Martins, S.A.C. Carabineiro, M.F.C. Guedes da Silva, J.G. Buijnsters, J.L. Figueiredo, A.J.L. Pombeiro, Oxidovanadium(V) complexes anchored on carbon materials as catalysts for the oxidation of 1-phenylethanol, ChemCatChem, 8 (2016) 2254-2266 (DOI : 10.1002/cctc.201600316))

[23] M. Vasconcellos-Dias, S.R.M.M. de Aguiar, C.D. Nunes, P.D. Vaz, T.G. Nunes, M.J. Calhorda, Pyridine carboxylate complex of Mo(II) as active catalysts in homogeneous and heterogeneous olefin epoxidation, Current Inorganic Chemistry, 1 (2011) 146-155 (DOI : 10.2174/1877944111101020146)

[24] D. Kołodyńska, R. Wnętrzak, J.J. Leahy, MH.B. Hayes, W. Kwapiński, Z. Hubicki, Kinetic and adsorptive characterization of biochar in metal ions removal, Chemical Engineering Journal 197 (2012) 295-305 (DOI/10.1016/j.cej.2012.05.025)

[25] A.Nieto-Márquez, A. Pinedo-Flores, G. Picasso, E. Atanes, R. Sun Kou, Selective adsorption of Pb^{2+}, Cr^{3+} and Cd^{2+} mixtures on activated carbons prepared from waste tires, Journal of Environmental Chemical Engineering 5 (2017) 1060-1067 (DOI /10.1016/j.jece.2017.01.034)

Simple routes for the functionalization of carbon nanoparticles and potencial applications

María C. Paiva[1] and M. Fernanda Proença[2]

[1] Instituto de Polímeros e Compósitos, Universidade do Minho, 4804-533 Guimarães, Portugal
[2] Centro de Química, Universidade do Minho, 4710-057 Braga, Portugal

The article describes briefly the investigation carried out on carbon-based materials along the past years as well as the current research and aims for the future.

1. Framework

The interest in the field of carbon materials started for M.C. Paiva in the early nineties with the emerging ideas for the development of carbon fibers that could reach the automotive industry. After a brief investigation on the surface characterization of vapor grown carbon fibers produced by J. L. Figueiredo research group, the focus turned into pitch and PAN-based carbon fibers, their surface physical and chemical modification towards strong interfaces with polymers. This was the PhD topic under the supervision of C.A.A. Bernardo, in good collaboration with J. M. D. Tascón and co-workers (Instituto del Carbón, Oviedo, Spain), M. Nardin (Institut des Surfaces et Interfaces, Mulhouse, France) and D. D. Edie (Center for Advanced Engineering Fibers and Films, Clemson University, SC, USA) [2-5]. The research extended to carbon nanotubes in collaboration with Ya-Ping Sun's group, at Clemson University [6], and continued at Instituto de Polímeros e Compósitos (IPC), Universidade do Minho, in partnership with M. Fernanda Proença (Centro de Química, Universidade do Minho), with a long experience in organic chemistry, the synthesis and reactivity of organic carbon-based molecules, in particular heterocyclic compounds. The research carried out and ongoing includes the chemical modification of carbon nanofibers (CNF), multiwall carbon nanotubes (MWCNT), single wall carbon nanotubes (SWCNT), exfoliated graphite and graphene, using covalent and non-covalent approaches. The functionalized carbon nanoparticles showed great stability in water, formed stable polymer aqueous suspensions and were used namely to produce composites with strong interfaces in thermoset resins or thermoplastic polymers, or to anchor metal nanoparticles at their surface. A brief overview of the investigation carried out for the functionalization of sp^2 carbon nanoparticles (CNP) is presented below, as well as some of the outcomes and possible applications. Along the way collaboration work was developed with researchers from different fields, which will be referred along the text and references.

2. Covalent functionalization of carbon nanoparticles

The design of strategies for covalent functionalization of CNP walls aimed at simple reactions that would inflict a low level of damage upon the CNP structure. The use of solvents was avoided whenever possible in order to minimize waste and facilitate their scale up.

The reactions investigated were based on cycloadditions to the π-electrons of the CNP, carried out in solution or under solvent-free conditions, mostly using one-pot procedures. One of the approaches was based on the 1,3-dipolar cycloaddition of azomethine ylides (DCA), generated in situ from *N*-benzyloxycarbonylglycine and paraformaldehyde, under solvent-free. The procedure was carried out to functionalize CNF [7,8], MWCNT [9], SWCNT [10], and graphite nanoplatelets (GnP) [11], in good yield and without relevant structural damage to the CNP, as illustrated by scanning tunneling microscopy in Figure 1a. The cyclic amine (pyrrolidine) formed was observed to be a good anchoring group for silver and copper nanoparticles [10].

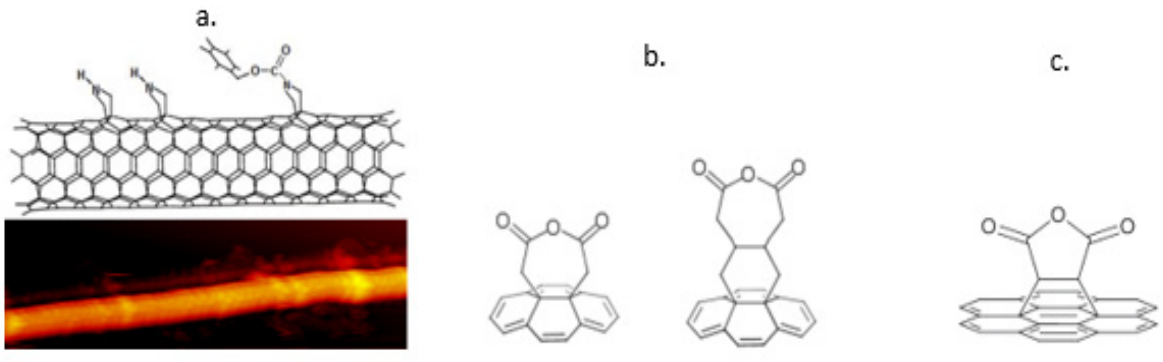

Figure 1. MWCNT observed by scanning tunneling microscopy and schematic representation of the functional groups bonded through the DCA reaction (a); functional groups at the CNP wall identified after DA cycloaddition of 1,3-butadiene (b) and of maleic anhydride (c).

Another covalent functionalization approach investigated was the Diels-Alder (DA) cycloaddition of 1,3-butadiene. The reaction was carried out on CNF [12] and MWCNT [13] in solution (diglyme) or under solvent-free conditions. It was shown that under the conditions used, the alkene initially formed undergoes a cascade oxidation process, yielding mainly carboxylic anhydride groups as final products (Figure 1b). The DA cycloaddition of maleic anhydride to MWCNT was also investigated. In this case, the hydrolysis of the anhydride was facilitated by the presence of MWCNT. However, the process could be reversed by heating in a high boiling point solvent thus recovering the anhydride form (Figure 1c) [14].

3. Non-covalent functionalization of carbon nanoparticles

In the context of non-covalent functionalization of CNP a selection of symmetrical perylene bisimides (PBI) were prepared by reaction of perylene tetracarboxylic dianhydride and a series of alpha-amino acids [15]. Their ability to adsorb at the MWCNT surface to form stable aqueous suspensions was investigated. The alpha-amino acid plays an important role on the stability of the suspensions, as was observed experimentally and confirmed by theoretical calculations (Figure 2a). It was demonstrated that PBI functionalized with Boc-lysine and phenylalanine led to stable suspensions of CNT in water at a quite low PBI concentration (5 x 10^{-5} M).

A water-soluble pyrene derivative was also prepared in high yield using a simple and low-cost functionalization methodology, easy to scale up. The synthesized pyrene derivative, depicted in Figure 2b, was tested for the stabilization of different types of GnP in aqueous solution [16], at low pyrene concentrations (5 x 10^{-5} M).

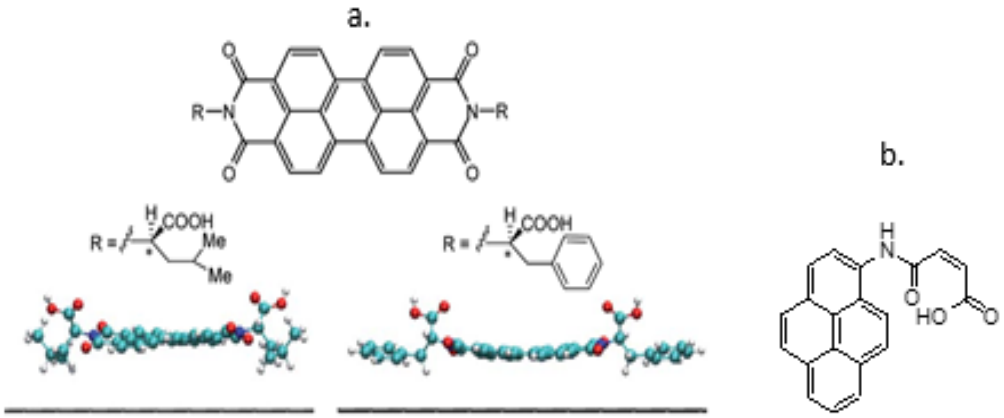

Figure 2. Equilibrium of different PBI geometries on the CNT surface (a); representation of the structure of the synthesized pyrene derivative (b).

4. Carbon nanoparticle-polymer interface

The CNP/polymer interface in a composite is strengthened by strong interactions between the two materials. However, the atomically smooth surface of the CNP will interact weakly with most polymers and the CNT tends to cluster and remain in the agglomerate form, hindering the dispersion and formation of homogeneous composites. The functionalization of CNP by covalent chemistry changes the interfacial energy and, if the functional groups are adequately selected, they may react covalently with the polymer forming a strong interface (Figure 3). Even when low reactivity between the functional groups and the polymer is predicted, the reaction may be favored under specific mixing conditions. For thermoplastic polymers reaction may proceed under melt mixing conditions, at relatively high temperature and viscosity. This was observed for MWCNT and GnP functionalized by the DCA reaction, decorated with a cyclic amine that is thermally stable and reactive in the polymer melt, using poly(lactic acid) (PLA) and polypropylene (PP) mixed with PP modified with maleic anhydride [17-20].

Covalent chemistry also had a positive contribution for interfacial bonding in CNP/thermoset polymers, particularly when the functional groups bonded to the CNP surface participate in the crosslinking reactions during the cure of the resin.

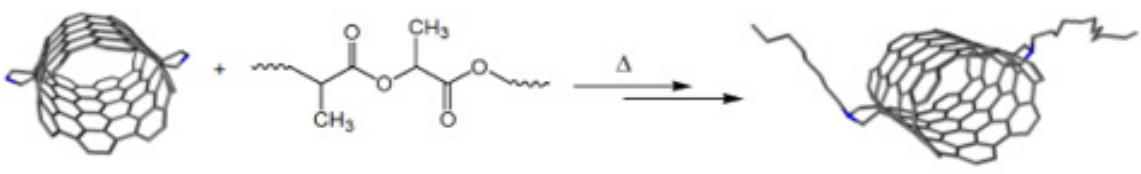

Figure 3. Reaction of a DCA functionalized CNT with PLA yielding the polymer functionalized CNT.

5. Formation of few-layer graphene from bulk graphite and carbon nanotubes

The production of graphene and graphene nanoribbons from graphite and carbon nanotubes, respectively, is a topic of intensive research. We observed that the DCA-functionalized MWCNT could undergo unzipping forming graphene nanoribbons (GNR) during their analysis by scanning tunneling microscopy (STM) [21]. The production of GNR from MWCNT in ethanol was successful [22] and the yield was sufficient to allow the production of composite films with enhanced mechanical properties, using layer-by-layer deposition [11].

Few layer graphene (FLG) was prepared by liquid phase exfoliation of graphite. The procedure was carried out in a dilute solution of the pyrene derivative depicted in Figure 2.b [16] and tested on graphite from various origins. The FLG thus produced was applied as mechanical reinforcement in natural polymer composites produced by layer-by-layer [23]. Composite films with good barrier properties and electrical conductivity were produced from aqueous polymer/FLG suspensions by spray coating [24].

6. Applications

The functionalized and pristine CNP were applied in a range of areas in collaboration with colleagues from different fields and institutions.

In the field of thermoplastic polymer composites the dispersion of CNP was investigated using different techniques in collaboration with J. A. Covas (IPC) [17-20, 25-28]. The characterization of these composites in terms of thermal properties and liquid sensing activity was carried out in collaboration with P. Poetschke (Leibniz Institute for Polymer Research, Dresden) [18, 25-26]. In the aim of Project Inteltex (European FP6 project) electrically conductive thin monofilaments were integrated into fabrics for the production of textiles with sensing activity towards temperature, strain, water, etc. (depending on the polymer) in collaboration with F. Ferreira (2C2T - Centro de Ciência e Tecnologia Têxtil, Universidade do Minho) [30]. Some of the project outcomes are illustrated in Figure 4.

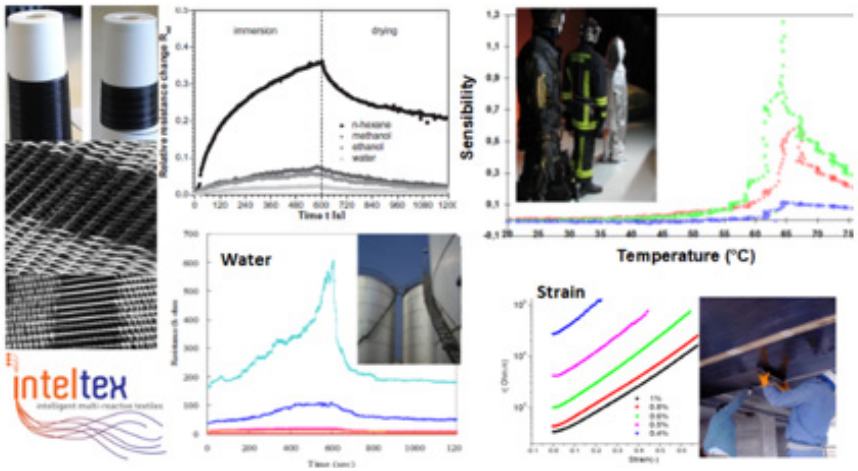

Figure 4. Textiles incorporating electrically conductive composite filaments and their sensing activity.

Composites with functionalized MWCNT were produced for testing sensing activity in a collaboration with P. K. Bhatnagar and P. C. Mathur (Department of Electronic Science, University of Delhi South Campus, Índia) [29].

Electrically conductive composite filaments were produced at IPC for application in 3D printing of conductive parts for aerospace applications, such as represented in Figure 5a [25]. The 3D printing was then carried out by Ugo Lafont's team (European Space Research and Technology Centre, Noordwijk, The Netherlands).

Thermoset polymer nanocomposites with electrical and thermal conductivity are under investigation in a collaboration project with Bosch Car Multimédia, Portugal, (project iFactory and ongoing project Factory of the Future) for the development of electrically conductive adhesives (ECAs) for PCB bonding (Figure 5b) [31]. The ECAs developed presented a shelf live larger than 6 months at temperature of -20 °C.

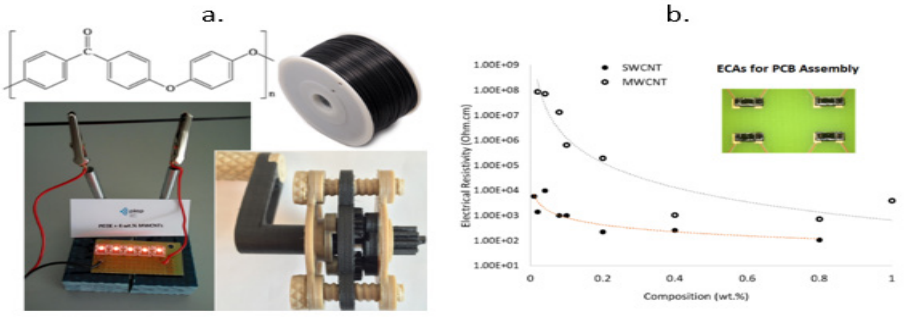

Figure 5. PEEK/MWCNT/GnP conductive filaments produced for 3D printing of complex parts (a); testing ECAs for PCB bonding (b).

In the field of electrochemistry the investigation of the effect of electrode modification with functionalized and pristine CNP, on the electrochemical response was carried out in collaboration with F. Bento and D. Geraldo from Centro de Química, group of Sustainable Chemistry: New Methods and Materials (Figure 6) [32-34].

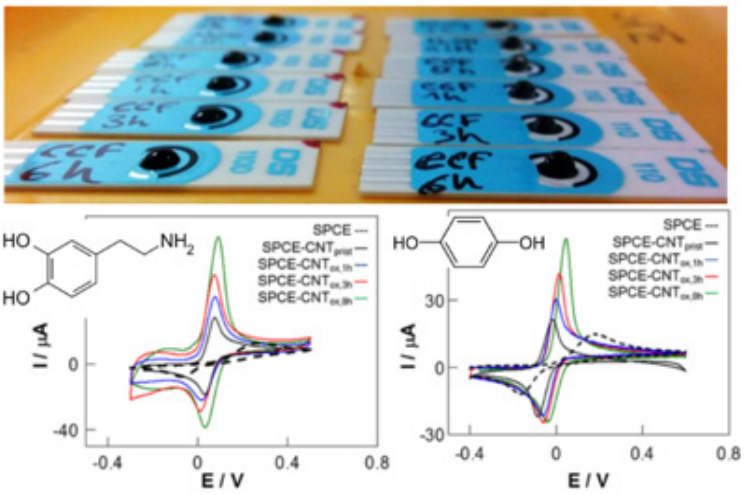

Figure 6. Testing the response of electrodes modified with functionalized MWCNT.

CNP play an important role in the biomedical field to act as mechanical reinforcement and allow electrical stimuli that may enhance cell growth in tissue engineering. In collaboration with N. M. Alves (Instituto de Investigação em Biomateriais, Biodegradáveis e Biomiméticos, I3Bs, Universidade do Minho) and J. F. Mano (formerly at I3Bs) films with enhanced mechanical properties were produced using layer-by-layer techniques, formed by natural polymers, GnP and GnR [11, 23, 35]. In a collaboration with R. F. Silva (CICECO – Aveiro Institute of Materials, Universidade de Aveiro) MWCNT functionalized by the DA reaction were used for tissue engineering with promising results [36].

Finally, the application of aqueous suspensions of MWCNT and SWCNT prepared via non-covalent functionalization, in cementitious matrices, was investigated in a collaboration with R. Fangueiro (2C2T, Universidade do Minho) and S. Rana (formerly at 2C2T) [37, 38].

References

[1] Carbon Fibers Filaments and Composites. Herausgeg. von J. L. Figueiredo, C. A. Bernardo, R. T. K. Baker and K. J. Hüttinger. Kluwer Academic Publishers Group, Dordrecht 1989.

[2] M.C. Paiva, M. Nardin, D.D. Edie, C.A. Bernardo, Ribbon Fibres from Naphtalene-Based Mesophase: Surface Studies and Fibre/Matrix Interactions in Polycarbonate Composites, Carbon, 1998, 36, 1, 71-77.

[3] M.C. Paiva, M. Nardin, C.A. Bernardo, "Mechanical, Surface and Interfacial Characteristics of Pitch and PAN-based Carbon Fibres", Carbon, 2000, 38, 1323-1337.

[4] M. Montes-Moran, A. Martinez-Alonso, J.M. Tascon, M.C. Paiva, C.A. Bernardo, "Effects of Plasma Oxidation on the Surface and Interfacial Properties of Carbon Fibres/ Polycarbonate Composites", Carbon, 2001, 39, 1057-1068.

[5] M.C. Paiva, C.A. Bernardo, D.D. Edie, "A Comparative Analysis of Alternative Models to Predict the Tensile Strength of Untreated and Surface Oxidised Carbon Fibers", Carbon, 2001, 39, 1091-1101.

[6] M.C. Paiva, B. Zhou, K.A.S. Fernando, Y. Lin, J.M. Kennedy, Y.-P. Sun, Mechanical and morphological characterization of polymer-carbon nanocomposites from functionalized carbon nanotubes, Carbon, 2004, 42, 14, 2849-2854.

[7] R. Araújo, M. C. Paiva, M. F. Proença, Carlos J. R. Silva, Functionalization of Carbon Nanofibers by 1,3 - Dipolar Cycloaddition Reactions and its Effect on Composite Properties, Composite Science and Technology, 2007, 67, 806-810.

[8] R. F. M. Fernandes, M. F. Proença, C. J. R. Silva, M. C. Paiva, The 1,3-dipolar cycloaddition reaction in the functionalisation of carbon nanofibres, J. Nanosci. Nanotechnol., 2007, 7, 3441–3445.

[9] M. C. Paiva, F. Simon, R. M. Novais, T. Ferreira, M. F. Proença, W. Xu, F. Besenbacher, Controlled Functionalization of Carbon Nanotubes by a Solvent-free Multicomponent Approach. ACS Nano 2010, 4, 12, 7379-7386.

[10] M. M. Silva, D. Ribeiro, E. Cunha , M. F. Proença, R. J. Young, M. C. Paiva, A Simple Method for Anchoring Silver and Copper Nanoparticles on Single Wall Carbon Nanotubes, Nanomaterials 2019, 9, 1416.

[11] M. Silva, S. G. Caridade, A. C. Vale, E. Cunha, M. P. Sousa, J. F. Mano, M. C. Paiva, N. M. Alves, Biomedical films of graphene nanoribbons and nanoflakes with natural polymers, RSC Advances, 2017, 7, 27578 – 27594.

[12] M. F. Proença, R. F. Araújo, M. C. Paiva, C. J. R. Silva, The Diels-Alder Cycloaddition Reaction in the Functionalization of Carbon Nanofibers, J. Nanosci. Nanotechnol. 2009, 9, 6234-6238.

[13] R. F. Araújo, M. F. Proença, C. J. Silva, T. G. Castro, M. Melle-Franco, M. C. Paiva, S. Vilar-Rodil, J. M. D. Tascón, Grafting of adipic anhydride to carbon nanotubes through a Diels-Alder cycloaddition/oxidation cascade reaction. Carbon, 98 (2016) 421-431.

[14] R. F. Araújo, M. F. Proença, C. J. Silva, M. C. Paiva, S. Villar-Rodil, J. M. D. Tascón, The solvent effect on the sidewall functionalization of multi-walled carbon nanotubes with maleic anhydride, Carbon 78 (2014) 401–414.

[15] R. F. Araújo, C. J. R. Silva, M. C. Paiva, M. Melle Franco, M. F. Proença, Efficient Dispersion of Multi-walled Carbon Nanotubes in Aqueous Solution by Non-covalent Interaction with Perylene Bisimides, RSC Advances 3, 46 (2013), 24535-24542.

[16] E. Cunha, M.F. Proença, M.G. Pereira, M.J. Fernandes, R.J. Young, K. Strutynski, M. Melle-Franco, M. Gonzalez-Debs, P.E. Lopes, M.C. Paiva, Water Dispersible Few-Layer Graphene Stabilized by a Novel Pyrene Derivative at Micromolar Concentration, Nanomaterials 2018, 8, 675.

[17] R. M. Novais, F. Simon, M. C. Paiva, J. A. Covas, The influence of carbon nanotube functionalization route on the efficiency of dispersion in polypropylene by twin-screw extrusion, Composites: Part A 43 (2012) 2189–2198.

[18] R. M. Novais, F. Simon, P. Pötschke, T. Villmow, J. A. Covas, M. C. Paiva. Poly(lactic acid) composites with poly(lactic acid)-modified carbon nanotubes. Journal of Polymer Science Part A: Polymer Chemistry 51 (2013) 3740-3750.

[19] R. M. Santos, C. Vilaverde, E. Cunha, M. C. Paiva, J. A. Covas, Probing dispersion and re-agglomeration phenomena upon melt mixing of polymer-functionalized graphite nanoplates, Soft Matter, 12 (2016) 77-86.

[20] R. M. Santos, S.T. Mould, P. Formánek, M.C. Paiva, J.A. Covas. Effects of Particle Size and Surface Chemistry on the Dispersion of Graphite Nanoplates in Polypropylene Composites, Polymers (2018) 10(2) 222 (14 pages).

[21] M.C. Paiva, W. Xu, M.F. Proença, R.M. Novais, E. Lægsgaard, F. Besenbacher. Unzipping of Functionalized Multiwall Carbon Nanotubes Induced by STM. Nano Lett. (2010) 10, 1764–1768.

[22] E. Cunha, M.F. Proença, F. Costa, A.J. Fernandes, M. A. C. Ferro, P.E. Lopes, M. González-Debs, M. Melle-Franco, F.L. Deepak, M.C. Paiva, Self-assembled functionalized graphene nanoribbons from carbon nanotubes, ChemistryOpen, 4, 2 (2015) 115-119.

[23] C. Silva, S. G. Caridade, E. Cunha, M. P. Sousa, H. Rocha, J. F. Mano, M. C. Paiva, N. M. Alves, Nanostructured Biopolymer/Few-Layer Graphene Freestanding Films with Enhanced Mechanical and Electrical Properties, Macromol. Mater. Eng. (2018) 1700316 (16 pages).

[24] E. Cunha, M. C. Paiva, Composite Films of Waterborne Polyurethane and Few-Layer Graphene—Enhancing Barrier, Mechanical, and Electrical Properties, J. Compos. Sci. 2019, 3(2), 35.

[25] J. Gonçalves, P. Lima, B. Krause, P. Pötschke, U. Lafont, J.R. Gomes, C.S. Abreu, M.C. Paiva, J.A. Covas, Electrically Conductive Polyetheretherketone Nanocomposite Filaments: From Production to Fused Deposition Modeling, Polymers, 2018, 10, 925.

[26] P. Potschke, K. Kobashi, T. Villmow, T. Andres, M. C. Paiva, J. A. Covas, Liquid sensing properties of melt processed polypropylene/poly(ε-caprolactone) blends containing multiwalled carbon nanotubes, Composites Science and Technology, 71(12), 1451-1460, 2011.

[27] J. A. Covas, M. C. Paiva, R. M. Novais, The Effect of Flow Type and Chemical Functionalization on the Dispersion of Carbon Nanofiber Agglomerates in Polypropylene, Composites: Part A, 43, 833-841, 2012.

[28] S. Jamali, M.C. Paiva, J.A. Covas, Dispersion and re-agglomeration phenomena during melt mixing of polypropylene with multi-wall carbon nanotubes, Polymer Testing 32 (2013) 701-707.

[29] A. Kaur, I. Singh, J. Kumar, C. Bhatnagar, S. K. Dixit, P. K. Bhatnagar, P. C. Mathur, J. A. Covas, M. C. Paiva, Enhancement in the performance of multi-walled carbon nanotube: Poly(methylmethacrylate) composite thin film ethanol sensors through appropriate nanotube functionalization, Materials Science in Semiconductor Processing, 31 (2015) 166-174.

[30] A. Ferreira, F. Ferreira, M. C. Paiva, Textile Sensor Applications with Composite Monofilaments of Polymer / Carbon Nanotubes, Advances in Science and Technology Vol. 80 (2013) 65-70.

[31] P. E. Lopes, D. Moura, D. Freitas, M.F. Proença, H. Figueiredo, R. Alves, and M. C. Paiva, Advanced electrically conductive adhesives for high complexity PCB assembly. AIP Conference Proceedings 2055, 090009 (2019).

[32] R. Gusmão, E. Cunha, M. C. Paiva, D. Geraldo, M. F. Proença, F. Bento, Role of Carbonaceous Fragments on the Functionalization and Electrochemistry of Carbon Materials, ChemElectroChem (2016) 3 (12) pp. 2138-2145.

[33] R. Gusmão, M. Melle-Franco, D. Geraldo, F. Bento, M. C. Paiva, M. F. Proença, Probing the surface of oxidized carbon nanotubes by selective interaction with target molecules, Electrochemistry Communications, 57 (2015) 22-26.

[34] R. Gusmão, V. López-Puente, I. Pastoriza-Santos, J. Perez-Juste, M. F. J R P Proença, F. Bento, D. Geraldo, M. C. Paiva and E. Gonzalez-Romero, Enhanced electrochemical sensing of polyphenols by oxygen-mediated surface, RSC Adv., 5 (2015) 5024-5031.

[35] D. Moura, S.G. Caridade, M.P. Sousa, E.P. Cunha, H. Rocha, J.F. Mano, M.C. Paiva, N.M. Alves, High performance free-standing membranes by layer-by-layer assembly of graphene flakes and ribbons with natural polymers, Journal of Materials Chemistry B, (2016) 4 (47) 7718-7730.

[36] D. Mata, M. Amaral, A. J. S. Fernandes, B. Colaço, A. Gama, M. C. Paiva, P. S. Gomes, R. F. Silva, M. H. Fernandes, Diels–Alder functionalized carbon nanotubes for bone tissue engineering: in vitro/in vivo biocompatibility and biodegradability. Nanoscale, 7, 20 (2015) 9238-9251.

[37] S. Parveen, S. Rana, R. Fangueiro, M. C. Paiva, Microstructure and mechanical properties of carbon nanotube reinforced cementitious composites developed using a novel dispersion technique, Cement and Concrete Research, 73 (2015) 215-227.

[38] S. Parveen, S. Rana, R. Fangueiro, M. C. Paiva, Characterizing Dispersion and Long Term Stability of Concentered Carbon Nanotube Aqueous Suspensions for Fabricating Ductile Cementitious Composites, Powder Technology, 307 (2017) 1-9.

A short review on carbon-based nanomaterials and their hybrids

Bohdan Kulyk, Alexandre Faia Carvalho, Nuno Santos, Antonio José Fernandes, Florinda Mendes Costa

Physics Departament & I3N, University of Aveiro, 3810-067, Aveiro, Portugal

Abstract

A wide range of carbon allotropes exists, each with different properties and characteristics that make them appealing for various practical applications. In this brief review, our work on carbon-based nanomaterials is presented. Particular attention is given to hybrid materials, characterized by a simultaneous growth of different carbon allotropes, which in turn allows to integrate the often-complementary properties of each one in the same material. Using chemical vapour deposition (CVD) as a basis, the synthesis conditions, properties, and potential applications of these hybrids are described. Additionally, ongoing work on other carbon materials, such as CVD-grown and laser-induced graphene is presented.

Keywords: CVD; Nanocarbons; Carbon Hybrids; Nanocrystalline diamond; Graphene; Sensors.

1. Introduction

The possibility of synthesizing diamond from a gas mixture using the chemical vapour deposition (CVD) technique triggered an intense area of research, allowing to obtain monocrystals and a wide range of crystal sizes in the form of thin films [1], [2]. The synthesis is generally performed at relatively low pressures and temperatures, prompting the production of multifunctional films (from nanocrystalline to microcrystalline diamond) by tuning the growth parameters towards a specific application. The purely covalent nature of diamond, along with its strong atomic structure and low mass density, offers excellent mechanical properties [3].

Exploring these characteristics was the original motivation behind the work performed by our group, focusing on the synthesis of diamond films towards a wide range of applications. Some examples are: i) highly adherent CVD diamond coatings on Si3N4 based materials [4]–[7]; ii) CVD diamond deposition on steel substrates using suitable interlayers [8], [9]; iii) cutting tools made of free-standing thick diamond plates brazed to hard metal inserts [10], [11]; and iv) CVD diamond for medical applications, taking advantage of the chemical inertness, good biocompatibility, and resistance to harsh cleaning processes [12]–[15].

This knowledge, along with the existence of a wide range of stable carbon allotropes with distinct properties, encouraged the group to developed new functional materials by integrating different carbon nanostructures in the form of hybrid materials [16]–[20]. The CVD technique, allowing the synthesis of different allotropes by properly selecting the growth parameters, is ideal for exploring this new approach. Indeed, the integration of different nanocarbons in the form of hybrids could benefit from the conjugation of the unique properties of each allotrope. The strong connection between the allotropes due to the simultaneous synthesis allows to obtain specific properties which may exceed those obtained from just the individual contributions of each component.

In this context, the group explored the synthesis of different hybrids, namely the integration of: i) carbon nanotubes (CNTs) well interconnected with nanocrystalline diamond (NCD) clusters [16]; ii) diamond-graphite nanoplatelets (DGNPs) composed of vertically aligned crystalline diamond nanoplatelets as thin as 5 nm, covered by a highly conductive nanographite coating [21]–[23]; and iii) graphene-diamond hybrids (GDHs), formed by highly crystalline longitudinal few-layer graphene (FLG) sprinkled with NCD clusters [17], [24].

More recently, the group has been dedicated to the production of CVD graphene and also laser-induced graphene (LIG) by the irradiation of polyimide films with a laser (wavelengths of 10.6 μm or 355 nm), under ambient conditions [25]. Under the laser source, the polymer graphitizes and forms a graphene-like foam with interesting characteristics for many applications, namely for electrodes, as a platform to pattern piezoresistive strain sensors, and for electrochemical biosensors.

It is worthwhile to note that all these structures can be integrated with other materials, namely intermetallic oxides, envisaging a wide range of composites' applications. Previous works [26], [27] already explored the synergistic properties of ZnO with carbon-based materials. Indeed, an enhancement of the ZnO photoluminescence was observed when nanostructures of this semiconductor were deposited on a forest of vertically-aligned carbon nanotubes (VACNT) [27]. Also, ZnO/CNT buckypaper composites were seen to maintain the strong luminescent properties of the ZnO structures, while exhibiting the electrical properties associated with the CNTs [28]. More recently, an approach for the synthesis of ZnO-decorated LIG samples through a direct-laser scribing was developed, allowing the simultaneous production of ZnO and LIG [26]. The idea is to explore the simplicity of the fabrication process and the interesting electrochemical and optical properties that result from the combination of ZnO with graphene in flexible and miniaturized devices, to develop cheap and disposable biosensors, combining both optical and electrochemical transducing mechanisms in the same device.

The main goal of this paper is to report the development of some multifunctional nanocarbon hybrid materials able to be applied in specific applications.

2. Carbon synthesis by Chemical Vapour Deposition

The broad spectrum of application possibilities offered by carbon materials is highly dependent on the synthesis techniques by which such materials are obtained. Chemical Vapour Deposition (CVD) has a long history in the context of carbon materials' growth, with a vast amount of experience and deep understanding of the intervening processes having been accumulated in this field along the years [29], [30].

The basic principle behind CVD growth is the decomposition of a precursor followed by the deposition of the resulting species. These processes occur by means of chemical reactions in the vapour phase, which can be activated by an appropriate energy input (thermal, electromagnetic, plasma) and may also be facilitated by catalysts. Thus, the control of temperature, precursor and environment chemistry, activation power, pressure, and substrate nature are key factors for successful CVD growth.

Methane is by far the most often selected carbon precursor, although other ones are also frequently referred in the literature (ex.: ethanol [31], methanol [32], acetone [33], and even tequila [34]). Hydrogen is also commonly employed in CVD synthesis of carbons, namely to provide chemical etching, passivation of the growth surface, and assistance in hydrocarbon precursor breakdown [35], [36]. Argon and oxygen are also often used to dilute the gas mixtures [37] and to reduce the energy barrier for growth [38], respectively. Furthermore, the addition of other specific gases enables in-situ doping [39], [40].

As for the precursor breakdown, this can be enabled by external energy sources, through, for instance, direct exposure to a hot filament (HFCVD) [41]–[43] or by radiative heating coming from heating elements (TCVD) [44], [45]. The precursor breakdown can also be achieved in a plasma (either induced by DC or microwave) [46]–[48], or by heating the substrate through induction (another form of TCVD) [49], [50].

In what concerns the substrate, its choice must be compatible with the chemical and physical conditions of the growth process. Moreover, substrates with very low carbon solubility are typically preferred, one exception being the CVD growth by carbon dissolution and consequent precipitation at the latter's surface [51], [52].

In CVD synthesis of carbons, the growth parameters can be tuned to favour a specific allotrope, by promoting a particular hybridization of the carbon bonds.

For diamond, composed by highly stable sp^3 carbon bonds, the sp2 forms are to be suppressed. Typically, this can be achieved by decreasing the concentration of the precursor in hydrogen super-saturated mixtures, thus enhancing the etch rate of the sp2 phases [53]. The main species contributing to diamond growth are believed to be the [CH3]• radical and C2H2 [54]. A particular case of diamond growth is the synthesis of nanocrystalline diamond (NCD) [53]. Here, the small crystallite size is typically promoted by a constant renucleation mechanism [55], [56]. A carbon-lean precursor mixture chemistry typically results in higher quality materials, although growth in high hydrocarbon/hydrogen ratio mixtures is also possible [54].

In the case of carbon nanotubes (CNTs), on the other hand, the desired carbon bond hybridization is sp2. Here, the synthesis process differs in that it requires a catalyst on top of the substrate, which is typically composed by metal particles with high carbon solubility, such as Fe, Co, or Ni [57]. The growth is achieved by the carbon saturation of these particles, followed by carbon precipitation which then results in CNTs growth. By properly selecting the size and morphology of the catalyst particles, as well as the rest of the CVD process parameters, CNTs with different diameters and number of walls (either single-wall, SWCNTs, or multi-wall, MWCNTs) and varying morphologies can be achieved [58].

For graphene, another sp^2-carbon-based allotrope, the important aspects are the number of layers and the nucleation density. These are controlled by choosing an appropriate substrate, with Ni, for example, typically resulting in multilayer graphene films, by a growth process somewhat similar to that of CNTs (carbon saturation and precipitation) [52]. On Cu, on the other hand, the growth is, in principle, self-limited, due to the fact that once the entire surface of the substrate is covered by graphene, no further catalytic breakdown of the precursor can occur [45]. In practice, however, secondary layers are typically observed in CVD graphene grown on copper, with different mechanisms having been proposed for this effect [44], [59]–[61].

Other allotropes can be grown by CVD, such as, for example, graphite [62]–[64], highlighting the versatility of this synthesis technique. Moreover, by a carefully controlled interplay between the conditions required for the growth of each allotrope, their simultaneous synthesis can be achieved, resulting in hybrid carbon-based nanomaterials. The different hybrids synthesized by our group are briefly discussed below.

3. Carbon-based hybrids

3.1. Nanocrystalline diamond/carbon nanotubes hybrids

As stated above, the accurate control of the CVD synthesis parameters, envisaging a given specific carbon allotrope, is of crucial importance. This leads to the definition of parameter windows that, for some particular CVD techniques, can be very narrow, yet still overlap in a way that allows simultaneous synthesis of different carbon allotropes. Although this fact typically represents a limitation, it also opens the possibility of combining more than one carbon allotrope in a hybrid approach, taking advantage of the best features in each one. When grown simultaneously, different carbon forms potentially develop strong chemical links in a closely interconnected structure, especially

if this connection takes place at the nanoscale.

Inside the parameter window for microcrystalline diamond (MCD) grown by MPCVD, when the upper limit for methane concentration is crossed, the new diamond crystallites grow to much smaller sizes [29, p. 35]. Alongside, graphitic material develops at the grain boundaries, resulting in an sp^2 rich nanostructured diamond layer, formerly regarded as poor-quality CVD diamond [16]. Under these strict conditions, if catalytic particles of adequate sizes and nature are present, carbon nanotubes start to form, and both nanocrystalline diamond and CNTs grow at the same time.

According to the above described mechanism, hybrid films combining NCD and CNTs were successfully synthetized on silicon substrates using the MPCVD technique [16]. This was accomplished by producing an initial thin layer (~2 µm) of nanocrystalline diamond in a setup where the Si substrate was surrounded by millimetre-sized cast iron particles. These supplied the substrate surface with nanoparticles of Fe (it being a wellknown catalyst element for the growth of CNTs), formed by both co-deposition and diffusion. During the deposition process of the diamond layer, the Fe nanoparticles spread uniformly throughout the surface began to promote the nucleation and growth of CNTs, after the methane flow was increased. This eventually resulted in a diamond film with a surface comprising a neuronal-like network of diamond nanocrystalline clusters interconnected by CNTs [19], as shown if **Figure 1-a**. The presence of both carbon allotropes is evidenced by Raman spectroscopy (**Figure 1-b**). Additionally, since the obtained surface exposes a porous CNTs network, we were able to undertake an NCD overgrowth, filling the empty spaces between the clusters, thus embedding the CNTs structure in an NCD matrix (**Figure 2**). The resulting material resembles that of reinforced concrete, where NCD plays the role of the cement matrix and the CNTs correspond to the reinforcing metal bars [20]. This structure, composed by a brittle intrinsic electrical insulator (diamond) and a tough electrical/thermal conductor (CNTs), evokes applications where this combination can be useful, such as in cold cathodes, nano- and microelectromechanical systems (NEMS/MEMS), and sensors (gases, biochemical species, etc.).

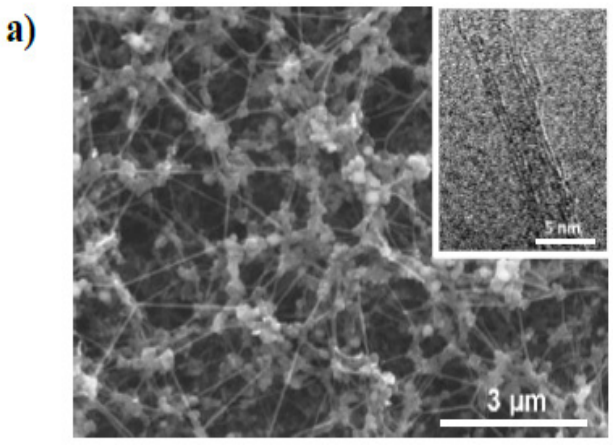

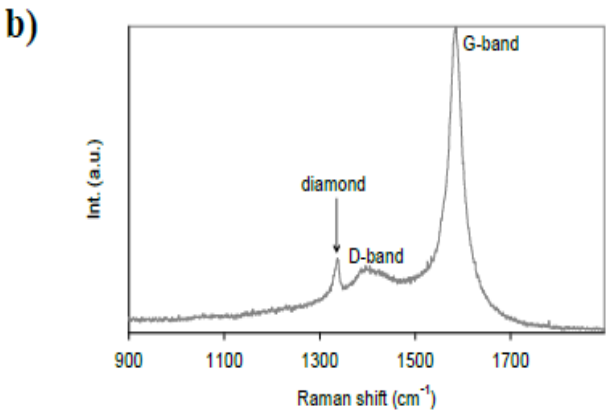

Figure 1. a) Scanning Electron Microscopy (SEM) micrograph of the NCD/CNT hybrid, where the straight CNT structures define a network connecting nanocrystalline diamond clusters. Although the average diameter of these multiwall CNTs is some tens of nanometres, some can get as thin as ~5 nm. The inset shows a High Resolution Transmission Electron Microscopy (HR-TEM) image showing one of these CNTs with 3 walls. **b)** UV (325 nm) micro Raman spectrum taken from the surface of the NCD/CNT hybrid. The assignment of diamond is well patent in the peak at ~1332 cm-1, along with the typical CNT features, the D and G bands at ~1390 cm-1 and 1581 cm-1, respectively.

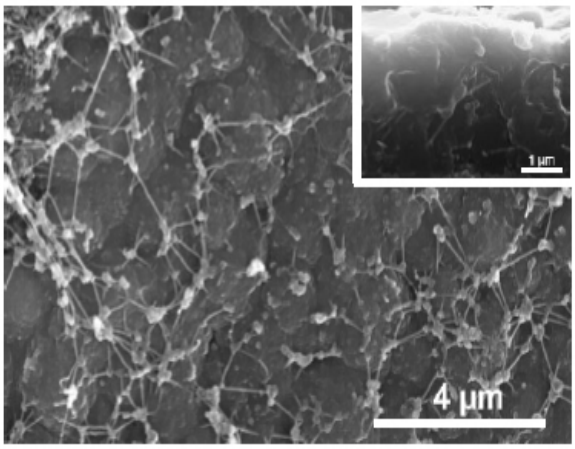

Figure 2. The hybrid surface after diamond overgrowth. CNTs can still be seen protruding from the diamond surface and embedding into it. The inset corresponds to a cross section view of the same structure where CNTs, surrounded by a continuous NCD layer, are evident.

3.2. Diamond/graphite nanoplatelets hybrids

Interfaces of crystalline diamond and graphene/graphite have been studied theorethically before [65]–[70], in order to gain insights into their mechanisms of formation, stability, expected properties, and possible applications. Some experimental studies regarding their synthesis and fundamental properties were also conducted [71]–[73]. NCD/graphite multilayer structures, obtained after thermal annealing of nanodiamond particles in vacuum, were observed to greatly influence the electric conductivity and field electron emission characteristics of these structures [71]. Hence, this class of hybrids is interesting for applications in micro and nanoelectronics [71], [72]. Recently, diamond/graphite hybrids were employed as electrodes for trace-level detection of heavy metal ions, providing low background currents and detection limit, as well as good sensor linearity within the 10 ppb to 1 ppm range [73].

The proper combination of nanographite and nanodiamond allotropes in a hybrid could unite important physico-chemical properties, such as mechanical strength and electrical conductivity, whilst retaining chemical stability and biocompatibility in a wide range of conditions generally attributed to both allotropes. A particularly interesting morphology of these hybrids synthesized by our group are the diamond-graphite nanoplatelets (DGNP), which can be obtained via high temperature (> 1000 ºC) MPCVD in a single-step procedure, using appropriate growth parameteres without the need of catalysts [20]–[23].

SEM images of the DGNP hybrids (**Figure 3-a**) depict a porous-like structure defined by nearly vertically-aligned nanoplatelets. The platelets are about 100 nm thick, with lengths of about 1-2 μm, having walls and top edges covered with irregular, non-faceted particulates. Transmission Electron Microscopy (TEM) observations (**Figure 3-b – d**) clarify the allotrope arrangement in the DGNP, which is composed of a thin (<10 nm) inner diamond platelet covered by nanographite grains. The presence of both allotropes was also confirmed via Raman spectroscopy [20]–[22]. Hence, nanodiamond acts as a mechanically strong and chemically stable template onto which the nanographite can be formed, providing electrical conductivity to the hybrid. Interestingly, it has been shown that the addition of N_2 to the H_2/CH_4 growth chemistry greatly increases the DGNP film electrical conductivity (by more than one order of magnitude), associated to a better crystallinity degree of the nanographite phase, while also promoting the vertical growth of the platelets [22].

These materials have been studied in a wide range of applications with promising results regarding their multifunctionality. The preferential vertical alignment and particular arrangement of the sp^2 and sp^3 carbon allotropes of the DGNPs presents two main advantages compared to smooth films, namely a much higher surface area and sharp edges. Vertically-aligned nanocarbons, in general, are of interest for electrochemistry, as, for example, bio-analytical surfaces [74] or enzyme-free amperometric biosensors for glucose and dopamine [75], [76]. Similar arguments led to the widespread application of vertically-aligned nanocarbons in field emission studies, given that the ridge geometry is known to lower the turn-on electrical fields for electron ejection to vacuum [77], [78]. Another application area where this material can play an important role is heat management. In particular, our group has shown that DGNP coatings improve heat dissipation compared to smooth nanodiamond, enhancing the heat flux from heated surfaces under natural convection-governed conditions [21]. This effect is expected to be more pronounced in forced convection conditions due to added turbulence on the high aspect ratio DGNPs. Hence, the morphostructural aspects of these hybrids, combined with their low production cost, thickness, and weight, are conceptually appealing to be employed as heat dissipators in miniaturized, high-power density devices such as computer chips. Taking advantage of the conductivity provided by nanographite, DGNP are shown to be an interesting alternative in the field of biomedical applications (**Figure 4**). Indeed, the DGNP films provide a high degree of biocompatibility concerning eukaryotic preosteoblastic cells [22] (see viability in **Figure 4-a**, at the bottom). Furthermore, the films' electric characteristics allow to build simple prototypes to induce morphological and functional alterations in cells, such as induced differentiation as well as increased proliferation and metabolic activity (see proliferation and metabolic activity (MTT) in **Figure 5-a**, at the bottom), thus constituting an interesting platform for tissue regeneration and growth purposes [22].

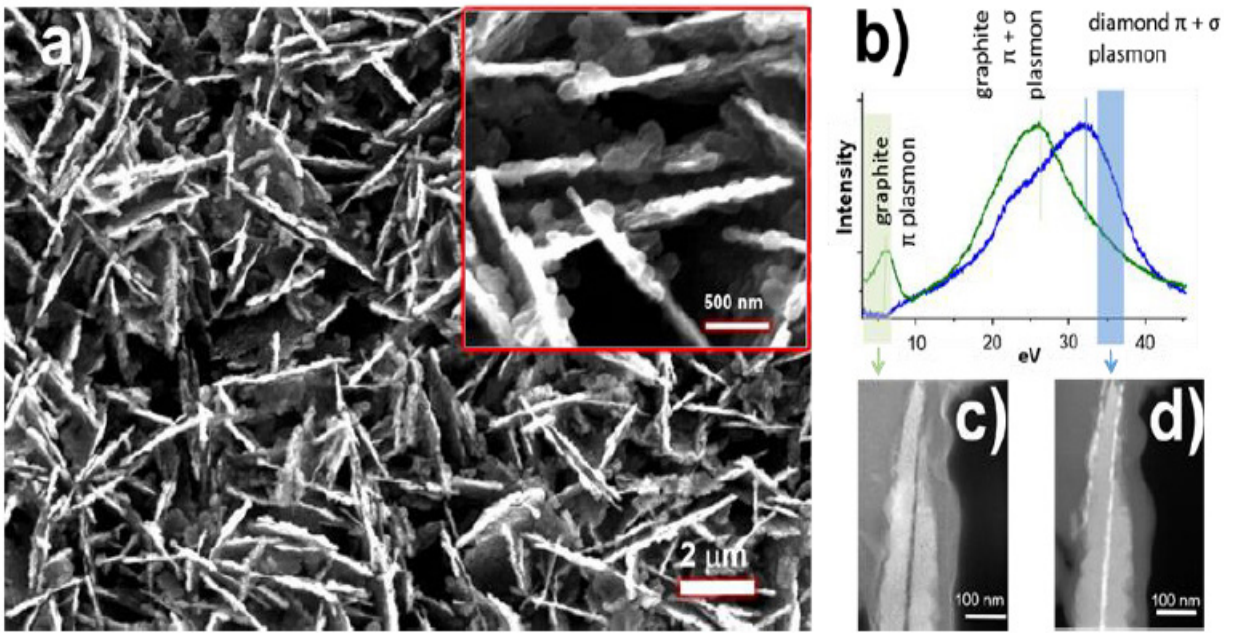

Figure 3. a) SEM micrographs of DGNP thin films. b) Low energy region of the electron energy loss spectra acquired from a nanographite (green) and nanodiamond (blue) sites. Energy windows are adequately chosen to form the energy-filtered images of c) and d), where the brighter contrast identifies nanographite and nanodiamond, respectively.

DGNPs have also shown an interesting electrochemical response, particularly concerning stability, reproducibility and fast faradaic electron transfer rates (faster than other carbons in the literature, such as some types of CNTs, glassy carbon, and graphene) [23]. Using the biotin-avidin affinity pair, biotin-functionalized DGNP electrodes are able to quantify avidin molecules at nM levels (**Figure 4-b**, at the bottom) using electron impedance spectroscopy (EIS, see **Figure 4-b**, at the top). Although several aspects can be further optimized, the results are encouraging regarding the fabrication of simple and efficient electrochemical biosensors for the point-of-care detection of several analytes, from cancer biomarkers to biological cells [23].

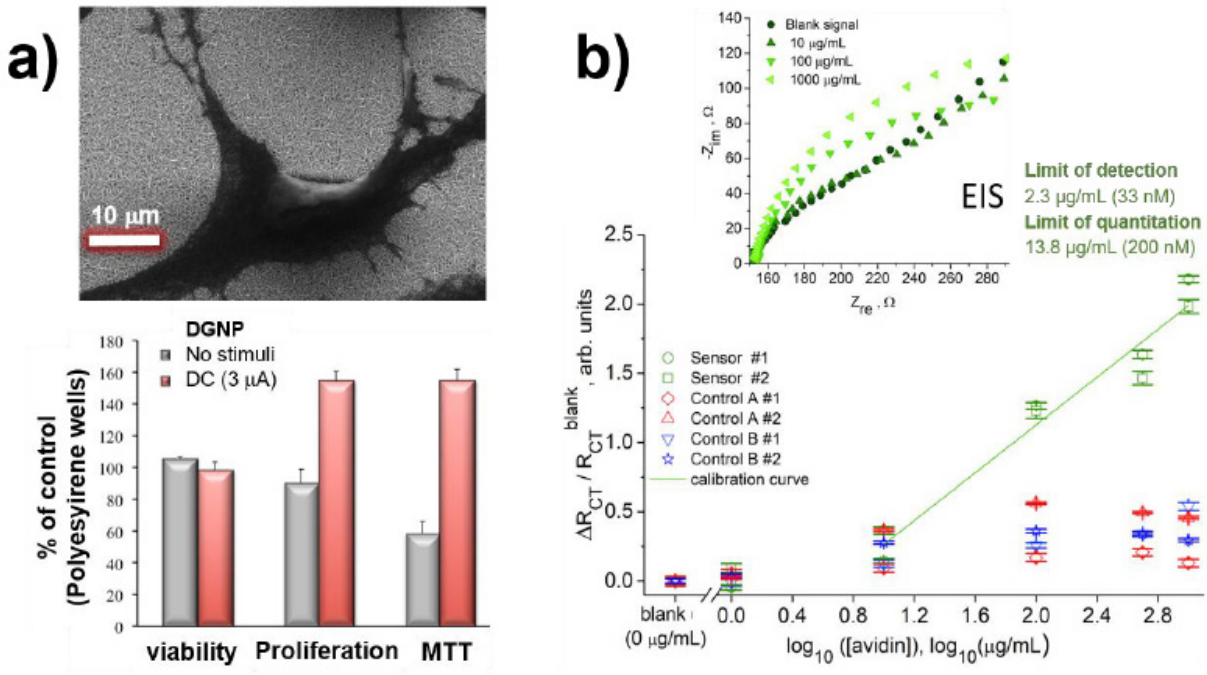

Figure 4. Biomedical applications of DGNP films. a) Top: SEM micrograph of a murine MC3T3-E1 preosteoblast (mouse bone-forming cell) adhered to DGNP substrates. Bottom: MC3T3-E1 cell viability, proliferation and metabolic activity calculated via MTT (3-(4,5-dimethylthiazol-2-yl)-2,5-diphenyltetrazolium bromide) test, expressed as function of percentage of control (standard cell culture plates). The cells were cultured on DGNP substrates with and without application of DC periodic stimuli.

b) Top: EIS spectra of biotin-functionalized DGNP electrodes after incubation in solutions of different concentrations of avidin in phosphate buffer saline. Bottom: From the EIS spectra, charge transfer resistances (RCT) values can be extracted and used to produce the calibration curve (at green), which clearly differentiates from control samples after incubation in avidin solutions.

3.3. Graphene/diamond hybrids

Catalytic graphene synthesis on copper substrates is one of the most successful routes to produce high-quality single layer graphene films [79]–[81]. In the pursuit of a way to promote a faster alternative to conventional thermal CVD, our group tried to explore the high efficiency in the dissociation of gaseous species in the plasma of the MPCVD technique. This improved efficiency in creating highly reactive carbon radical species was also expected to allow for a decrease in the substrate temperature. However, the first attempts revealed that it was still necessary to have the copper substrates close to the melting point, at around 1000 °C, to be able to deposit graphene by this technique. More interestingly, in certain conditions, we found that besides the multilayer graphene films that can be obtained by this technique [82], [83] with very short growth times in the minute range, nanocrystalline diamond clusters appeared sprinkled all over the surface of the sample [17]. These clusters are dome-like structures of diamond that, with increasing growth time, evolve into flower-like clusters with diamond petals (**Figure 5-a**). The linkage between these cluster and graphene was found to be a strong covalent bonding between the sp2 multilayer graphene films and the sp3 diamond clusters, as can be observed in the TEM micrograph in **Figure 5-b**. Micro Raman spectroscopy allows for the specific identification and characterization of the two allotropic phases, with graphene exhibiting strong G and 2D peaks, as well as a non-negligible D peak, associated to disorder and defects (**Figure 5-c**). In this case, due to the narrow FWHM of the bands, that should increase with disorder, we believe that the fact that the hybrid is formed in a highly reactive hydrogen plasma induces a certain degree of hydrogenation of the sp2 phase of this hybrid. These hydrogen plasma conditions are also what contributes to the simultaneous growth of diamond with graphene. In terms of applications for this material, we explored its potential use as cold-cathode field emitter [24]. Diamond has a negative electron affinity [84], which makes it a good candidate for electron emission under an applied electric field. However, due to its poor electrical conduction properties, charge injection is a challenge. So, to supress this hindrance, the covalently bound graphene should allow a good charge transfer to the diamond clusters, while the latter would act as the electrode emitters. To better control the density of diamond without increasing

too much the number of graphene layers, a pulsed methane deposition was explored. As sp3 carbon bonds are more stable to the etching produced by the hydrogen radicals during growth than their sp2 counterparts [29, p. 59], [85], by controlling the methane to hydrogen ratio it is possible to tune the etching or growth of graphene. Thus, diamond growth is promoted in hydrogen-rich atmospheres, while graphene is etched in the same conditions. So, a phased growth with alternating periods with and without methane flow allows the growth of diamond clusters without the formation of graphite. The field emission properties of these hybrids were explored for different cluster sizes and densities and it was found that, by fitting the emission with a Fowler–Nordheim relationship, there were two emission mechanisms: one from the diamond cluster and another from the edges and defects of the underlying graphene film.

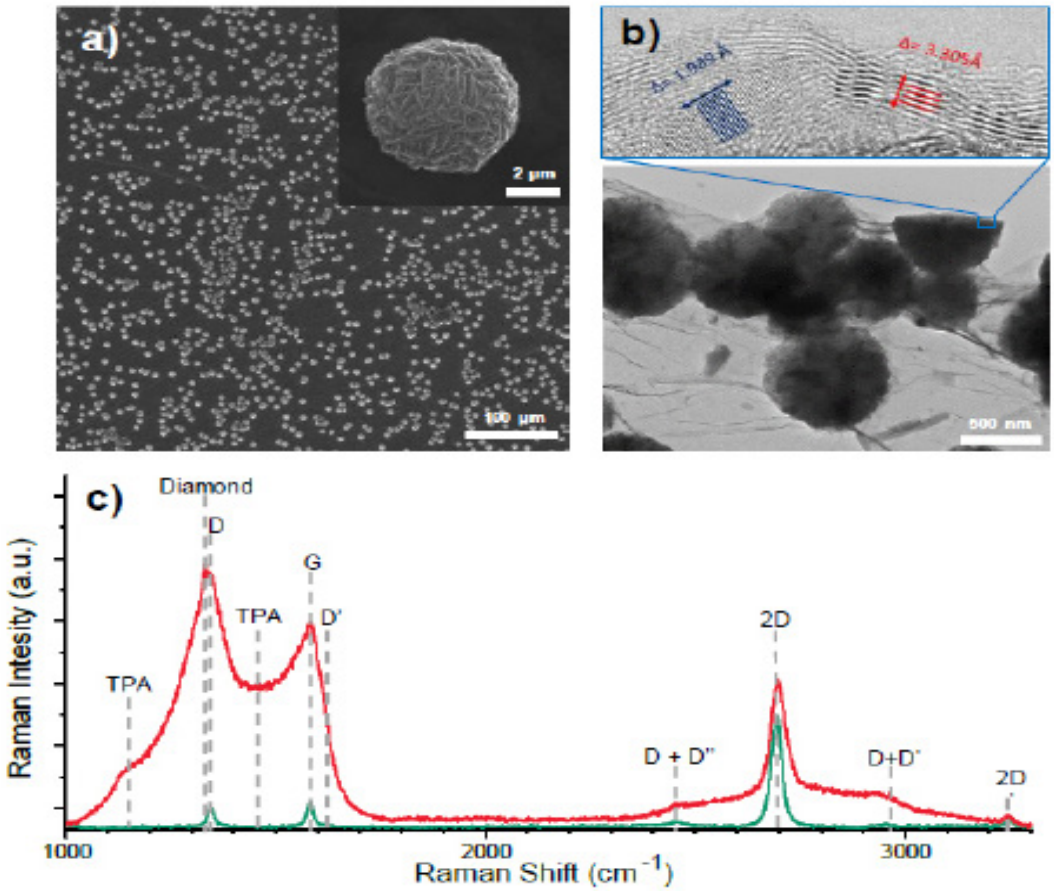

Figure 5. a) Raman spectra of the graphene/diamond hybrids (GDH). Red represents the spectrum over a diamond cluster, with some contribution from the underlying graphene while green is a spectrum from the graphene sheet. b) TEM micrographs of the hybrids, with a detailed region showing epitaxy between the diamond (111) planes and graphene basal plane. c) SEM micrographs of a hybrid film over copper with the diamond clusters sprinkled over the graphene. The inset shows the structure of a cluster after a long deposition run.

4. Other carbon-based materials

4.1 CVD Graphene

Graphene, a single-atom-thick sheet of sp2-bonded carbon atoms arranged in a honeycomb pattern [86], is known for its wide range of outstanding properties and characteristics, from extremely high electron mobility [81], [87] and impressive thermal conductivity [88], to a large Young's modulus and intrinsic tensile strength [89].

This material has been playing an important role in our group's research efforts for the last several years. CVD is the employed technique for the growth of graphene, building on our experience in CVD synthesis of carbon-based nanomaterials. The growth is performed on copper substrates which act as a catalyst, at temperatures close to its melting point. The heating of the substrate can be achieved by means of a plasma, resistive heating, or induction. A typical CVD growth process of graphene consists of a controlled heating stage, followed by an annealing of the substrate (typically in a reducing atmosphere) to clean its surface and promote grain reorientation and growth, with a subsequent growth stage in which the carbon precursor is introduced into the reactor, and finished with a cooling stage which can either be fast or controlled [44].

Regarding the synthesis process itself, we have focused on optimising the process parameters. In particular, attention was given to the treatment of the substrate, which led to a low graphene nucleation density and, consequently, millimetre-sized large single-crystal domains (**Figure 6**).

The application of CVD grown graphene in a wide range of devices has been an important focal point of our group's research. Suspended graphene membranes have been employed for the transduction of acoustic waves into an electrical signal in graphene-based microphones. The use of CVD graphene for fast and broadband third-harmonic generation is

also being explored, as are impedimetric biosensors using CVD graphene as a sensing platform.

In summary, the unique properties of graphene make it a highly attractive material for a wide spectrum of applications, with CVD synthesis being a particularly useful tool for the development of these applications, thanks to its ability to grow high quality graphene in fairly large quantities.

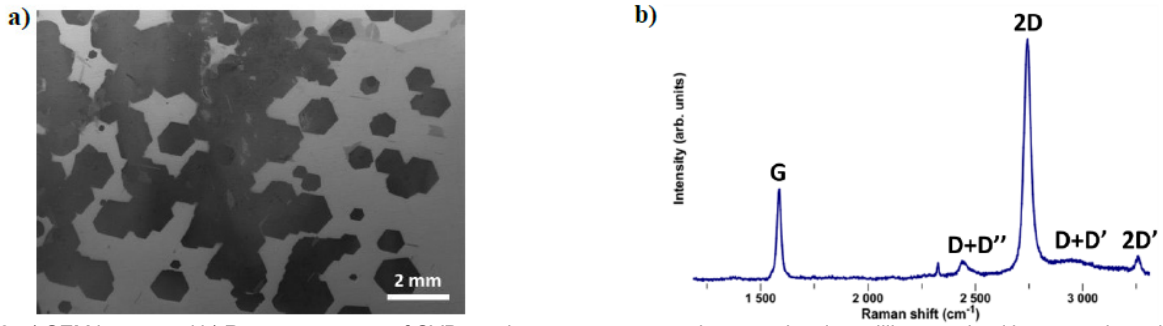

Figure 6. a) SEM image and b) Raman spectrum of CVD graphene on a copper substrate, showing millimetre-sized hexagonal graphene domains and a spectrum typical of single-layer graphene.

4.2 Laser-Induced Graphene

In many applications, non-pristine graphene-based materials are interesting, either because of characteristics conferred by the presence of defects, such as hydrophilicity due to a high degree of oxidation of the material, or by the ease of production and ability to directly pattern a device onto a substrate. Historically, the majority of such materials are chemically exfoliated graphene oxides (GO), that may or may not be reduced to form a less defective reduced graphene oxide (rGO) [90]–[93]. However, there is an alternative method to produce graphene foams with properties similar to rGO that relies simply on the irradiation of an organic material with a laser. This material, known as Laser-Induced Graphene (LIG) can be produced using a wide range of laser sources and relies on the rapid heating of a polymer, usually polyimide, and subsequent release of gases trough the dissociation of its molecular bonds and formation of a localized plasma at the surface of the polymer [25], [94]. This quick release creates a porous network (**Figure 7-a**) of multilayer graphene sheets with a low oxygen content, similarly to rGO, as can be attested by Raman spectroscopy in **Figure 7-b**. The ability to pattern virtually any geometry of a conductive graphene foam over an insulating platform hints at the large potential of this technique in the production of sensors. Traditionally, this material is produced using a CO2 laser (10600 nm), but our group showed that it is possible to produce LIG with a 355 nm laser, with higher resolution and lower depth of penetration into the polymer [25]. With this material we produced piezoresistive strain gauges and explored their applications in health monitoring, namely on the detection of the arterial pressure waveform (**Figure 7-c**). Some of the ongoing works are focused on the usage of LIG as a platform for electrochemical biosensors.

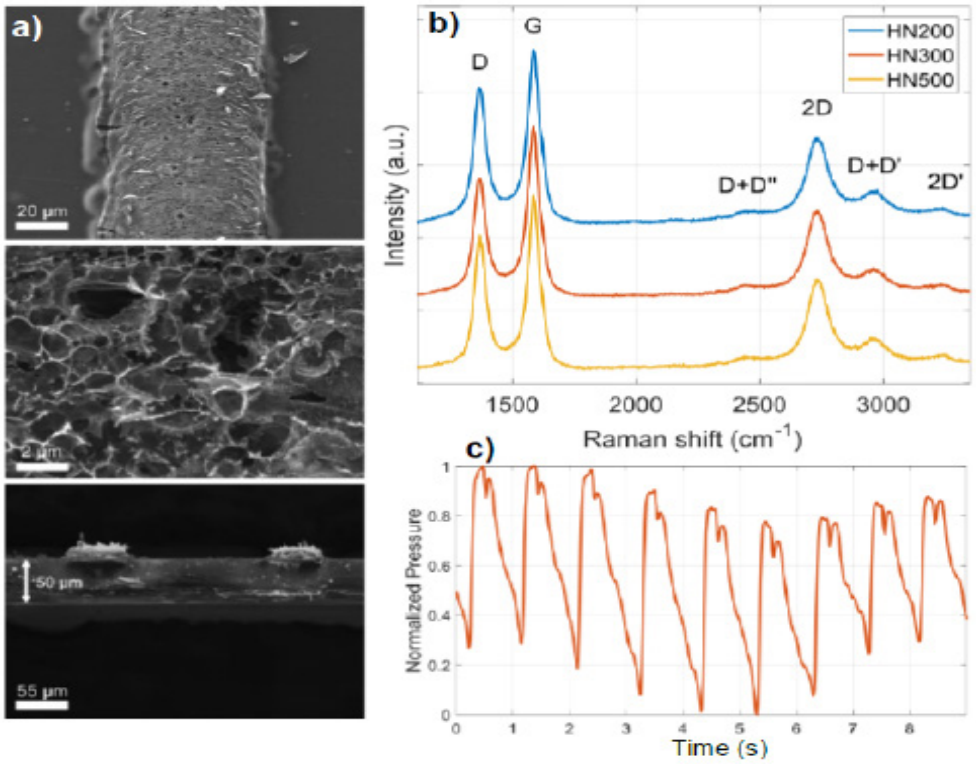

Figure 7. a) Raman spectra of LIG produced in Kapton with different thicknesses, showing an independence of the substrate thickness to the quality of the produce foam. b) Arterial pressure wave as measured by a LIG strain gauge at the carotid. c) SEM micrographs of a LIG stripe over Kapton. The last figure is a cross section image showing the short penetration length.

5. Conclusion

The large variety of carbon-based allotropes, with different properties and characteristics, allows to explore them for a wide range of applications. But perhaps more interestingly, the ability to synthesize hybrids based on a close interplay between these allotropes expands the possibilities offered by carbon nanomaterials, through combination of complementary properties of the different phases. In this brief review, our work on carbon-based nanomaterials, with a particular focus on hybrids, has been presented, along with the conditions and underlying processes inherent to their synthesis, their properties, and their potential applications. In particular, the importance of chemical vapour deposition as a versatile synthesis technique that allows for an overlap between the growth conditions' windows for each allotrope has been highlighted. Moreover, ongoing work on other novel carbon materials, such as CVD-grown and laser-induced graphene has been presented. Thus, and on the basis of the results shown here, it is our belief that this field continues to offer a lot to explore, from growth studies to practical applications.

References

[1] A. J. S. Fernandes, M. A. Neto, F. A. Almeida, R. F. Silva, and F. M. Costa, "Nano- and micro-crystalline diamond growth by MPCVD in extremely poor hydrogen uniform plasmas," Diam. Relat. Mater., vol. 16, no. 4-7 SPEC. ISS., pp. 757–761, 2007.

[2] J. E. Butler and A. V. Sumant, "The CVD of nanodiamond materials," Chem. Vap. Depos., vol. 14, no. 7-8 SPEC. ISS., pp. 145–160, 2008.

[3] P. Hess, "The mechanical properties of various chemical vapor deposition diamond structures compared to the ideal single crystal," J. Appl. Phys., vol. 111, no. 5, 2012.

[4] F. G. Silva, M. A. Neto, A. J. S. Fernandes, F. M. Costa, F. J. Oliveira, and R. F. Silva, "Adhesion and wear behaviour of NCD coatings on Si3N4 by micro-abrasion tests," J. Nanosci. Nanotechnol., vol. 9, no. 6, pp. 3938–3943, 2009.

[5] M. A. Neto, A. J. S. Fernandes, R. F. Silva, and F. M. Costa, "Nucleation of nanocrystalline diamond on masked/unmasked Si3N4 ceramics with different mechanical pretreatments," Diam. Relat. Mater., vol. 17, no. 4–5, pp. 440–445, 2008.

[6] M. Amaral, F. J. Oliveira, M. Belmonte, A. J. S. Fernandes, F. M. Costa, and R. F. Silva, "Tailored Si3N4 ceramic substrates for CVD diamond coating," Surf. Eng., vol. 19, no. 6, pp. 410–416, 2003.

[7] A. Tallaire, V. A. Silva, A. J. S. Fernandes, F. M. Costa, and R. F. Silva, "Effect of intergranular phase of Si3N4 substrates on MPCVD diamond deposition," Surf. Coatings Technol., vol. 151–152, pp. 521–525, 2002.

[8] F. J. G. Silva, A. J. S. Fernandes, F. M. Costa, V. Teixeira, A. P. M. Baptista, and E. Pereira, "Tribological behaviour of CVD diamond films on steel substrates," Wear, vol. 255, no. 7–12, pp. 846–853, 2003.

[9] F. J. G. Silva, A. P. M. Baptista, E. Pereira, V. Teixeira, Q. H. Fan, A. J. S. Fernandes, and F. M. Costa, "Microwave plasma chemical vapour deposition diamond nucleation on ferrous substrates with Ti and Cr interlayers," Diam. Relat. Mater., vol. 11, no. 9, pp. 1617–1622, 2002.

[10] P. Miranzo, M. I. Osendi, E. Garcia, A. J. S. Fernandes, V. A. Silva, F. M. Costa, and R. F. Silva, "Thermal conductivity enhancement in cutting tools by chemical vapor deposition diamond coating," Diam. Relat. Mater., vol. 11, no. 3–6, pp. 703–707, 2002.

[11] V. Silva, A. J. S. Fernandes, F. M. Costa, J. Sacramento, and R. F. Silva, "Abrasive resistance of CVD diamond brazed thick films in machining of WC pre-sintered forms," Key Eng. Mater., vol. 230–232, pp. 193–196, 2002.

[12] E. Salgueiredo, F. A. Almeida, M. Amaral, A. J. S. Fernandes, F. M. Costa, R. F. Silva, and F. J. Oliveira, "CVD micro/nanocrystalline diamond (MCD/NCD) bilayer coated odontological drill bits," Diam. Relat. Mater., vol. 18, no. 2–3, pp. 264–270, 2009.

[13] E. Salgueiredo, M. Vila, M. A. Silva, M. A. Lopes, J. D. Santos, F. M. Costa, R. F. Silva, P. S. Gomes, and M. H. Fernandes, "Biocompatibility evaluation of DLC-coated Si3N4 substrates for biomedical applications," Diam. Relat. Mater., vol. 17, no. 4–5, pp. 878–881, 2008.

[14] M. Amaral, E. Salgueiredo, F. J. Oliveira, A. J. S. Fernandes, F. M. Costa, and R. F. Silva, "NCD by HFCVD on a Si3N4-bioglass composite for biomechanical applications," Surf. Coatings Technol., vol. 200, no. 22-23 SPEC. ISS., pp. 6409–6413, 2006.

[15] A. J. S. Fernandes, E. Salgueiredo, F. J. Oliveira, R. Silva, and F. M. Costa, "Directly MPCVD diamond-coated Si3N4 disks for dental applications," Diam. Relat. Mater., vol. 14, no. 3–7, pp. 626–630, 2005.

[16] A. J. S. Fernandes, M. Pinto, M. A. Neto, F. J. Oliveira, R. F. Silva, and F. M. Costa, "Nano carbon hybrids from the simultaneous synthesis of CNT/NCD by MPCVD," Diam. Relat. Mater., vol. 18, no. 2–3, pp. 160–163, 2009.

[17] A. F. Carvalho, T. Holz, N. F. Santos, M. C. Ferro, M. A. Martins, A. J. S. Fernandes, R. F. Silva, and F. M. Costa, "Simultaneous CVD synthesis of graphene-diamond hybrid films," Carbon N. Y., vol. 98, no. November, pp. 99–105, 2016.

[18] T. Holz, D. Mata, N. F. Santos, I. Bdikin, A. J. S. Fernandes, and F. M. Costa, "Stiff Diamond/Buckypaper Carbon Hybrids," ACS Appl. Mater. Interfaces, vol. 6, no. 24, pp. 22649–22654, Dec. 2014.

[19] A. L. Horovistiz, A. J. S. Fernandes, R. F. Silva, and F. M. Costa, "Quantification of microstructural features in carbon nanotube/nanodiamond hybrids," Microsc. Microanal., vol. 18, no. SUPPL.5, pp. 85–86, 2012.

[20] N. F. Santos, A. Fernandes, T. Holz, R. F. Silva, and F. M. Costa, "Simultaneous CVD growth of nanostructured carbon hybrids," in Nanoscience Advances in CBRN Agents Detection, Information and Energy Security, P. Petkov, D. Tsiulyanu, W. Kulisch, and C. Popov, Eds. Springer Netherlands, 2015, pp. 111–117.

[21] N. F. Santos, T. Holz, T. Santos, A. J. S. Fernandes, T. L. Vasconcelos, C. P. Gouvea, B. S. Archanjo, C. A. Achete, R. F. Silva, and F. M. Costa, "Heat Dissipation Interfaces Based on Vertically Aligned Diamond/Graphite Nanoplatelets," ACS Appl. Mater. Interfaces, vol. 7, pp. 24772–24777, 2015.

[22] N. F. Santos, M. Cicuéndez, T. Holz, V. S. Silva, A. J. S. Fernandes, M. Vila, and F. M. Costa, "Diamond-Graphite Nanoplatelet Surfaces as Conductive Substrates for the Electrical Stimulation of Cell Functions," Appl. Mater. Interfaces, vol. 9, no. 2, pp. 1331–1342, Jan. 2017.

[23] N. F. Santos, S. O. Pereira, A. J. S. Fernandes, T. L. Vasconcelos, C. M. Fung, B. S. Archanjo, C. A. Achete, S. R. Teixeira, R. F. Silva, and F. M. Costa, "Physical Structure and Electrochemical Response of Diamond-Graphite Nanoplatelets: From CVD Synthesis to Label-Free Biosensors," ACS Appl. Mater. Interfaces, vol. 11, no. 8, pp. 8470–8482, Feb. 2019.

[24] N. F. Santos, U. Zubets, A. F. Carvalho, A. J. S. Fernandes, L. Pereira, and F. M. Costa, "Tuning the field emission of graphene-diamond hybrids by pulsed methane flow CVD," Carbon N. Y., vol. 122, pp. 726–736, 2017.

[25] A. F. Carvalho, A. J. S. Fernandes, C. Leitão, J. Deuermeier, A. C. Marques, R. Martins, E. Fortunato, and F. M. Costa, "Laser-Induced Graphene Strain Sensors Produced by Ultraviolet Irradiation of Polyimide," Adv. Funct. Mater., vol. 28, no. 52, pp. 1–8, 2018.

[26] J. Rodrigues, J. Zanoni, G. Gaspar, A. J. S. Fernandes, A. F. Carvalho, N. F. Santos, T. Monteiro, and F. M. Costa, "ZnO decorated laser-induced graphene produced by direct laser scribing," Nanoscale Adv., vol. 1, no. 8, pp. 3252–3268, 2019.

[27] J. Rodrigues, D. Mata, A. J. S. Fernandes, M. A. Neto, R. F. Silva, T. Monteiro, and F. M. Costa, "ZnO nanostructures grown on vertically aligned carbon nanotubes by laser-assisted flow deposition," Acta Mater., vol. 60, no. 13–14, pp. 5143–5150, 2012.

[28] J. Rodrigues, D. Mata, A. Pimentel, D. Nunes, R. Martins, E. Fortunato, A. J. Neves, T. Monteiro, and F. M. Costa, "One-step synthesis of ZnO decorated CNT buckypaper composites and their optical and electrical properties," Mater. Sci. Eng. B Solid-State Mater. Adv. Technol., vol. 195, pp. 38–44, 2015.

[29] H. Liu and D. S. Dandy, Diamond Chemical Vapor Deposition: Nucleation and Early Growth Stages. New Jersey, U.S.A.: Noyes Publications, 1995.

[30] Y. I. Zhang, L. Zhang, and C. Zhou, "Review of chemical vapor deposition of graphene and related applications," Acc. Chem. Res., vol. 46, no. 10, pp. 2329–2339, 2013.

[31] V. Baranauskas, H. J. Ceragioli, A. C. Peterlevitz, M. C. Tosin, and S. F. Durrant, "Effects of argon dilution of an ethanol/hydrogen gas feed on the growth of diamond by hot-filament chemical vapor deposition," Thin Solid Films, vol. 377, no. 378, pp. 303–308, 2000.

[32] L. Yang, C. Jiang, S. Guo, L. Zhang, J. Gao, J. Peng, T. Hu, and L. Wang, "Novel Diamond Films Synthesis Strategy: Methanol and Argon Atmosphere by Microwave Plasma CVD Method Without Hydrogen," Nanoscale Res. Lett., vol. 11, no. 1, pp. 4–9, 2016.

[33] T. H. Chein and Y. Tzeng, "CVD diamond grown by microwave plasma in mixtures of acetone/oxygen and acetone/carbon dioxide," Diam. Relat. Mater., vol. 8, no. 8–9, pp. 1393–1401, 1999.

[34] J. Morales, M. Apátiga, and V. M. Castaño, "Growth of Diamond Films from Tequila," vol. 21, pp. 134–138, 2008.

[35] J. E. Butler, Y. A. Mankelevich, A. Cheesman, J. Ma, and M. N. R. Ashfold, "Understanding the chemical vapor deposition of diamond: Recent progress," J. Phys. Condens. Matter, vol. 21, no. 36, 2009.

[36] I. Vlassiouk, M. Regmi, P. Fulvio, S. Dai, P. Datskos, G. Eres, and S. Smirnov, "Role of hydrogen in chemical vapor deposition growth of large single-crystal graphene," ACS Nano, vol. 5, no. 7, pp. 6069–6076, 2011.

[37] B. J. Jones, S. Wright, R. C. Barklie, J. Tyas, J. Franks, and A. J. Reynolds, "Nanostructure and paramagnetic centres in diamond-like carbon: Effect of Ar dilution in PECVD process," Diam. Relat. Mater., vol. 17, no. 7–10, pp. 1629–1632, 2008.

[38] J. Stiegler, T. Lang, M. Nygård-Ferguson, Y. Von Kaenel, and E. Blank, "Low temperature limits of diamond film growth by microwave plasma-assisted CVD," Diam. Relat. Mater., vol. 5, no. 3–5, pp. 226–230, 1996.

[39] A. L. Vikharev, A. M. Gorbachev, M. A. Lobaev, A. B. Muchnikov, D. B. Radishev, V. A. Isaev, V. V. Chernov, S. A. Bogdanov, M. N. Drozdov, and J. E. Butler, "Novel microwave plasma-assisted CVD reactor for diamond delta doping," Phys. Status Solidi - Rapid Res. Lett., vol. 10, no. 4, pp. 324–327, 2016.

[40] D. Wei, Y. Liu, Y. Wang, H. Zhang, L. Huang, and G. Yu, "Synthesis of N-Doped Graphene by Chemical Vapor Deposition and Its Electrical Properties," Nano Lett., vol. 9, no. 5, pp. 1752–1758, May 2009.

[41] Y. Chakk, R. Brener, and A. Hoffman, "Enhancement of diamond nucleation by ultrasonic substrate abrasion with a mixture of metal and diamond particles," Appl. Phys. Lett., vol. 66, no. 21, pp. 2819–2821, 1995.

[42] M. Amaral, A. J. S. Fernandes, M. Vila, F. J. Oliveira, and R. F. Silva, "Growth rate improvements in the hot-filament CVD deposition of nanocrystalline diamond," Diam. Relat. Mater., vol. 15, no. 11-12 SPEC. ISS., pp. 1822–1827, 2006.

[43] L. Marty, A. Iaia, M. Faucher, V. Bouchiat, C. Naud, M. Chaumont, T. Fournier, and A. M. Bonnot, "Self-assembled single wall carbon nanotube field effect transistors and AFM tips prepared by hot filament assisted CVD," Thin Solid Films, vol. 501, no. 1–2, pp. 299–302, 2006.

[44] R. Muñoz and C. Gómez-Aleixandre, "Review of CVD synthesis of graphene," Chem. Vap. Depos., vol. 19, no. 10–12, pp. 297–322, 2013.

[45] X. Li, W. Cai, J. An, S. Kim, J. Nah, D. Yang, R. Piner, A. Velamakanni, I. Jung, E. Tutuc, S. K. S. K. Banerjee, L. Colombo, and R. S. R. S. Ruoff, "Large-area synthesis of high-quality and uniform graphene films on copper foils," Science (80-.)., vol. 324, no. 5932, p. 1312, Jun. 2009.

[46] M. Kamo, Y. Sato, S. Matsumoto, and N. Setaka, "Diamond synthesis from gas phase in microwave plasma," J. Cryst. Growth, vol. 62, no. 3, pp. 642–644, 1983.

[47] M. Meyyappan, "A review of plasma enhanced chemical vapour deposition of carbon nanotubes," J. Phys. D. Appl. Phys., vol. 42, no. 21, 2009.

[48] C. J. Tang, A. J. S. Fernandes, F. Costa, and J. L. Pinto, "Effect of microwave power and nitrogen addition on the formation of {100} faceted diamond from microcrystalline to nanocrystalline," Vacuum, vol. 85, no. 12, pp. 1130–1134, 2011.

[49] R. Piner, H. Li, X. Kong, L. Tao, I. N. Kholmanov, H. Ji, W. H. Lee, J. W. Suk, J. Ye, Y. Hao, S. Chen, C. W. Magnuson, A. F. Ismach, D. Akinwande, and R. S. Ruoff, "Graphene synthesis via magnetic inductive heating of copper substrates," ACS Nano, vol. 7, no. 9, pp. 7495–7499, 2013.

[50] L. Tao, J. Lee, H. Li, R. D. Piner, R. S. Ruoff, and D. Akinwande, "Inductively heated synthesized graphene with record transistor mobility on oxidized silicon substrates at room temperature," Appl. Phys. Lett., vol. 103, no. 18, 2013.

[51] F. J. Derbyshire, A. E. B. Presland, and D. L. Trimm, “Graphite formation by the dissolution-precipitation of carbon in cobalt, nickel and iron,” Carbon N. Y., vol. 13, no. 2, pp. 111–113, 1975.

[52] Q. Yu, J. Lian, S. Siriponglert, H. Li, Y. P. Chen, and S. S. Pei, “Graphene segregated on Ni surfaces and transferred to insulators,” Appl. Phys. Lett., vol. 93, no. 11, pp. 1–4, 2008.

[53] M. Wang and P. K. Chu, “Nanocrystalline Diamond Coatings,” in Encyclopedia of Plasma Technology - Two Volume Set, J. L. Shohet, Ed. CRC Press, 2016, pp. 857–873.

[54] P. W. May and Y. A. Mankelevich, “From ultrananocrystalline diamond to single crystal diamond growth in hot filament and microwave plasma-enhanced CVD reactors: A unified model for growth rates and grain sizes,” J. Phys. Chem. C, vol. 112, no. 32, pp. 12432–12441, 2008.

[55] P. W. May and Y. A. Mankelevich, “Experiment and modeling of the deposition of ultrananocrystalline diamond films using hot filament chemical vapor deposition and Ar/CH4/H 2 gas mixtures: A generalized mechanism for ultrananocrystalline diamond growth,” J. Appl. Phys., vol. 100, no. 2, 2006.

[56] C. J. Tang, A. J. Neves, S. Pereira, A. J. S. Fernandes, J. Grácio, and M. C. Carmo, “Effect of nitrogen and oxygen addition on morphology and texture of diamond films (from polycrystalline to nanocrystalline),” Diam. Relat. Mater., vol. 17, no. 1, pp. 72–78, 2008.

[57] M. L. Terranova, V. Sessa, and M. Rossi, “The world of carbon nanotubes: An overview of CVD growth methodologies,” Chem. Vap. Depos., vol. 12, no. 6, pp. 315–325, 2006.

[58] M. Kumar and Y. Ando, “Chemical vapor deposition of carbon nanotubes: A review on growth mechanism and mass production,” J. Nanosci. Nanotechnol., vol. 10, no. 6, pp. 3739–3758, 2010.

[59] X. Li, L. Colombo, and R. S. Ruoff, “Synthesis of Graphene Films on Copper Foils by Chemical Vapor Deposition,” Adv. Mater., pp. 6247–6252, 2016.

[60] Q. Li, H. Chou, J.-H. Zhong, J.-Y. Liu, A. Dolocan, J. Zhang, Y. Zhou, R. S. Ruoff, S. Chen, and W. Cai, “Growth of Adlayer Graphene on Cu Studied by Carbon Isotope Labeling,” Nano Lett., vol. 13, no. 2, pp. 486–490, Feb. 2013.

[61] Y. Hao, L. Wang, Y. Liu, H. Chen, X. Wang, C. Tan, S. Nie, J. Won Suk, T. Jiang, T. Liang, J. Xiao, W. Ye, C. R. Dean, B. I. Yakobson, K. F. McCarty, P. Kim, J. Hone, et al., “Oxygen-activated growth and bandgap tunability of large single-crystal bilayer graphene,” Nat. Nanotechnol., vol. 11, no. 5, pp. 426–431, 2016.

[62] A. N. Obraztsov, E. A. Obraztsova, A. V. Tyurnina, and A. A. Zolotukhin, “Chemical vapor deposition of thin graphite films of nanometer thickness,” Carbon N. Y., vol. 45, no. 10, pp. 2017–2021, 2007.

[63] M. Yudasaka, R. Kikuchi, T. Matsui, H. Kamo, Y. Ohki, S. Yoshimura, and E. Ota, “Graphite thin film formation by chemical vapor deposition,” Appl. Phys. Lett., vol. 64, no. 7, pp. 842–844, 1994.

[64] A. S. Johansson, J. Lu, and J. O. Carlsson, “TEM investigation of CVD graphite on nickel,” Thin Solid Films, vol. 252, no. 1, pp. 19–25, 1994.

[65] W. R. L. Lambrecht, C. H. Lee, B. Segall, J. C. Angus, Z. Li, and M. Sunkara, “Diamond nucleation by hydrogenation of the edges of graphitic precursors,” Nature, vol. 364, no. 6438, pp. 607–610, Aug. 1993.

[66] O. Shenderova and D. W. Brenner, “Coexistence Of Two Carbon Phases At Grain Boundaries In Polycrystalline Diamond,” MRS Proc., vol. 442, p. 693, Jan. 1996.

[67] V. M. Ayres, M. Farhan, D. Spach, J. Bobbitt, J. A. Majeed, B. F. Wright, B. L. Wright, J. Asmussen, M. G. Kanatzidis, and T. R. Bieler, “Transitions in morphology observed in nitrogen/methane-hydrogen depositions of polycrystalline diamond films,” J. Appl. Phys., vol. 89, no. 11, pp. 6062–6068, 2001.

[68] A. T. Balaban, D. J. Klein, and C. A. Folden, “Diamond-graphite hybrids,” Chem. Phys. Lett., vol. 217, no. 3, pp. 266–270, Jan. 1994.

[69] Davidson and Pickett, “Graphite-layer formation at a diamond (111) surface step.,” Phys. Rev. B. Condens. Matter, vol. 49, no. 20, pp. 14770–14773, May 1994.

[70] A. De Vita, G. Galli, A. Canning, and R. Car, “A microscopic model for surface-induced diamond-to-graphite transitions,” Nature, vol. 379, no. 6565, pp. 523–526, Feb. 1996.

[71] A. V. Okotrub, L. G. Bulusheva, V. L. Kuznetsov, D. V. Vyalikh, and M. V. Poyguin, “Electronic structure of diamond/graphite composite nanoparticles,” Eur. Phys. J. D, vol. 34, no. 1–3, pp. 157–160, Jul. 2005.

[72] I. I. Vlasov, O. I. Lebedev, V. G. Ralchenko, E. Goovaerts, G. Bertoni, G. Van Tendeloo, and V. I. Konov, “Hybrid diamond-graphite nanowires produced by microwave plasma chemical vapor deposition,” Adv. Mater., 2007.

[73] Y. Guo, N. Huang, B. Yang, C. Wang, H. Zhuang, Q. Tian, Z. Zhai, L. Liu, and X. Jiang, “Hybrid diamond/graphite films as electrodes for anodic stripping voltammetry of trace Ag+ and Cu2+,” Sensors Actuators, B Chem., vol. 231, pp. 194–202, 2016.

[74] W. P. Kang, J. L. Davidson, A. Wisitsora-At, Y. M. Wong, R. Takalkar, K. Holmes, and D. V. Kerns, “Diamond vacuum field emission devices,” in Diamond and Related Materials, 2004, vol. 13, no. 11–12, pp. 1944–1948.

[75] C. Y. Ko, J. H. Huang, S. Raina, and W. P. Kang, “A high performance non-enzymatic glucose sensor based on nickel hydroxide modified nitrogen-incorporated nanodiamonds,” Analyst, vol. 138, no. 11, pp. 3201–3208, Jun. 2013.

[76] S. Raina, “Nanodiamond macroelectrodes and ultramicroelectrode arrays for bio-analyte detection,” Vanderbilt University, 2011.

[77] Y. Tzeng, C. L. Chen, Y. Y. Chen, and C. Y. Liu, “Carbon nanowalls on graphite for cold cathode applications,” Diam. Relat. Mater., vol. 19, no. 2–3, pp. 201–204, 2010.

[78] H. G. Chen and L. Chang, “Growth of diamond nanoplatelets on nanocrystalline diamond substrates,” Diam. Relat. Mater., vol. 18, no. 2–3, pp. 141–145, 2009.

[79] X. Xu, Z. Zhang, J. Dong, D. Yi, J. Niu, M. Wu, L. Lin, R. Yin, M. Li, J. Zhou, S. Wang, J. Sun, X. Duan, P. Gao, Y. Jiang, X. Wu, H. Peng, et al., “Ultrafast epitaxial growth of metre-sized single-crystal graphene on industrial Cu foil,” Sci. Bull., vol. 62, no. 15, pp. 1074–1080, 2017.

[80] Z. Yan, J. Lin, Z. Peng, Z. Sun, Y. Zhu, L. Li, C. Xiang, E. L. Samuel, C. Kittrell, and J. M. Tour, "Toward the Synthesis of Wafer-Scale Single-Crystal Graphene on Copper Foils," ACS Nano, vol. 6, no. 10, pp. 9110–9117, Oct. 2012.

[81] C. Stampfer, F. Haupt, T. Taniguchi, M. Schmitz, L. Banszerus, K. Watanabe, M. Oellers, J. Dauber, S. Engels, and B. Beschoten, "Ultrahigh-mobility graphene devices from chemical vapor deposition on reusable copper," Sci. Adv., vol. 1, no. 6, p. e1500222, 2015.

[82] A. Kumar, A. A. Voevodin, D. Zemlyanov, D. N. Zakharov, and T. S. Fisher, "Rapid synthesis of few-layer graphene over Cu foil," Carbon N. Y., vol. 50, no. 4, pp. 1546–1553, Apr. 2012.

[83] A. Kumar, A. A. a. Voevodin, R. Paul, I. Altfeder, D. Zemlyanov, D. N. N. Zakharov, and T. S. S. Fisher, "Nitrogen-doped graphene by microwave plasma chemical vapor deposition," Thin Solid Films, vol. 528, pp. 269–273, 2013.

[84] J. B. Cui, J. Ristein, and L. Ley, "Electron Affinity of the Bare and Hydrogen Covered Single Crystal Diamond (111) Surface," Phys. Rev. Lett., vol. 81, no. 2, pp. 429–432, Jul. 1998.

[85] M. J. Behr, E. A. Gaulding, K. A. Mkhoyan, and E. S. Aydil, "Hydrogen etching and cutting of multiwall carbon nanotubes," J. Vac. Sci. Technol. B Microelectron. Nanom. Struct., vol. 28, no. 6, p. 1187, 2010.

[86] A. Bianco, H. M. Cheng, T. Enoki, Y. Gogotsi, R. H. Hurt, N. Koratkar, T. Kyotani, M. Monthioux, C. R. Park, J. M. D. Tascon, and J. Zhang, "All in the graphene family - A recommended nomenclature for two-dimensional carbon materials," Carbon, vol. 65. pp. 1–6, 2013.

[87] K. I. Bolotin, K. J. Sikes, Z. Jiang, M. Klima, G. Fudenberg, J. Hone, P. Kim, and H. L. Stormer, "Ultrahigh electron mobility in suspended graphene," 2008.

[88] A. A. Balandin, S. Ghosh, W. Bao, I. Calizo, D. Teweldebrhan, F. Miao, and C. N. Lau, "Superior thermal conductivity of single-layer graphene," Nano Lett., vol. 8, no. 3, pp. 902–907, 2008.

[89] I. W. Frank, D. M. Tanenbaum, A. M. van der Zande, and P. L. McEuen, "Mechanical properties of suspended graphene sheets," J. Vac. Sci. Technol. B Microelectron. Nanom. Struct., vol. 25, no. 6, p. 2558, 2007.

[90] M. Fathy, A. Gomaa, F. A. Taher, M. M. El-Fass, and A. E. H. B. Kashyout, "Optimizing the preparation parameters of GO and rGO for large-scale production," J. Mater. Sci., vol. 51, no. 12, pp. 5664–5675, 2016.

[91] S. Abdolhosseinzadeh, H. Asgharzadeh, and H. S. Kim, "Fast and fully-scalable synthesis of reduced graphene oxide," Sci. Rep., vol. 5, pp. 1–7, 2015.

[92] K. H. Lee, B. Lee, S. J. Hwang, J. U. Lee, H. Cheong, O. S. Kwon, K. Shin, and N. H. Hur, "Large scale production of highly conductive reduced graphene oxide sheets by a solvent-free low temperature reduction," Carbon N. Y., vol. 69, pp. 327–335, 2014.

[93] S. Stankovich, D. A. Dikin, R. D. Piner, K. A. Kohlhaas, A. Kleinhammes, Y. Jia, Y. Wu, S. T. Nguyen, and R. S. Ruoff, "Synthesis of graphene-based nanosheets via chemical reduction of exfoliated graphite oxide," Carbon N. Y., vol. 45, no. 7, pp. 1558–1565, Jun. 2007.

[94] A. R. Cardoso, A. C. Marques, L. Santos, A. F. Carvalho, F. M. Costa, R. Martins, M. G. F. Sales, and E. Fortunato, "Molecularly-imprinted chloramphenicol sensor with laser-induced graphene electrodes," Biosens. Bioelectron., vol. 124–125, pp. 167–175, 2019.

An Overview of CVD Diamond Growth on Ceramics and Synthesis of CNTs at the University of Aveiro

Eduardo Silva[1], Sérgio Pratas[1], aneeta Jaggernauth[1], Ricardo Silva[1], Miguel Neto[1], Filipe Oliveira[1], Rui Silva[1]

[1] CICECO - Aveiro Institute of Materials, Departament of Materials and Ceramic Engineering, University of Aveiro, 3810-193 Aveiro, Portugal

The Carbon and Ceramic Composites Group from the University of Aveiro has been active for almost 25 years, working mostly on applied research. Led by Professor Rui Silva, it all started with a study about the wear properties of tungsten carbide coated CVD diamond [1]. Since then, diamond coatings synthesized by hot filament assisted chemical vapour deposition (HFCVD) became the core developed material both for machining and biological applications, especially due to the simultaneous development of a special silicon nitride (Si_3N_4) composition, an outstanding substrate for CVD diamond coatings due to the strong bonding between both materials. This dual system has found its most notable performance in cutting tools and hip joint prosthetics.

Along with the nanomaterials revolution, the group didn't fall behind and started working on the CVD synthesis of carbon nanotubes (CNTs) as materials with bone growth stimulation properties, and later on, as core electrode materials for electrochemical capacitors. The research on CVD diamond also went a step forward. By doping diamond with boron, it could be used as a semiconducting material, which in combination with its intrinsic chemical inertness, biocompatibility and mechanical robustness, could yield sensors with unique properties for biological and corrosion related applications.

This group along with other colleagues from the University of Aveiro has placed Portugal in the map of CVD diamond research, making it the 15th country worldwide with most published articles on the topic. This has only been possible through the networking efforts and expertise of Prof. Rui Silva and Dr. Filipe Oliveira, along with the ability to fabricate in-house HFCVD reactors, mostly through the skills of Dr. Miguel Neto. The innovation towards higher-end applications such as biosensors and smart regenerative materials didn't stay behind closed doors. By focusing on applied research, the Carbon and Ceramic Composites Group has also contributed for the development of the regional economy through the many partnerships with local industries.

In the following pages, we present a brief overview of the most relevant work that our group has been developing in recent years.

Diamond coatings by HFCVD for tribological applications

Mostly known for great beauty and high value, diamond is a much more important and useful material in a form and scale that departs from the shiny crystals that people tend to admire. Chemical vapor deposition (CVD) is one of the techniques that allow the synthesis of diamond coatings. These are polycrystalline layers where diamond crystallites within the micro- to nanometer range are bound together and can be grown in the form of well adherent and homogeneous coatings. CVD diamond coatings exhibit unique properties such as extreme hardness and thermal conductivity, as well as chemical inertness. These properties make them ideal for harsh mechanical and/or chemical conditions, such as cutting of highly abrasive materials and mechanical seals for pumping of corrosive liquids [2].

H_2 and CH_4 are the most commonly used gas species for diamond growth by hot filament-assisted CVD. The gases require activation, which can be thermally assisted by hot wires at low pressure ranging roughly from 20 to 200 mbar. Following the activation step, the radicals are transported to a previously seeded substrate where diffusion of species occurs. At the growing surface, the hydrogen abstraction reaction is very important to promote the substitution of atomic hydrogen by methyl radicals, resulting in the growth of diamond crystals (Figure 1). Carbide forming substrates are preferred for the growth of CVD diamond, to improve mechanical adhesion, among other reasons. As a pre-conditioning step, substrates are "seeded" with diamond particles that create preferential nucleation spots. The morphology of diamond crystals can be controlled by proper parameter adjustment on the CVD system, allowing the crystallite size to vary within the micrometer to nanometer range (Figure 1).

While microcrystalline diamond (MCD) exhibits overall better adhesion to substrates, its surface is also rougher, which can be a disadvantage. On the other size range, nanocrystalline diamond (NCD) exhibits a much smoother surface but its adhesion is inferior. A typical route to grow nanodiamond crystals is to promote renucleation. Under such conditions, diamond crystals do not grow in the typical columnar structure of MCD, with large crystals, giving place to agglomerates of densely packed diamond nanocrystals instead [32,33].

Adhesion and wear rate are two of the most critical aspects governing the performance and cost/benefit relation of CVD diamond coatings. With this in mind, our group has developed a series of important works in the field of CVD diamond tribology, mainly concerning their application for machining, mechanical seals and biotechnology.

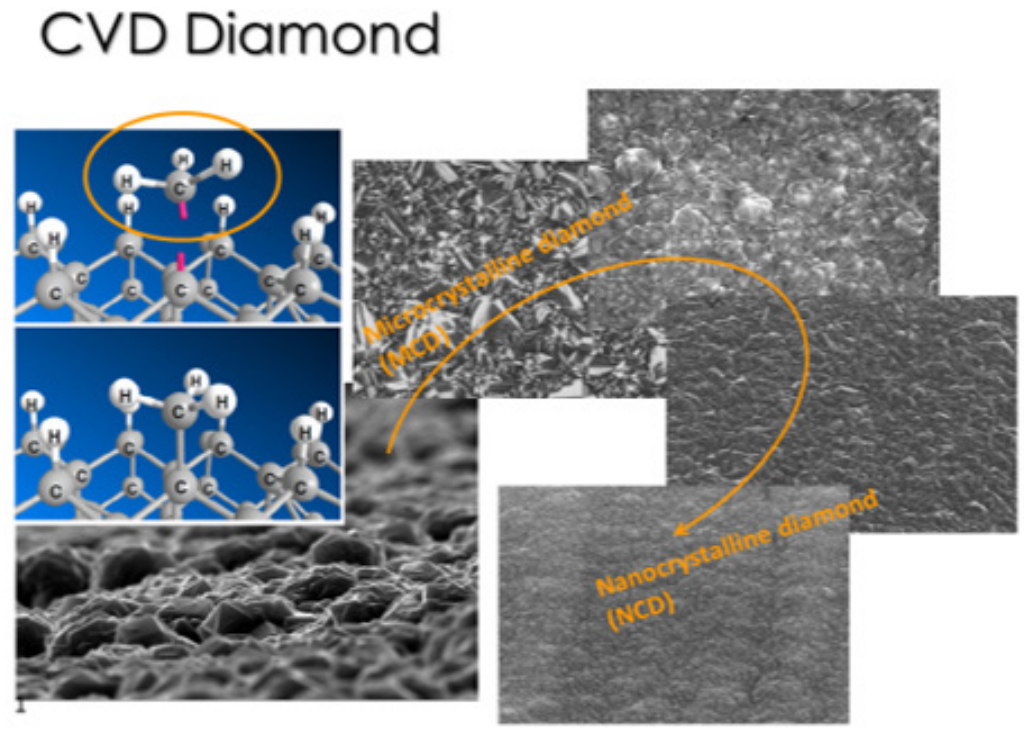

Figure 1. Growth mechanism and the different morphologies of CVD diamond.

Flávia Almeida was one of the main contributors in this regard, presenting works about the tribological properties and machining performance of CVD diamond coatings on Si_3N_4 and hard metal (WC-Co, or cemented carbide) substrates. In [3] the adhesion of different diamond morphologies to Si3N4 substrates was evaluated with the objective of optimizing the properties of nanocrystalline diamond, especially adhesion. Three different morphologies were synthesized by hot filament assisted CVD and studied: microcrystalline (MCD), submicrocrystalline (SMCD) and nanocrystalline diamond (NCD). Although all morphologies showed good adhesion, MCD registered the highest. It was found that pre-treating the Si_3N_4 substrates with CF4 plasma provided an enhanced mechanical interlocking at the matrix/coating interface. The MCD film showed highest adhesion, supporting a normal load of 1600 N without peeling-off, with an interfacial crack resistance of 12.0 N μm^{-1}. This represented a significant advance in adhesion level for the referred system. The highest adhesion exhibited by MCD in comparison to SMCD and NCD was attributed to less amount of graphitic phase at the interface, which enabled a stronger bonding to Si_3N_4.

In fact, in a dedicated interfacial study by HRTEM and HRSEM-EELS analysis, the high adhesion levels of MCD were attributed to the spontaneous growth of DLC (Diamond-Like Carbon) interlayers, which relax the thermal residual stress in the interfacial region [4]. These layers are intercalated with diamond direct nucleation regions exhibiting grain-to-grain epitaxial growth.

Despite its superior bonding, MCD is hardly a choice in certain applications due to its characteristic high roughness, due to the micro-sized pyramidal asperities of diamond crystals, which lead to mechanical interlocking [5]. Consequently, high initial friction values in sliding contacts are observed leading to higher stress levels, temperature and ultimately to the increase in the wear rate [6]. Hence NCD represents a better solution, especially for sliding surfaces under high load. A work from Cristiano Abreu showed that NCD on NCD tribopairs under water lubrication led to very mild to mild wear regimes, with the wear coefficient values varying from 10^{-9} to 10^{-8} mm3$N^{-1}m^{-1}$ [7].

Diamond coatings were also investigated for the turning of hardmetal, a process which provides energy savings and better finishing quality that wheel grinding [8]. While polycrystalline diamond and polycrystalline cubic boron nitride are the standard materials for this process, Almeida has demonstrated that CVD diamond coated hardmetal tools enabled a much better performance than PCD (Polycrystalline Diamond) and PCBN (Polycrystalline Cubic Boron Nitride) ones, leading to much lower wear rates and higher tool durability [8]. While the friction coefficient between the chip and rake face reached values of 0.6–0.7 for the CVD tools after 180 m, the PCD one attained the same 0.7 coefficient value after mere 70 m. Moreover, it was found that the PCD tool also had a larger amount of adhered workpiece material than the CVD ones, which was caused by the chemical affinity of common Co binder in the PCD tool and the hardmetal workpiece.

In another report, further investigation and comparison between uncoated and NCD coated drill bits showed a remarkably superior performance of the later tools in drilling of pre-sintered cemented carbide (WC-5.5 wt.% Co) [9]. While the bare hardmetal drill bit exhibited a low infeed rate (20 mm/min) and increase of axial force from 4 to 20 N after four holes, the NCD-coated hardmetal tool allowed for infeed rates of 940

mm/min, reaching the same axial force of 20 N only at 500 mm/min. All this was done keeping the integrity of the tool and good surface finishing of the resulting hole. But the secret to such high performance of hardmetal tools coated with CVD diamond comes from even before the tools enter the CVD chamber. A two step pre-treatment with Murakami and Aqua regia is used for the purpose of removing cobalt from the surface of hardmetal due to its inhibitory effect on diamond nucleation, promoting formation of graphitic phases instead [10]. With this kind of pre-treatment, diamond seeding, nucleation and anchoring are much more effective, allowing the hardmetal tool to benefit from the intrinsic properties of the diamond coating, without compromising its mechanical integrity.

A more environmentally friendly alternative to acid pre-treatment of hardmetal tools has been recently employed by Sérgio Pratas. Via this route, a tungsten carbide interlayer is formed by means of tungsten vaporization and carburization during 1 hour (i.e. saturation of the hardmetal surface with a high CH4/H2 ratio of thermally activated gas) (Figure 2). After this period the pretended diamond synthesis parameters are introduced and the growth begins. As a result of this one-step solution, diamond films with high adherence can be produced, thanks to the absence of graphite at the harmetal/diamond interface.

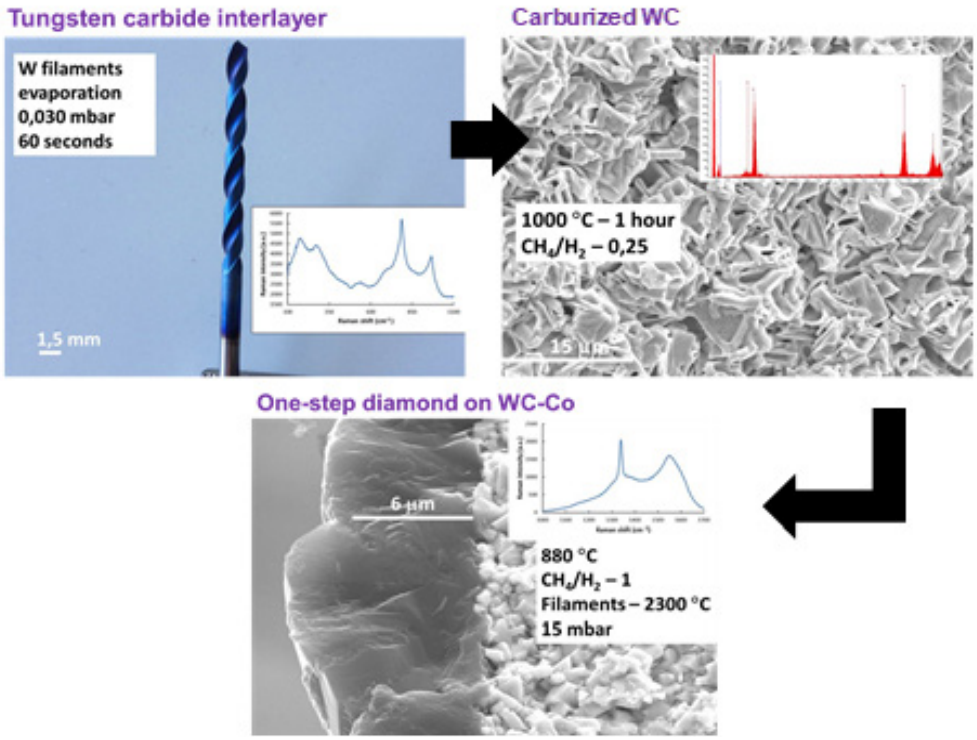

Figure 2. Growth procedure for CVD diamond on WC-Co with tungsten carbide interlayer.

By now it is clear that NCD is an excelling coating for more efficient tools and tribological systems because it is smooth, while still providing high hardness and low wear rate. However, it is also clear that MCD provides for higher adhesion due to better bonding at the interface. In order to combine the advantages of both morphologies, Ermelinda Salgueiredo has investigated the behaviour of multilayer diamond coatings [11]. Besides the above-mentioned advantages, multilayer diamond coatings were developed with two main goals: to mitigate catastrophic crack propagation, typical of ceramic materials, and to take advantage of NCD for stress relieving within the coating. Single, bilayer and multilayer coatings were compared. In order to evaluate adhesion and fracture propagation mode, the coatings were submitted to sandblasting with SiC particles. For single MCD and NCD layers, it was found that a substrate (Si3N4) pre-conditioning step of CF4 plasma attack plus flat lapping with diamond suspension was vital to transition from catastrophic and extensive delamination of the coatings, to more localized removal of smaller parts of the coatings. For the multilayered ones, under sandblasting with SiC particles, the tests were stopped after more than two hours without any signal of extensive delamination [11]. Damage occurred only by gradual loosening of material from the surface. A stress field distribution model was developed in order to characterize the different behaviour of the multilayered diamond coatings. According to this model, the maximum value of the von Mises parameter J21/2 is found at MCD/NCD interfaces. Crack propagation occurs along this region, working as a toughening mechanism by absorbing impact energy of SiC particles, and ultimately delaying delamination of the coatings.

The transitory interfaces between diamond layers on multilayer coatings have been investigated by HRTEM (High Resolution Transmission Electron Microscopy), STEM-EDX (Scanning Transmission Electron Microscopy – Energy Dispersive X-Ray Spectroscopy), and EELS (Electron Energy Loss Spectroscopy) [12]. This study showed that the

nature of the interface depends on which type of layer is on the base. While for MCD to NCD transitions graphite-like structures where more prominent, (as shown by the π* C peak at 285 eV in spatially resolved STEM-EELS), for NCD to MCD transitions, non-diamond material is absent. This is caused by the new gas composition at the start of a new layer: higher methane and lower hydrogen for NCD and the opposite for MCD. Hence, at the NCD-to-MCD interface graphite could not be detected because it was most likely etched away by atomic hydrogen.

Going a step further, the tribological behaviour of the multilayer architecture was tested on self-mated ball-on-flat setup [6]. Comparison between monolayers, bi- and fourfold multilayers of micro- and nanocrystalline CVD diamond morphologies revealed that none of the tested architectures showed coating delamination on both high-load & short-term tests (max 200 N; 86 m) and endurance tests (60 N; 691 m). The experiments were performed in the absence of lubrication, showing very low values of friction coefficient ranging from 0.02 to 0.09. The four fold multilayer coating with NCD on the top most layer outperformed the coatings with less layers by combining high wear resistance (~2.4×10^{-7} mm3N^{-1} m^{-1}) and a low friction coefficient (0.06) under an applied load of 200 N, without delamination [6]. The top nanocrystalline diamond layer was found to progressively wear out, as a sacrificial layer, while the harder microcrystalline diamond layer underneath kept the residual stresses low.

Such superior performance undoubtedly makes multilayer diamond coatings ideal for highly demanding tribological applications subjected to high contact pressures where lubrication is unpractical, or when low friction coefficient and high wear resistance are mandatory. A practical example of multilayer diamond coatings in action comes from another work of Almeida as leading author. The idea was to investigate the tribological behaviour of bare Si_3N_4, Si_3N_4 coated with micro/nano multilayers of CVD diamond, and AISI 52100 hardened chrome alloy steel [13]. The choice of materials was related to the possible application of CVD diamond in biodiesel lubricated systems. Because of the higher electric conductivity in comparison to petrol-based fuels, biodiesel creates conditions for higher corrosion rates, to which CVD diamond is resistant. As main outcome, this study demonstrated that the friction coefficient (COF) for multilayer diamond is lower than for steel (0.07 vs 0.1) and the wear regimes in lubricated and unlubricated condition are very similar (k~10^{-8} mm3$N^{-1}m^{-1}$) [13]. As for the bare Si3N4 both the friction and wear coefficients proved it unreliable for the considered application, especially in dry condition.

A more recent study was designed to understand the effects of relative humidity (RH), and temperature on the sliding and wear behaviour of multilayer diamond [14]. As mentioned before, the material is suited for high abrasion applications and poor lubrication conditions. The ten-fold multi-layered coating was synthesized on top of Si3N4 by alternating micro- and nanocrystalline diamond layers with A/B/A sequence, starting with MCD for higher adhesion to Si3N4 and ending with a top NCD layer for a smoother surface (Figure 3). Immediately, a difference in the critical indentation load of 600 N for single NCD layer and 900 for the 10-fold multilayer coating was established. Self-mated ball-on-plate tribological tests with RH (10 to 90 %) and temperature (25-100 ºC) as main variables revealed that while the effect of RH on the friction coefficient is minimal, it is very pronounced on the critical load value (load above which the coating detaches), increasing from 40 N at 10% RH to 120 N at 90% [14]. This was explained by the formation of a water layer between the surfaces of the ball and the plate which extends the contact area during sliding, inducing a load bearing effect. The static friction coefficient was observed to increase with temperature, most likely due to lower lubrication induced by the dryer conditions. The effect of temperature on the critical load was very pronounced, ranging from 40 to 55 N within the studied temperature range [14]. Overall the study points out the importance of water as load bearing medium, even for materials that are suitable for operation under low lubrication sliding.

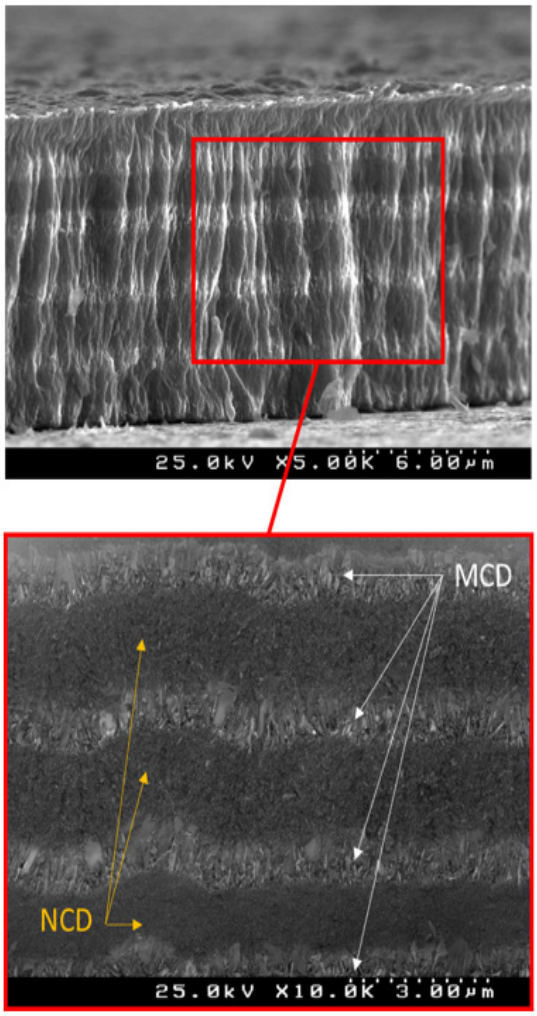

Figure 3. A/B/A multilayer CVD diamond alternanting between MCD and NCD with NCD as finishing layer for a smoother surface.

CVD diamond is not just a super hard, chemically inert and wear resistant material, it is also biocompatible

and a very interesting material for various biotechnology applications [15]. Margarida Amaral has conducted a non-specific cytotoxicity and biocompatibility analysis on NCD with human gingival fibroblast cells, where the typical morphology and cell growth could be reproduced [16]. With osteoblast cells, NCD was found to increase cell proliferation as well as stimulation of markers such as ALP activity and matrix mineralization, in comparison to polystyrene tissue culture plates.

This study open the door for the application of NCD as a coating for implant applications such as articular joint prosthesis for total hip replacement (THR) [17–19]. With the modern days increase of the life expectancy, there is a corresponding increase of THR interventions. Ceramic materials exhibit good biocompatibility in general, especially when compared to metals, for which ion release may cause osteolysis among other effects. While alumina-on-alumina tribopairs are surgeons' first choice for patients younger than 50 years, Si_3N_4 has been demonstrated to considerably excel the fracture toughness of Al_2O_3, which implies lower fracture probability and less chance of implant replacement or readjustment.

Following the group's previous results with NCD, Amaral presented a work describing a new articular joint prosthesis material consisting of NCD coated Si3N4 ceramic hip joints comprising an NCD/ Si3N4 ceramic femoral head working against an NCD/ Si3N4 acetabular liner [18]. After withstanding one million cycles, which correspond to approximately one year of a hypothetical patient's life, this tribosystem exhibited a wear rate of 0.005 mm3 per million cycles in the second half of the test. This was one order of magnitude lower than the best ceramic-on-ceramic hip joints available at the time. Furthermore, the resulting residual amount of debris did not present cytotoxicity. The Raman spectra collected after the tribological testing demonstrated no significant structural transformations of the coating [18].

In the same line of research, Salgueiredo reported on bilayer MCD/NCD coated Si3N4 odontological drill bits to drill a laminated block that mimics the cortical and trabecular bone [20]. Besides the tribological advantage of this system, NCD debris is harmless and the films exhibit a high resistance to bacterial colonization. The produced drill bits presented a superior performance when compared to AISI 420 steel: reduction of the maximum force applied by about four times in the speed range 350–1400 rpm; cooler operation temperature of less ~4ºC; drilling at low spindle speeds (100 rpm); and higher infeed rates (30 mm/min) which is important to reduce to duration of the surgical procedure. More than just numbers, these figures represent a significant reduction of trauma for the patient.

Boron doped diamond

The extreme hardness and thermal conductivity of CVD diamond determine its main application in cutting and anti-wear parts, as also in heat sinks for electronic and optical components. However, CVD diamond can be doped, which widens the range of applications of this material, as it becomes electrically conductive. For a given film thickness, the conductivity of CVD diamond films may vary from 1×10^{-9} $\Omega^{-1}cm^{-1}$, for lightly doped films, to 100 $\Omega^{-1}cm^{-1}$, for heavily doped ones [21]. When heavily doped ([B] > 1×10^{20} atoms/cm^3), CVD diamond becomes a conducting material or even superconducting at sufficient low temperature (~2K) [21,22]. Accordingly, what determines the conductivity value is going to be the doping source, the concentration of the relevant doping element (boron, nitrogen, phosphorus or sulphur) and the location of B atoms within the diamond lattice. Boron doping yields p-type semiconductivity by introducing an acceptor energy level 0.37 eV above the valence band, while nitrogen or phosphorus doping yield n-type semiconduction [21]. While the latter elements have been reported to successfully dope CVD diamond films, boron exhibits higher doping efficiency due to its lower charge carrier activation energy [21].

In our group, a boron doping system was developed, targeting the application of CVD diamond for corrosion-related sensing and biosensing. Miguel Neto pioneered our works with boron doped diamond (BDD) starting from interfacial studies. The author has characterized the surface of BDD films addressing specifically the boron doping setup of used in our group B2O3 mixed in pure ethanol and dragged by argon gas into the reaction chamber [23]. It is generally accepted that CVD diamond surfaces are H-terminated, mainly due to hydrogen rich gas mixture used for its synthesis. However, with oxygen introduced as part of the mixture it was important to characterize the resulting surface, since this element is known to be detrimental to doping efficiency by compensation of boron-introduced electronic holes. Therefore, by X-ray photoelectron spectroscopy (XPS) and water contact angle measurements, the author studied the surface termination of boron doped NCD and MCD coatings grown on silicon nitride (Si3N4) ceramics, via a boron oxide containing solution carried by argon gas. A dependency between the resulting diamond morphology, the flow of argon and the system pressure could be established. Although the water contact angle of ~90º revealed a hydrophobic surface, the XPS characterization revealed that the surface is only partially H-terminated with the remaining area consisting mainly of C–O–C and C=O terminating groups. The experimental data shows that oxygen is not restricted to the surface and may also be incorporated in the film during the CVD process [23].

In a subsequent study, the focus was the development of suitable electrical contacts for the development of BDD based electronic devices [24]. These should possess low electrical resistivity to minimize device losses at the metal–semiconductor interface and they must adhere well to the semiconductor material. The presented solution was the deposition of single-

-phase WC layers, an electrically conducting material, providing high thermal stability at the interface [24]. Diamond was grown uninterruptedly from the interior of the tungsten layer instead of from its surface. The process consisted on vaporizing tungsten oxide (WO_2) from the system's own heating filaments, under vacuum (10^{-2} bar) in a heating range of 1500-1900ºC [24]. The methane used for diamond growth will convert the oxide layer to WC during the first minutes of diamond growth. The success of the entire process was shown to rely on the substrate preconditioning with diamond particle seeding to ensure dense nucleation of the BDD film.

Later on, Neto has demonstrated the synthesis of metal-like boron doped diamond coatings on highly dielectric silicon nitride ceramic substrates [25]. The boron source was boron oxide mixed in ethanol. It was found that doping efficiency increases significantly with higher growth temperature and pressure, as well as lower methane content. Characterization by SIMS (Secondary Ion Mass Spectroscopy) depth profile analysis demonstrated that boron was uniformly distributed throughout the deposited diamond coatings [25]. In the case of NCD, boron was predominantly incorporated in passive electrical sites at the grain boundaries, which compromised the conductivity of the film.

A practical application of diamond as a temperature sensitive coating has been demonstrated in the form of an NTC (negative temperature coefficient) thermistor. The idea was to address the issues of tooth overheating and vitality in dental medicine. The deposition parameters in a HFCVD reactor were optimized for electrical resistance and B parameter using Taguchi's method. The device was assembled by applying in-situ ohmic contacts, isolating with undoped CVD diamond and using a PCB strip for electrical contacts and temperature measurements (Figure 4). The base of a pig molar tooth was placed inside a hot/cool water circuit and the temperature of the exposed surface was measured with the new NTCs. The sensors exhibited fast response time, high thermal sensitivity, while being bio-inert and biocompatible (Figure 5).

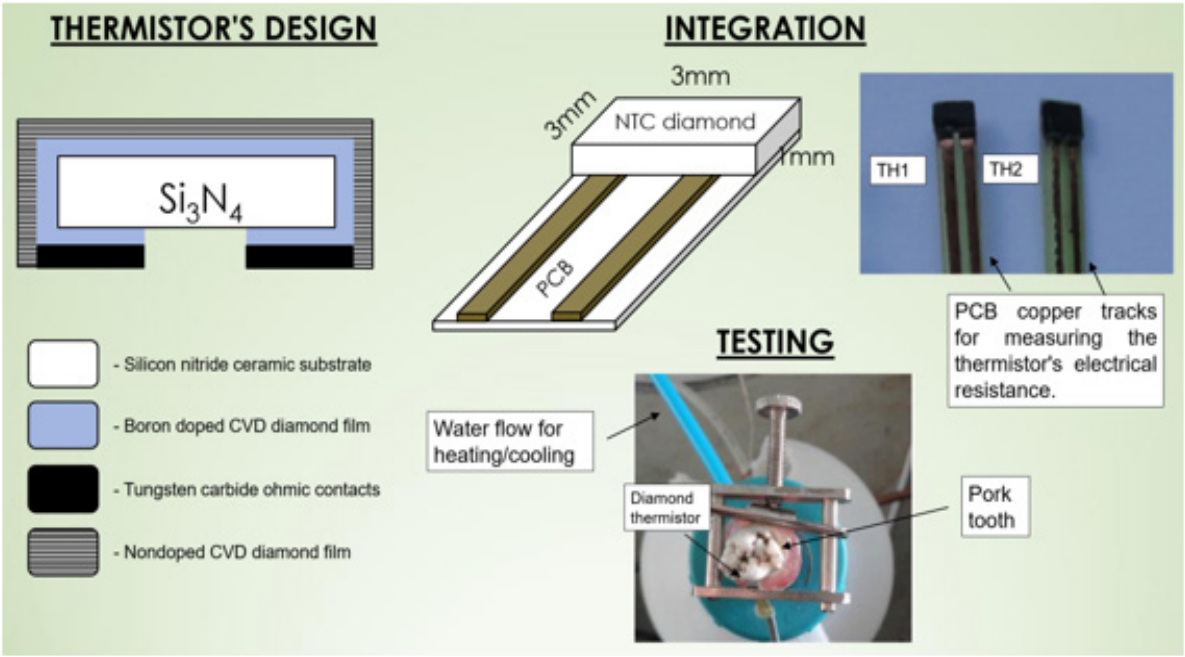

Figure 4. Diamond thermistor design and testing setup.

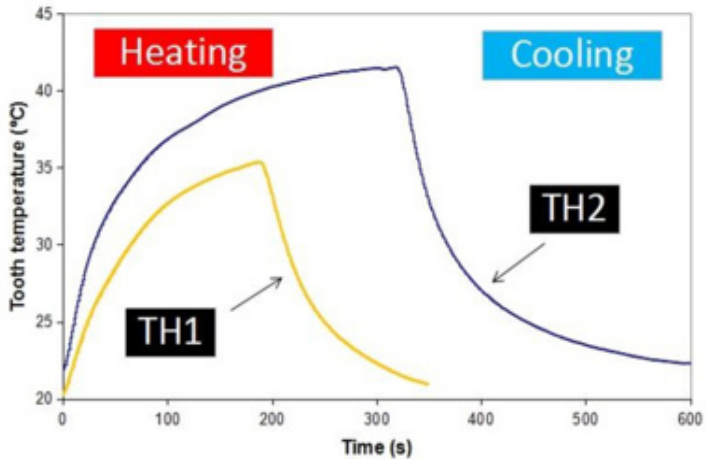

Figure 5. CVD diamond film behavior as NTC thermistor during heating/cooling cycle.

Boron doped diamond (BDD) is also an electrochemically active and functional material. It has gathered the interest of the scientific community due to its unmatched combination of properties: wide electrochemical potential window for water electrolysis, high-signal-to-noise ratio, high chemical stability, resistance to fouling, among others [26]. At a smaller scale Eduardo Silva started developing BDD microelectrodes applied to the field of corrosion, in particular for pH and dissolved oxygen (DO) sensing.

In a recent study BDD microelectrodes were developed as a possible alternative to suppress the limitations of glass membrane and glass capillary microelectrodes based on a selective ionophore-based oil-like membrane [27]. Although they are the standard for pH measurement, especially at the microscale, these electrodes present some disadvantages like spontaneous leakage of the liquid membrane, low mechanical robustness and short life time [28]. Moreover, the sensitivity and selectivity of such electrodes are constrained by adverse effects such as trans-membrane ion fluxes, which change the composition of the sample solution near the membrane, affecting the lower detection limit [29]. pH sensitivity of the microelectrodes was achieved by means of oxygen plasma treatment, after coating sharp tungsten wires with BDD. At this hydrophilic surface differently charged surface groups like C-OH, C-O^- and C-OH_2^+ can form, by a protonation–deprotonation mechanism, depending on the proton concentration in solution. The developed microelectrodes (Figure 6a) exhibited fast response and linearity with 50.8 ± 1.0 mV/pH in a wide range from pH 2 to 12. When tested on a galvanic Zn-Fe couple immersed in 0.05 M NaCl, the BDD microelectrodes successfully allowed mapping the local pH which varied from ~4.8 above the zinc under anodic dissolution and 9.3 over the iron cathodic area [27]. Although not illustrated in the same article, Figure 6b shows the typical behaviour that can be expected by BDD pH sensitive microelectrodes.

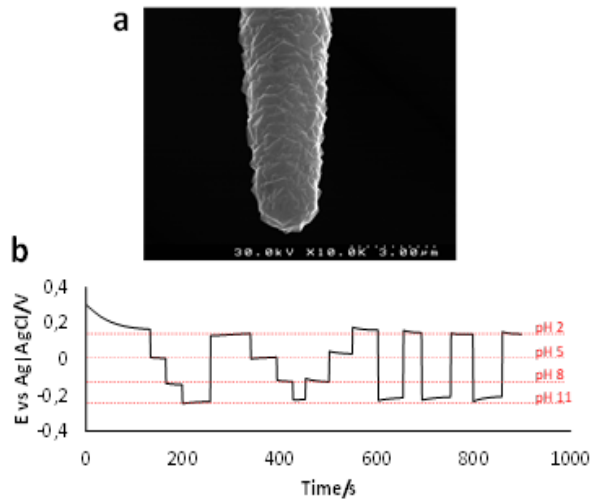

Figure 6. a) BDD pH sensitive microelectrode. b) The recorded potential in different pH solutions, shows a fast and stable response.

In another work, BDD microelectrodes were optimized for the detection of dissolved oxygen (DO) [30]. DO is one of the most important oxidizing species involved in cellular metabolism as well as in microbiological and corrosion processes. In the latter case, DO is the main cathodic reactant at neutral and alkaline pH for most engineering metals and alloys [31]. The development of corrosion protection strategies involves assessing the surface of metals with high degree of spatial resolution, which can be done by techniques such as SVET (Scanning Vibrating Electrode Technique) or microamperometry. The developed BDD microelectrodes were submitted to a surface modification with CF_4 plasma, which enabled high sensitivity to DO, by means of complexation with surface fluorine groups and electrochemical reduction [30]. A model galvanic cell immersed in aqueous electrolyte was used as setup for DO detection by using a SVET system in the amperometric mode (Figure 7a). It was demonstrated that BDD microelectrodes exhibited fast response and a detection limit of 0.63 µM. When scanning the near-surface of the model galvanic cell, the measured DO followed the expected distribution. Accordingly, the oxygen concentration was lower above the cathodic area, which is to expect since it is consumed mainly at the cathode (Figure 7b).

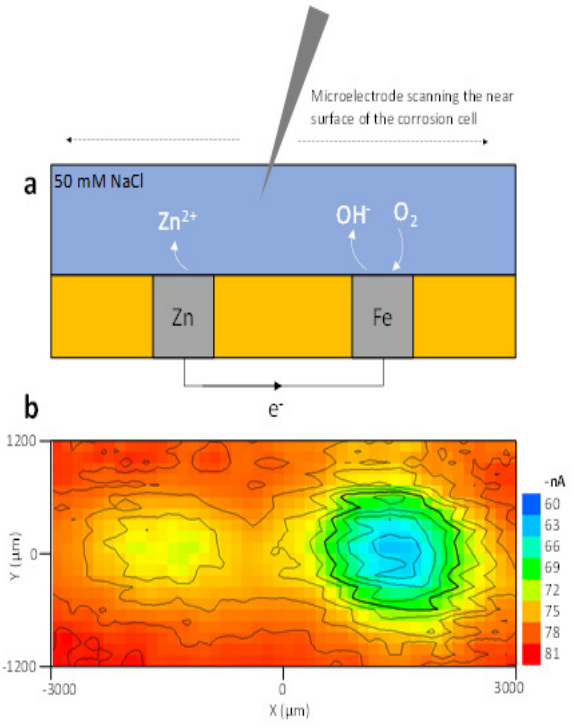

Figure 7. a) Model galvanic Zn-Fe system. b) DO oxygen map recorded with a BDD microelectrode. Less negative currents mean higher DO depletion. Since there is less oxygen available above the iron cathode, this is translated into lower DO reduction current at the BDD microelectrode.

Among the most relevant aspects of microelectrode construction is the choice for its geometry, which is related to the size tolerable for application, and needs to be dimensionally well defined, for analyte quantification purposes. A defective or irregular insulating shroud can give origin to the misinterpretation of electrochemical data. An alternative to insulation

with polymeric coatings has been presented by Silva: boron doped diamond microelectrodes insulated with undoped diamond [32]. Upon FIB (Focused Ion Beam) cutting, chemically and dimensionally stable all-diamond microelectrodes were obtained. A central, electroactive disk (BDD) insulated by a thin undoped diamond coating. This concept was demonstrated for local oxygen measurements on the Al–Cu–CFRP (Carbon Fiber Reinforced Polymer) system, which is of high relevance for the development of new composite materials for the aeronautics industry.

CNTs and hybrid materials

Asides from diamond, CVD synthesis of carbon nanotubes have been investigated in our group. It is well known that CNTs have been one of the cornerstones of the nanotechnology revolution worldwide. Due to their low cost and supreme electrical, mechanical and optical properties these rolled graphene sheets have been attracting a lot of scientific and industrial interest from sectors such as biotechnology for drug delivery and in vitro diagnosis, to energy production and storage, as high surface area electrodes or supercapacitors [33,34]. With several thousands of tons of produced worldwide, CNTs are finding their way to real world widespread usage, although limitations still persist, such as precisely controlling orientation and chirality. Diogo Mata was the first author to focus on CNT based materials, directing most of his endeavors to biotechnology. Endogenous electric signals are involved in the regeneration mechanism of bone through activation of Ca^{2+} channels located in the plasma membrane of osteoblasts. In the case of injury, the electric signals are disrupted. Accordingly, several authors reported accelerated bone regeneration when stimulated by electrically conductive composite bone grafts. In comparison with metal fillers, CNT do not exhibit corrosion-related toxicological risks, while still having high electric conductivity (~100 $S.m^{-1}$) at low percolation values of 0.6–3.5 vol.% [35]. In one of his works with smart CNT-based bone grafts, Mata reported on the development of CNT/HA/glass composites, focusing on the optimization of their mechanical, electrical and cytotoxic behaviour [36]. Comparing with non-electrically stimulated HA/glass matrix, it was demonstrated that the addition of CNTs enabled an increase in the cellular metabolic activity and DNA content of 130% and 60%, respectively, after only 3 days of daily stimulation of 15 μA for 15 min. Furthermore, the osteoblastic gene expression for Runx2, OC and ALP was enhanced by 80%, 50% and 25%, respectively, after 5 days of stimulation [36]. Such improvement in the functional activity of osteoblast cells were directly related to the local increase in the culture medium conductivity and the ability to apply confined electrical stimulate.

Although this work successfully demonstrated the viability of smart CNT-based bone grafts, the toxicological aspects of CNTs have been a matter of dispute for a long time. Metal impurities, tube morphology, hydrophobicity and non-biodegradability are mostly responsible for the toxicological profiles of CNTs. While transition-metal impurities (used as catalysts for CNT production) may induce cellular oxidative stress, the morphology of CNTs is responsible for the success of clearance, by means of the urinary and/or lymphatic systems [37]. However, even CNTs with proper size, dispersion and purity may still present cytotoxicity, due to hydrophobicity and biopersistency [38]. This can be solved by means of chemical functionalization that restricts CNT agglomeration and increases their mobility in physiological serums, avoiding accumulation in tissues and organs [37]. The functionalization of multi-walled carbon nanotube (MWCNTs) membranes by the [4 + 2] Diels–Alder cycloaddition reaction of 1,3 butadiene has been studied by Mata and co-workers in terms of functionalization yield, functional groups recognition, surface charge, wettability and roughness [39]. The biocompatibility and biodegradability of Diels–Alder functionalized CNT membranes were assessed in vitro with human-like osteoblasts and in vivo through implantation in Wister rats. While both functionalized and non-functionalized CNTs demonstrated adequate cell adhesion, enhanced cell spreading was observed for the functionalized ones [39]. This behaviour was attributed to the difference in surface energy, which also marked the improved proliferation and osteogenic differentiation, supported by higher MTT reduction values and ALP activity values, for the functionalized CNT membranes. When implanted in the Wistar rats, the Diels-Alder functionalized membranes induced less inflammatory response than their non-functionalized counterpart, as well as improved biodegradation [39]. Hence, this report demonstrated that cycloaddition reactions provide an optimal balance between preservation of CNT properties and in vivo biodegradability, providing a suitable route for bone healing modulation.

Although Mata has also developed fabrication approaches for smart bone grafts [26], perhaps the most innovative work regarding this topic was presented by Elsa Gonçalves. The author studied the behaviour of a 3D printed composite scaffold composed of silicon-doped nanocrystalline hydroxyapatite (HA) (similar composition to bone with better biological response), polycaprolactone (biodegradable polymer), and carbon nanotubes (to improve mechanical properties and electrical conductivity) [42]. The outcome of this rapid prototyping process was a composite with homogeneous distribution of HA and CNTs on a porous PCL (Polycaprolactone) matrix. An optimal CNT loading of 2% wt. was found to make the composite conductive and exhibit a compressive strength of 4 MPa, which is similar to trabecular bone. Increasing the CNT load to 10% wt. resulted in better cell adhesion due to improved protein adsorption [42].

In comparison to horizontally aligned CNTs and agglomerates, vertically aligned carbon nanotubes (VACNTs) enable the maximization of the intrinsic properties of CNTs, providing a fully accessible surface area, high electrical conductivity and ballistic

mass transport through tube porosity, along with high mechanical, chemical, and electrochemical stability. Other characteristics of VACNTs include growth with residual amorphous carbon (or none at all) and low amount of catalyst. This CNT morphology leads to the realization of the most noticeable proposed applications of this unique material such as supercapacitors, advanced yarns and fabrics, electronic interconnects, among many others [43].

In our group Ricardo Silva, is currently the main author developing VACNT based materials. In one of his works the author stressed the importance of growing VACNTs directly on metallic substrates (Inconel600). However, there is an obvious limitation to this procedure: diffusion of the catalyst particles that are required for CNT growth into the metal substrate. Hence a typical synthesis by CVD either involves a two-step process of growing VACNTs independently and then bind them to a metal collector or using an oxide buffer layer between the metal substrate and the catalyst particles. Either of the two is problematic because good electrical contact between the VACNTs and the metal substrate is required for optimal performance. The presented solution was annealing of the Inconel600 alloy in air, which led to the formation of uniformly dispersed and densely packed nano-sized catalytic particles (Figure 8) [44]. Hence, the metallic substrate plays two key roles: (i) the Inconel600 itself provides catalytic active sites for the nanotube growth process and (ii) acts as a current collector. This formation of catalyst particles in situ directly from the Inconel substrate, allows the successful growth of VACNTs with excellent adhesion and electrical contact [44].

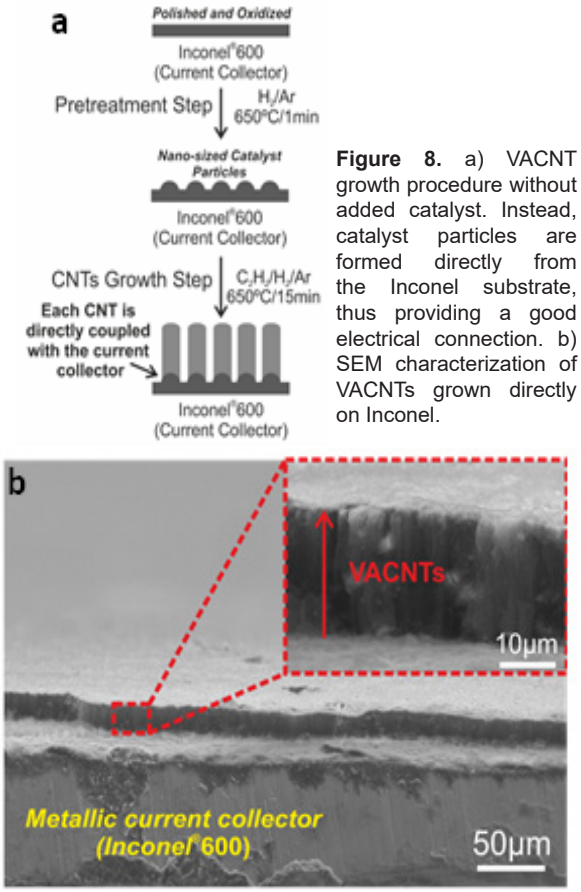

Figure 8. a) VACNT growth procedure without added catalyst. Instead, catalyst particles are formed directly from the Inconel substrate, thus providing a good electrical connection. b) SEM characterization of VACNTs grown directly on Inconel.

Other scientific contributions from the author include the development of novel hybrid materials for supercapacitors, particularly coating VACNTs with transition metal oxides by atomic layer deposition (ALD). An example of such approach was the coating of VACNTs with manganese oxide by ALD [45]. Electrochemical capacitors can generally be divided in two types: double layer capacitors and pseudocapacitors. While in the first type the capacitance is provided by the charge separation at the electrode–electrolyte interface, in the case of pseudocapacitors it has its origin in fast and reversible Faradaic redox reactions taking place at the electrode. Manganese oxide is very attractive as pseudocapacitor because it presents high theoretical capacitance and low environmental impact. The VACNTs were grown on Inconel600 through the catalyst free process mentioned above, while manganese oxide was deposited by ALD from MeCpMn(I)(CO)3 and O3 as the sources for manganese and oxygen, respectively (Figure 9). As a hybrid material, the VACNTs/Mn3O4 exhibited a synergistic effect, yielding enhanced capacitance for the pair, as compared with pristine VACNTs (Figure 10). The specific capacitance was observed to increase with the number of ALD cycles of Mn_3O_4 (i.e. the thickness of the coating) up to 78.62 $mF.cm^{-2}$, which demonstrates the pseudocapacitive contribution of the Mn_3O_4 in increasing the total capacitance of the nanocomposite [45].

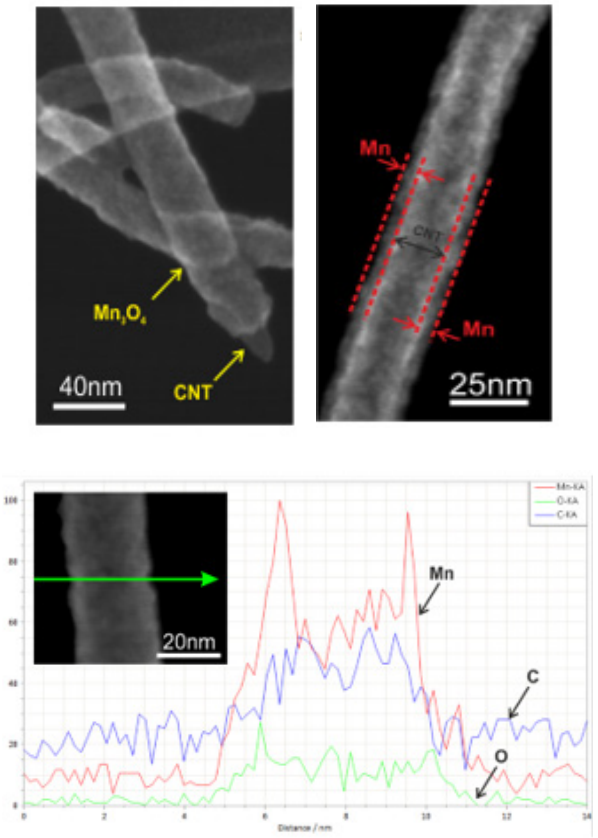

Figure 9. STEM images and corresponding EDS characterization of Mn3O4 coated CNTs, showing a core-shell configuration.

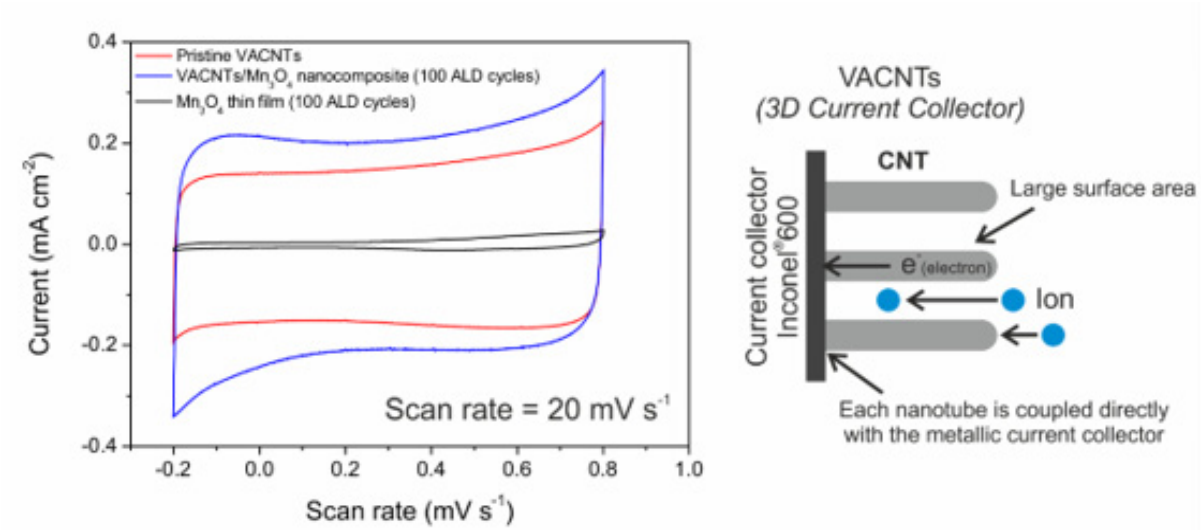

Figure 10. Voltammetric behavior of the VACNTs/Mn3O4 nanocomposite showing a significant capacitance increase for the Mn3O4 coated VACNTs.

The versatility of ALD was used in combination with CVD diamond as well. This study is being developed by Aneeta Jaggernauth. The focus is to take advantage of the high thermal conductivity, high breakdown field and chemical inertness of boron doped diamond for electronic devices operating under extreme or harsh conditions. Challenges of transistors, for example, include high leakage currents and low capacitive coupling between the transistor gate contact and the semiconductor itself. The incorporation of high-κ dielectric materials both as gate insulator and passivation layer on the semiconductor surface, accomplishes surface stability, charge carrier concentration and leakage current minimization. One such high-κ material is Al_2O_3 which is shown in Figure 11 grown by ALD on BDD, with the final goal being the assembly of even higher κ nanolaminates with HfO_2 and Ta_2O_5 deposited on BDD via atomic layer deposition (ALD) for enhanced transistor performance on high power devices and under high temperature conditions.

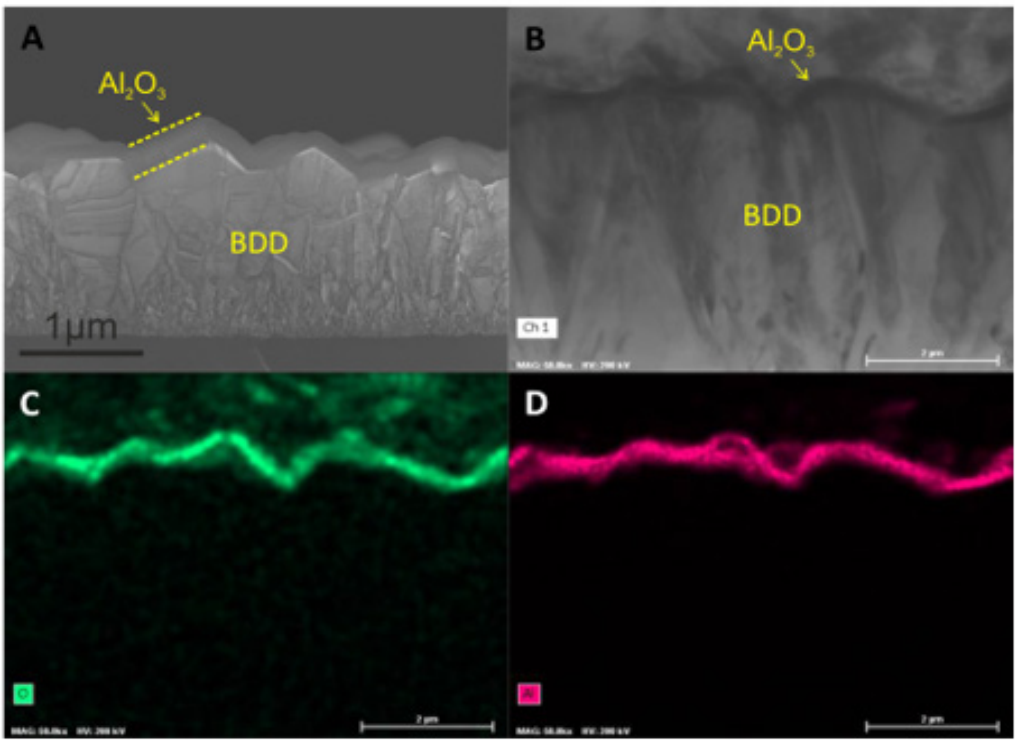

Figure 11. Boron doped diamond coated with Al2O3 by ALD; SEM image shown in A, TEM images in B, C & D with elemental analysis.

References

[1] N.M. Everitt, R.F. Silva, J. Vieira, C.A. Rego, C.R. Henderson, P.W. May, Diam. Relat. Mater. 4 (1995) 730–734.

[2] R.S. Balmer, J.R. Brandon, S.L. Clewes, H.K. Dhillon, J.M. Dodson, I. Friel, P.N. Inglis, T.D. Madgwick, M.L. Markham, T.P. Mollart, N. Perkins, G.A. Scarsbrook, D.J. Twitchen, A.J. Whitehead, J.J. Wilman, S.M. Woollard, J. Phys. Condens. Matter 21 (2009).

[3] F.A. Almeida, M. Amaral, F.J. Oliveira, A.J.S. Fernandes,

R.F. Silva, Vacuum 81 (2007) 1443–1447.

[4] F.A. Almeida, F.J. Oliveira, R.F. Silva, D.L. Baptista, S.B. Peripolli, C.A. Achete, Appl. Phys. Lett. 98 (2011) 1–4.

[5] E. Salgueiredo, M. Amaral, F.A. Almeida, A.J.S. Fernandes, F.J. Oliveira, R.F. Silva, Surf. Coatings Technol. 236 (2013) 380–387.

[6] E. Salgueiredo, C.S. Abreu, M. Amaral, F.J. Oliveira, J.R. Gomes, R.F. Silva, Wear 303 (2013) 225–234.

[7] C.S. Abreu, M. Amaral, F.J. Oliveira, J.R. Gomes, R.F. Silva, Diam. Relat. Mater. 18 (2009) 271–275.

[8] F.A. Almeida, A.J.S. Fernandes, F.J. Oliveira, R.F. Silva, Vacuum 83 (2009) 1218–1223.

[9] F.A. Almeida, J.M. Carrapichano, A.J.S. Fernandes, J. Sacramento, R.F. Silva, F.J. Oliveira, Int. J. Refract. Met. Hard Mater. 29 (2011) 618–622.

[10] F.A. Almeida, E. Soares, A.J.S. Fernandes, J. Sacramento, R.F. Silva, F.J. Oliveira, Vacuum 85 (2011) 1135–1139.

[11] E. Salgueiredo, F.A. Almeida, M. Amaral, M.A. Neto, F.J. Oliveira, R.F. Silva, Wear 297 (2013) 1064–1073.

[12] F.A. Almeida, E. Salgueiredo, F.J. Oliveira, R.F. Silva, D.L. Baptista, S.B. Peripolli, C.A. Achete, ACS Appl. Mater. Interfaces 5 (2013) 11725–11729.

[13] F.A. Almeida, M.M. Maru, M. Shabani, F.J. Oliveira, R.F. Silva, C.A. Achete, Wear 302 (2013) 1370–1377.

[14] M. Shabani, A. C.S., G. J.R., R.F. Silva, O. F.J., Diam. Relat. Mater. 73 (2017) 190–198.

[15] M. Amaral, C.S. Abreu, A.J.S. Fernandes, F.J. Oliveira, J.R. Gomes, R.F. Silva, Surf. Coatings Technol. 204 (2010) 1962–1969.

[16] M. Amaral, P.S. Gomes, M.A. Lopes, J.D. Santos, R.F. Silva, M.H. Fernandes, J. Nanomater. 2008 (2008).

[17] M. Amaral, C.S. Abreu, F.J. Oliveira, J.R. Gomes, R.F. Silva, Diam. Relat. Mater. 17 (2008) 848–852.

[18] M. Amaral, M.M. Maru, S.P. Rodrigues, C.P. Gouvêa, R.M. Trommer, F.J. Oliveira, C.A. Achete, R.F. Silva, Tribol. Int. 89 (2015) 72–77.

[19] M.M. Maru, M. Amaral, S.P. Rodrigues, R. Santos, C.P. Gouvea, B.S. Archanjo, R.M. Trommer, F.J. Oliveira, R.F. Silva, C.A. Achete, J. Mech. Behav. Biomed. Mater. 49 (2015) 175–185.

[20] E. Salgueiredo, F.A. Almeida, M. Amaral, A.J.S. Fernandes, F.M. Costa, R.F. Silva, F.J. Oliveira, Diam. Relat. Mater. 18 (2009) 264–270.

[21] A. Kraft, Int. J. Electrochem. Sci. 2 (2007) 355–385.

[22] W. Gajewski, P. Achatz, O.A. Williams, K. Haenen, E. Bustarret, M. Stutzmann, J.A. Garrido, Phys. Rev. B - Condens. Matter Mater. Phys. 79 (2009) 1–14.

[23] M.A. Neto, G. Pato, N. Bundaleski, O.M.N.D. Teodoro, A.J.S. Fernandes, F.J. Oliveira, R.F. Silva, Diam. Relat. Mater. 64 (2016) 89–96.

[24] M.A. Neto, E.L. Silva, A.J.S. Fernandes, F.J. Oliveira, R.F. Silva, Surf. Coatings Technol. 206 (2012) 3055–3063.

[25] M.A. Neto, E.L. Silva, C.A. Ghumman, O.M. Teodoro, A.J.S. Fernandes, F.J. Oliveira, R.F. Silva, Thin Solid Films 520 (2012) 5260–5266.

[26] N. Yang, S. Yu, J. V. MacPherson, Y. Einaga, H. Zhao, G. Zhao, G.M. Swain, X. Jiang, Chem. Soc. Rev. 48 (2019) 157–204.

[27] E.L. Silva, A.C. Bastos, M.A. Neto, R.F. Silva, M.G.S. Ferreira, M.L. Zheludkevich, F.J. Oliveira, Electrochem. Commun. 40 (2014) 31–34.

[28] D. Amman, Ion-Selective Micro-Electrodes, Principles, Design and Application, Springer-Verlag, 1986.

[29] T. Sokalski, A. Ceresa, T. Zwickl, E. Pretsch, J. Am. Chem. Soc. 119 (1997) 11347–11348.

[30] E. Silva, A.C. Bastos, M. Neto, A.J. Fernandes, R. Silva, M.G.S. Ferreira, M. Zheludkevich, F. Oliveira, Sensors Actuators, B Chem. 204 (2014) 544–551.

[31] E.E. Stansbury, R.A. Buchanan, Fundamentals of Electrochemical Corrosion, ASM International, 2000.

[32] E.L. Silva, C.P. Gouvêa, M.C. Quevedo, M.A. Neto, B.S. Archanjo, A.J.S. Fernandes, C.A. Achete, R.F. Silva, M.L. Zheludkevich, F.J. Oliveira, Anal. Chem. 87 (2015) 6487–6492.

[33] R.H. Baughman, A.A. Zakhidov, W.A. De Heer, Science (80-.). 297 (2002) 787–792.

[34] P. Simon, Y. Gogotsi, Nat. Mater. (2008) 845–854.

[35] J. Tatami, T. Katashima, K. Komeya, T. Meguro, T. Wakihara, J. Am. Ceram. Soc. 88 (2005) 2889–2893.

[36] D. Mata, F.J. Oliveira, M.A. Neto, M. Belmonte, A.C. Bastos, M.A. Lopes, P.S. Gomes, M.H. Fernandes, R.F. Silva, J. Mater. Chem. B 3 (2015) 1831–1845.

[37] L. Lacerda, A. Soundararajan, R. Singh, G. Pastorin, K.T. Al-Jamal, J. Turton, P. Frederik, M.A. Herrero, S. Li, A. Bao, D. Emfietzoglou, S. Mather, W.T. Phillips, M. Prato, A. Bianco, B. Goins, K. Kostarelos, Adv. Mater. 20 (2008) 225–230.

[38] A. Bianco, K. Kostarelos, M. Prato, Chem. Commun. 47 (2011) 10182–10188.

[39] D. Mata, M. Amaral, A.J.S. Fernandes, B. Colaço, A. Gama, M.C. Paiva, P.S. Gomes, R.F. Silva, M.H. Fernandes, Nanoscale 7 (2015) 9238–9251.

[40] D. Mata, F.J. Oliveira, N.M. Ferreira, R.F. Araújo, A.J.S. Fernandes, M.A. Lopes, P.S. Gomes, M.H. Fernandes, R.F. Silva, Nanotechnology 25 (2014).

[41] D. Mata, R.M. Silva, A.J.S. Fernandes, F.J. Oliveira, P.M.F.J. Costa, R.F. Silva, Carbon N. Y. 50 (2012) 3585–3606.

[42] E.M. Gonçalves, F.J. Oliveira, R.F. Silva, M.A. Neto, M.H. Fernandes, M. Amaral, M. Vallet-Regí, M. Vila, J. Biomed. Mater. Res. - Part B Appl. Biomater. 104 (2016) 1210–1219.

[43] W. Shi, D.L. Plata, Green Chem. 20 (2018) 5245–5260.

[44] R.M. Silva, A.C. Bastos, F.J. Oliveira, D.E. Conte, Y. Fan, N. Pinna, R.F. Silva, J. Mater. Chem. A 3 (2015) 17804–17810.

[45] R.M. Silva, G. Clavel, Y. Fan, P. Amsalem, N. Koch, R.F. Silva, N. Pinna, Adv. Mater. Interfaces 3 (2016).

Bamboo-Like Carbon fibers growth mechanism

Luis Sousa Lobo

Requimte Research Centre, Chemistry Dep., Universidade Nova de Lisboa, Portugal. Email: sousalobo266@gmail.com

Abstract

Bamboo-like growth behavior of carbon fibers is explained. There is a requirement to have this type of growth: to operate above the Tammann temperature of the catalyst. The metal nanoparticle can change shape during reaction (sintering-like behavior) so that CNT growth adjusting geometry. At nanoscale, Fick's laws still apply. Nanoparticles with a diameter below 20 nm show a reduction of melting point (mp) and Tammann temperature (T_{Ta}).

1. Introduction

The mechanism of bamboo-like carbon nanotubes growth requires clarification. Detailed kinetic studies are an efficient key to understand a mechanism. This has been evidenced in catalytic graphene growth [1-3]. The main scope of the present proposal is to evidence the need to operate above the Tammann temperature to enable bamboo-like growth. A comprehensive review of CNTs bamboo-like growth has been published recently, covering design, synthesis and production methods [4]. The need to enable solid-state shape changes also led to the conclusion that in *carbon gasification* operating above Tammann temperature (T_{Ta}) is required to have efficient carbon/catalyst contact and so, good catalytic activity: catalyst nanoparticles showing "carbon worm" behavior [5].

2. Growth of carbon nanotubes above catalyst's Tammann temperature.

The different role of the different crystal faces in catalytic carbon growth has been known for decades. Nickel has an fcc crystal structure. It is known that (111) faces facilitate nucleation and growth. Of the 3 alternative carbon growth routes (*catalytic, hybrid* and *pyrolytic* [1-3]) bamboo-like growth is usually a *hybrid* growth route mechanism, operating above the Tammann temperature of the catalyst particle being used. Values of the T_{Ta} for 10 metals are included in Table 1. Bamboo-like growth is an example of nanoparticle's shape changes by solid-solid interaction above T_{Ta}.

Crystal shape and crystal orientation of the faces of catalyst nanoparticle is crucial to get a desired shape and a fast rate of the growing graphene structure.

Shape changes due to contact interaction are facilitated above the Tammann temperature (Fig.1). Bamboo-like growth is a good example of the importance of T_{Ta} in shape adjustment of a nanoparticle by solid-solid interaction.

METAL	Melting (^{0}C)	T_{Ta} (^{0}C)
Fe	1538	632
(Fe_3C)	1223	475
Co	1495	611
Ni	1455	590
Cu	1083	405
Ru	2334	1030
Rh	1964	845
Pd	1555	641
Ag	962	346
Pt	1768	747
Au	1064	396

Table 1. *Melting points and Tammann temperatures of metals frequently used.*

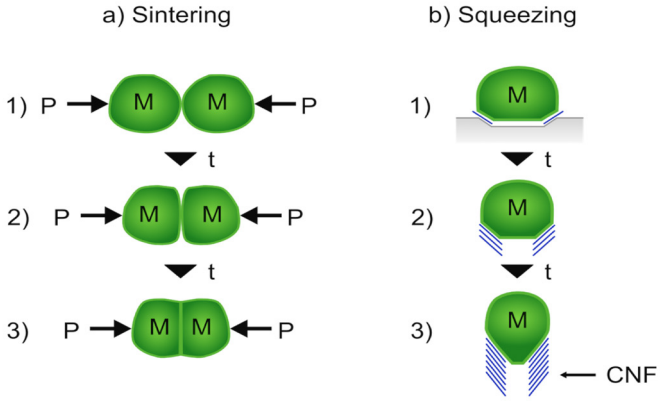

Figure 1. *Shape changes of nanoparticles above the Tammann temperature under surface pressure.*

M - metal; P - pressure; t - time

3. Alternative types of growth and bamboo-like growth variant.

There are alternative types of multiple wall carbon nanotubes (check Table 2):

a) Tube growth by successive graphene layer nucleation and growth *below* the previous one, via the catalytic route or the hybrid route; b) Successive pyrolytic formed layers grow via the pyrolytic route - *over* tubes previously formed (Fig. 2).

In the catalytic route or hybrid route a new graphene layer nucleates below the previous one, expands and bends by growth in the periphery, near the active catalyst surface border. This requires the formation of 6 pentagons at the periphery of the new expanding graphene layer.

KINETIC ROUTES	T range (ºC)	C GROWTH TYPE	ACTIVE CATALYSTS
I Catalytic	300-550	Surface catalysis	Fe, Co, Ni
II Hybrid	550-(700)	C black atoms dissolve/grow	Pt, Ru, Mo, Ni, Cu…
III Pyrolytic	600-(1200)	C black forms layers	No catalysis, shape adjusts

Table 2. *Alternative graphene formation routes.*

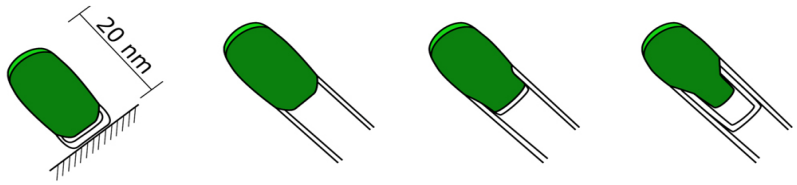

Figura 2. *Bamboo-like CNT growth. After a 1st graphene nucleus and 90º bending (6 pentagons) a second nucleation is formed 15 minutes later.*

In Table 3 we list 21 bamboo-like growth studies, including the work of Lee et al. in 2000 (C_2H_2, Fe, 750-950 ºC) In our view, these authors proposed a correct approach to the mechanism. The studies of Saito in 1995 [18] and Li et al. in 1999 [19] gave interesting information about growth modes and clues to understand the carbon growth mechanism. Two carbon growth alternatives - octopus carbon (formed at 500 ºC) vs. bamboo-like (formed at 650 ºC) - with the same gas (CH_4/N_2) and the same catalyst (Ni-Cu) evidenced kinetics and geometry roles. Octopus carbon requires easy and selective carbon nucleation on the 8 (111) facets [5]. A scheme of bamboo-like growth initiation is shown in Fig. 4, adapted from He et al. [21].

CATALYST	GAS	T ºC	1st author	Year	Ref-
Ni-Cu/Al	CH_4/N_2	500-730	Li YD	1999	[18]
Fe/SiO_2	C_2H_2	750-950	Lee CJ	2000	[6]
Fe/SiO_2	CH_4/NH_3	650-950	Cui H	2000	[20]
$Ni-Cu/Al_2O_3$	CH_4/H_2	720-830	Chen J	2001	[21]
Ni	$C_2H_2/N_2/H_2$	750-950	Jung M	2001	[33]
Ni	Phthalocyanine	600-850	Katayama T	2002	[22]
Co/Al_2O_3-Ti	C_2H_2/NH_3	750-950	Jang JY	2002	[23]
Fe, Co, Ni	CH_4/H_2	850-1100	Bartsch K	2005	[35]
Fe	$C_2H_2/NH_3/H_2$	700	Ting JM	2007	[24]
Ni	C_2H_2	650	Lin MT	2007	[25]
Ni/Al	CH_4/N_2	500-600	He C	2007	[19]
Cu	$CH_4/H_2/H_2S$	500-900	Katar SL	2008	[26]
Cu/Al_2O_3	C_2H_5OH	700-850	Xue B	2009	[34]
Ni $(AC)_2$	C_4H_4S/H_2-S	Detonation	Wang C	2010	[37]
Ni, Ni-Cu	CH_4/N_2	550-830	Gonzalez I	2011	[8]
Cu/Al_2O_3	C_2H_4/He	700-900	Lin JH	2012	[27]
Fe, Co, Ni, Al_2O_3	C_2H_2	720	Kekzenovity	2013	[28]
Cu/SiO_2	C_2H_4/He	500-900	Lin YC	2013	[29]
Cu/Al_2O_3	C_2H_2/N_2	550-800	Krishna VM	2014	[30]
La/NiO_3	Glicerol/Ethanol	700-900	Velasquez	2014	[36]
$Fe-Mo/Al_2O_3$	$C_3H_4N_2$	800-900	Wang Q	2017	[31]
Fe/Al_2O_3	Polyamide	750	Amaiz N	2018	[32]

Table 3. *A selection of bamboo-like CNTs growth studies. Operating temperatures are always above the Tammann temperature of the metal (see Table 2) facilitating shape adjustment of the particle and 90º turning in graphene growth.*

CNF growth includes a graphene layer that covers the tip and an extension: a conical catalyst shape graphene layer. The adjustment is possible due to sintering-like reshaping of the metal nanoparticle, but growth of the more regular CNT structure is not possible. In this case the structure must include pentagons and heptagons to adjust the growing graphene layer to the conical shape.

Table 3 evidences that successful experiments to produce bamboo-like nanotubes are run above catalyst's T_{Ta}. So, catalyst particles can change shape progressively under pressure, like in sintering. At nanoscale the change of *shape* is much easier. Li et al. used Ni with about 18% Cu [18], which lowers mp and T_{Ta} of Ni-Cu alloy compared to pure Ni.

Conclusions

1. Bamboo-like growth behavior of carbon fibers occurs most likely by a sintering-like shape change mechanism of the catalyst particles, enabling a new graphene layer to bend and grow further (inside). This is possible above the Tammann temperature of the metal particle under *catalytic* or *hybrid* carbon growth routes but not under *pyrolytic* growth. Shape changes are not due to liquefaction but to movements of the metal atoms of the external layer of the catalyst nanoparticle - under surface contact pressure.

2. This sintering-like behavior should not be described as melting or liquid-like behavior. Catalysis by solids is based on a surface structure: liquids do not have a stable surface structure.

3. Kinetics is a key to understand the behavior observed, particularly the concept of rate determining-step. Isothermal kinetic studies are required. Scanning temperature studies give useful *initial* information. However, reaction orders and activation energy evaluation in new systems require *isothermal* experiments.

References

[1] L.S. Lobo. Catalytic carbon formation: clarifying the alternative kinetic routes and defining a *kinetic linearity for sustained growth* concept. Reac Kinet Mech Cat 118 (2016) 393-414.

[2] L.S. Lobo. Nucleation and growth of carbon nanotubes and nanofibers: Mechanism and catalytic geometry control. Carbon 114 (2017) 411-417.

[3] L.S. Lobo. Mechanism of Catalytic CNTs Growth in 400-650 ^{0}C Range: Explaining Volcano Shape Arrhenius Plot and Catalytic Synergism Using both Pt (or Pd) and Ni, Co, or Fe. C, J. of Carbon Research 5,42 (2019).

[4] Z. Jia, K. Kou, M. Qin, H. Wu, F. Puleo, F. Liotta. Controllable and large- scale synthesis of carbon Nanostructures: A Review of Bamboo-Like Nanotubes. Catalysts 7,8 (2017) 256.

[5] L.S. Lobo. Intrinsic kinetics in carbon gasification: Understanding linearity, "nanoworms" and alloy catalysts. App, Cat. B: Environmental 148-149 (2014) 136-143.

[6] C.J. Lee, J. Park. Growth model of bamboo-shaped carbon nanotubes by thermal chemical vapor deposition. App. Phys. Letters 77,21 (2000) 3397-9.

[7] B. Brown, C.B. Parker, B.R. Stoner, J.T. Glass. Growth of vertically aligned bamboo-like carbon nanotubes from ammonia/methane precursors using a platinum catalyst. Carbon 49 (2011)

[8] I. Gonzalez, J. De Jesus, E. Canizales. Bamboo-shaped CNTs generated by methane thermal decomposition using Ni nanoparticles synthesized in water-oil emulsions. Micron 42 (2011) 819-825.

[9] V.I. Zaikovski1, V.V. Chesnokov, R.A. Buyanov. The Relationship between the State of Active Species in a Ni/Al_2O_3 Catalyst and the Mechanism of Growth of Filamentous Carbon. Kinetics and Catalysis 42,6 (2001) 890-931.

[10] D.W. McKee. Metal oxides as catalysts for oxidation of graphite. Carbon 8,5 (1970) 623-626.

[11] C.A. Bernardo, L.S. Lobo. Kinetics of carbon formation from acetylene and 1-butene on cobalt. In: B. Delmon, G. Froment (eds). Catalyst Deactivation. Elsevier, Amsterdam (1980) 409-420.

[12] L.S. Lobo, M.D. Franco. Kinetics of catalytic carbon formation on steel surfaces from light hydrocarbons. Cat. Today 7 (1990) 247-256.

[13] R. Sharma, P. Rez, M. Brown, G. Du, M.M.J. Treacy. Dynamic observations of the effect of pressure and temperature conditions on the selective synthesis of carbon nanotubes. Nanotechnology 18 (2007) 125620;

[14] S. Hofmann, R. Sharma, C. Ducati, G. Du, et al. In situ observations of Catalyst Dynamics during Surface-Bound Carbon Nanotube Nucleation. Nano Lett 7,3 (2007) 603-608.

[14] Z. Yu, D. Chen, B. Totdal, A.H. Holmen. Effect of support and Reactant on the Yield and Structure of Carbon Growth by Chemical vapor deposition. J Phys Chem B 109 (2005) 6096-6102.

[15] H.B. Liu, J.A. Ascensio, M. Perez-Alvarez, M.J. Yacaman. Melting behavior of nanometer sized gold isomers. Surf Sci 491 (2001) 88-98.

[16] Y. Saito. Nanoparticles and filled nanocapsules. Carbon 33 (1995) 979-88.

[17] Y.D. Li, J. Chen, Y. Ma, J. Zhao, Y. Qin, L. Chang. Formation of bamboo-like nanocarbon and evidence for the quasi-liquid state of nanosized metal particles at moderate temperatures. Chem Comm (1999) 1141-2.

[18] C. He, N. Zhao, C. Shi, X. Du, J. Li. TEM studies of the initial stage growth and morphologies of bamboo-shaped carbon nanotubes synthesized by CVD. J. Alloys Compounds 433 (2007) 79-83.

[19] H. Cui, O. Zhou, B. R. Stoner. Deposition of aligned bambo-like carbon nanotubes via microwave plasma enhanced chemical vapor deposition. J App Physics 88,10 (2000) 6072-4

[20] J. Chen, Y. Li, Y. Ma, Y. Qin, L. Chang. Formation of bamboo-shaped carbon filaments and dependence of their morphology on catalyst composition and reaction conditions. Carbon 39 (2001) 1467-1475.

[21] T. Katayama, H. Araki, K. Yoshino. Multiwalled nanotubes with bamboo-like structure and effects of heat treatment. J App Physics 91 (2002) 6675.

[22] Y. Jang, C. E. Lee, T. J. Lee, S. C. Lyu, C.J. Lee. Lateral force microscopy of bamboo-shaped multiwalled CNTs. Current App Physics 6 (2006) 141-4.

[23] J-M. Ting J-M, Lin S-H. Growth and characteristics of CNTs obtained under different $C_2H_2/H_2/NH_3$ concentrations. Carbon 45 (2007) 1934-40.

[24] M.T. Lin, J.P.I. Tan, C. Boothroyd, K.P. Loh, E.S. Tok, Y-L. Foo. Dynamical Observation of Bamboo-like Carbon Nanotube Growth. Nano Letters 7,8 (2007)

[25] S. L. Katar, A. Gonzalez-Berrios, J. De Jesus, B. Weiner, G. Morell. Direct deposition of Bamboo-Like Carbon Nanotubes on Copper Substrates by Sulfur-Assisted HFCVD. J Nanomaterials ID 515890 (2008) 7 pgs.

[26] J-H. Lin, C-S. Chen, Z-Y. Zheng, C-W. Chang, H-W. Chen. Sulphate-activated growth of bamboo-like carbon nanotubes over copper catalysts. Nanoscale 4 (2012) 4757

[27] E. Keczenovity, D. Fejes, B. Reti, K. Hernadi. Growth and characterization of bamboo-like carbon nanotubes synthesized on Fe-Co-Cu catalysts prepared by high-energy ball milling. Phys Status Solidi B 250 (2013) 2544.

[28] Y.C. Lin, J.H. Lin. Purity-controllable growth of bamboo-like multi-walled CNTs over copper-based catalysts. Cat Communications 34 (2013) 41-44.

[29] V. M. Krishna, A. Abilarassu, T. Somanathan, N. Gokulakrishnan. Effective synthesis of well graphitized high yield bamboo-like MWCNTs on copper loaded -alumina nanoparticles. Diamond and Rel. Mat. 50 (2014) 20-25.

[30] Wang, P.C. McIntyre, W. Cai. Phase Field Model for Morphological Transition in Nanowire Vapor-Liquid-Solid Growth. Crystal Growth & Design, 17 (2017) 2211-2227.

[31] N. Arnaiz , I. Martin-Gullon, R. Font, M.F. Gomez-Rico. Production of bamboo-type carbon nanotubes doped with nitrogen from polyamide pyrolysis gas. J. Anal. App Pyrolysis 130 (2018) 52-61.

[32] M. Jung, K.Y. Eun, J-K. Lee, Y-J. Baik, K-R. Lee, J.W. Park. Growth of CNTs by CVD. Diamond Rel. Mater. 10 (2001) 1235-1240.

[33] B. Xue, R. Liu, W-Z. Huang, Y-F. Zheng, Z-D. Xu. Growth and characterization of bamboo-like multiwalled carbon nanotubes over Cu/Al_2O_3 catalyst. J Mater Sci 44 (2009) 4040-46.

[34] K. Bartsch, J. Biedermann, T. Gemming, A. Leonhardt. On the diffusion-controlled growth of multi-walled CNTs. J. App. Physics 97 (2005) 114301.

[35] M. Velasquez, C. Batiot-Dupeyrat, J. Galego, A. Santamaria. Chemical and morphological characterization of multi-walled-carbon nanotubes syntheside by carbon deposition from an ethanol-glycerol blend. Diam. Relat. Mater. 50 (2014) 38-48.

[36] C. Wang, L. Zhan, W-L. Wang, W-M. Qiao, X. Liang, L-X. Ling. Effect of sulfur on the growth of carbon nanotubes by detonation-assisted CVD. App Surf Science 257 (2010) 932-36.

Preparation of submicron carbon fibers from lignocellulosic waste for energy and environmental applications

Francisco José García Mateos

garciamateos@uma.es
Presented in 2017, Departamento de Ingeniería Química, Andaluciía Tech, Universidad de Málaga, 29010, Málaga, Spain.
Supervisors: Tomás Cordero and José Rodríguez Mirasol (Universidad de Málaga, Spain)

Objective and Novelty

The objective of this PhD Thesis was the preparation of advanced fibrous carbon materials to be used in energy and environmental applications. For this purpose, coaxial electrospinning technique, a simple and versatile method, was used to prepare submicron diameter fibers. Alcell lignin was used as carbon precursor for the preparation of carbon fibers. In this Thesis work, the incorporation of phosphoric acid to the initial lignin/ethanol solutions was investigated with the objective to study its effect on the stabilization of the lignin fibers during an oxidative treatment at low temperature and on the textural and surface chemistry properties of the final carbon fibers obtained after a thermal treatment at high temperature. The presence of high thermally stable surface phosphorus group improved the development of porosity, surface acid character and oxidation and electro-oxidation resistance of the obtained carbon fibers. The incorporation of metal precursor to the lignin solutions was also studied in order to obtain carbon fibers doped with metal nanoparticles in a simple way. These carbon materials presented very interesting properties to be used in different applications of the chemical industry, confirming that electrospinning is a powerful tool for maximizing the value of lignin as carbon precursor.

Results

The third and fourth chapters of the PhD Thesis were focused on the study of lignin fibers stabilization step. Lignin, which has a low glass transition temperature, requires for long times to be stabilized, making crucial the stabilization step for the preparation of carbon fibers. Figure 1 shows the effect of the heating rate on the lignin and P-containing lignin fibers stabilization. Pure lignin fibers were obtained by the electrospinning of lignin/ethanol solutions (mass ratio of lignin/ethanol of 1/1). The stabilization stage required the use of a low heating rate (0.08 ºC/min) up to 200 ºC, then, this temperature is kept for 60 hours. Therefore, the total duration of the step necessary to stabilize the pure lignin fibers is 90 hours. This long stabilization time is necessary to get the crosslinking of the lignin structure.

The incorporation of small amount of H_3PO_4 to the initial lignin/ethanol solutions (0.3/1/1 H_3PO_4/lignin/ethanol) produces the generation of phosphates (and/or polyphosphates) groups in the lignin structure, improving the cross-linking of lignin structure and making faster the air stabilization step of P-lignin fibers. These lignin fibers can be stabilized at heating rates as high as 3-5 ºC/min and only maintained at 200 ºC for 1 hour. The comparison of stabilized lignin fibers at 1 ºC/min showed the melting of pure lignin fibers, meanwhile P-containing lignin fibers kept completely their morphology (Figure 1). The incorporation of low amounts of H_3PO_4 to the lignin solutions allows to stabilize fibers 50 times faster. In addition, the use of phosphoric acid also improved the development of the carbon fibers porosity, acid character and oxidation and electro-oxidation resistance of the resulting carbon fibers that make these carbon materials very interesting for different chemical engineering applications.

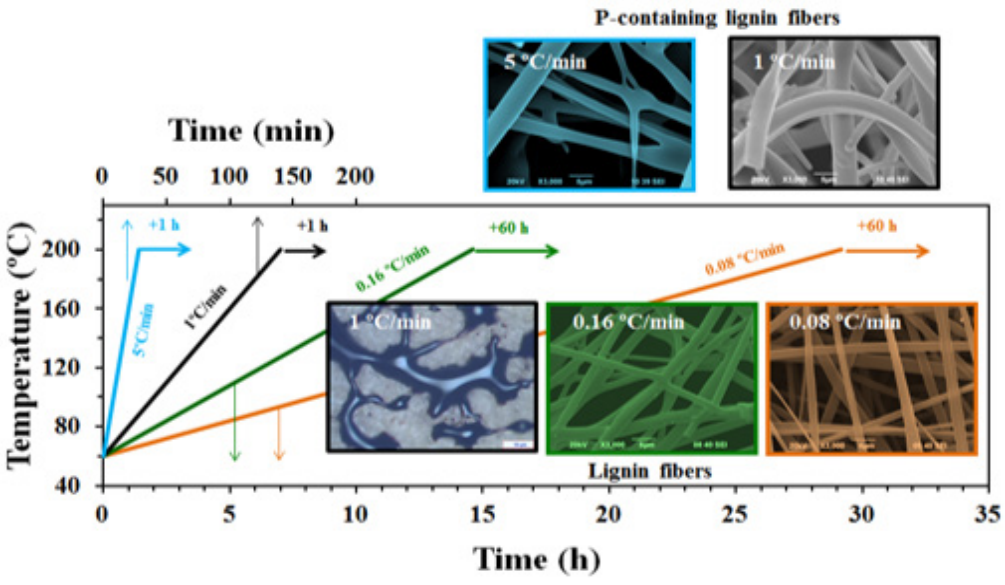

Figure 1. Effect of stabilization heating rates and times on lignin and P-lignin fibers

In the fifth chapter, the adsorbent characteristics of these microporous carbon fibers for phenol removal in liquid phase, with adsorption capacities as high as 180 mg/g at an equilibrium concentration of 25 mg/L and 25 ºC, was reported. The small carbon fibers diameters facilitate the diffusion of the pollutant to the surface of microporosity, making the adsorption process faster and, simultaneously, very low pressure drops are achieved when submicron diameter carbon fibers are used as adsorbent in a column adsorption. Furthermore, the incorporation of H_3PO_4 to the initial lignin solutions produces a widening of the carbon fibers porosity, improving the kinetic of the adsorption process. Equilibrium and kinetic adsorption experiments were carried out at different temperatures. A mathematical model was used to predict the breakthrough profiles in fixed-bed columns by using equilibrium and kinetics adsorption parameters obtained from the batch experiments. Figure 2 a) shows the experimental breakthrough profile for phenol adsorption (dots) on P-carbon fibers and the predicted values (lines) obtained from the mathematical model. The regeneration of the phenol saturated carbon fibers with a water stream at 25ºC was also studied and a regeneration yield of 55 and 14 % for P-containing and pure carbon fibers, respectively, was obtained.

In the sixth chapter, the preparation of P-containing carbon fibers at different temperatures and their use as acid catalysts for alcohol decomposition in a fixed bed reactor were reported. In this sense, isopropanol decomposition reaction was used as a test to characterize the surface acidity or basicity of the carbon fiber materials. The selectivity for isopropanol decomposition was 100 % to propylene, demonstrating the acid character of these materials. In Figure 2 b) a steady state conversion values of isopropanol on P-containing carbon fibers prepared at 900 ºC are reported. A relationship between the amount of P and the activity for isopropanol decomposition was found and conversions similar to those observed for a commercial acid catalyst (γ-Al_2O_3) were observed for the carbon fiber containing higher amount of surface P. The thermal stability of carbon catalysts is very important in applications under oxidizing conditions. The P-containing carbon fibers present high oxidation resistance, starting to gasify at temperatures as high as 525-550 ºC in the presence of air. Phosphorus surface groups are the responsible for this high oxidation resistance. Ethanol and methanol decomposition were also studied on P-containing carbon fibers in the presence of air. High selectivity to ethylene and dimethyl ether was observed for ethanol and methanol decomposition, respectively.

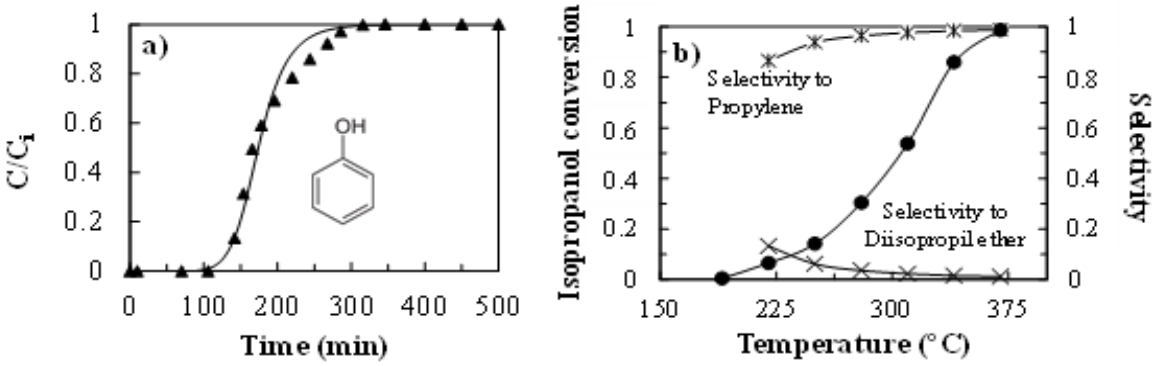

Figure 2. Breakthrough profile of phenol adsorption at 25 ºC on carbon fibers (a) and steady state conversion of isopropanol and selectivity on acid carbon fibers (b).

In the two last chapters, the use of the carbon fibers as carbon electrodes for energy storage and conversion was reported. Figure 3 shows some results about the utilization of carbon fibers in these applications. Interconnected carbon fibers obtained by electrospinning of lignin solutions were evaluated as binderless and flexible electrodes in supercapacitors, without using any type of conductive promoter. The interconnection of carbon electrodes (CF-I) improves the electrical conductivity with respect to the linear carbon electrodes (CF-L), enhancing the electrochemical behavior at higher scan rates (Figure 3). A symmetric two-electrode supercapacitor was constructed in aqueous electrolyte (H_2SO_4, 1M) showing 60 kW/kg of maximum power density and energy density of 10 Wh/kg. This supercapacitor was stable during 100000 cycles operating at 1.3 V and 5 A/g.

The preparation of electrospun Pt supported lignin-based carbon fibers was also evaluated as electrocatalyst for alcohol electro-oxidation. The effect of Pt and H_3PO_4 loadings on the physicochemical properties and activity of the catalyst was analyzed. A higher Pt content produces a development of the mesoporosity in carbon fibers. Differently, the presence of H_3PO_4 only delivers a slight increase in the specific surface area, even at the highest Pt loading, while Pt particle sizes decrease from 9.6 nm to 2.1 nm. The absence of Pt in the carbon electrode does not present electro-activity for alcohol electro-oxidation. On the contrary, when carbon electrodes with Pt were used an outstanding MOR and EOR is produced with a current density as high of 495 A/g_{Pt} (Figure 3). These carbon fibers showed promising results as anodes for the direct alcohol fuel cells for methanol (MOR) and ethanol (EOR) electro-oxidation, due to the well-dispersed Pt nanoparticles, their physicochemical properties and their adequate conformation in fuel cell devices.

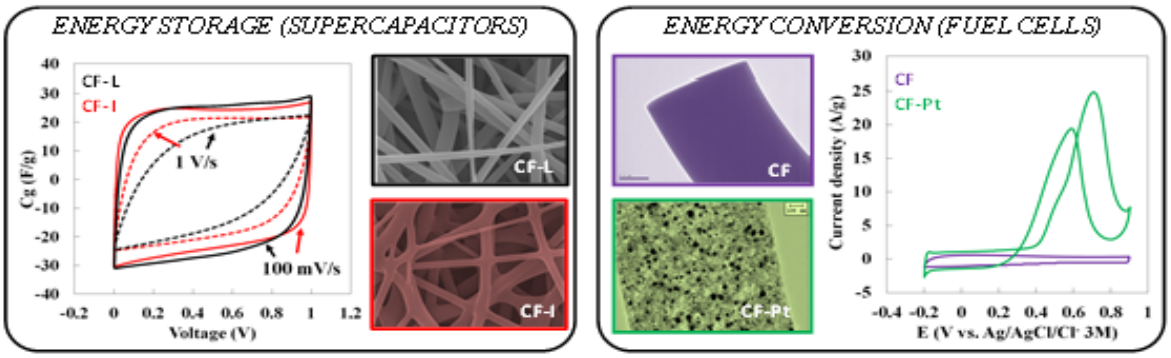

Figure 3. Steady state CVs from symmetric 2-electrode supercapacitors and from carbon electrodes in fuel cells in presence of methanol.

Conclusions

The advantages of electrospinning of Alcell lignin/ethanol solutions to produce carbon fibers have been presented in this PhD work. All combinations of physico-chemical, metal dispersion, electrical conductivity and mechanical properties make these carbon fibers excellent porous materials as catalysts, electrocatalysts, electrodes, and adsorbents.

Related Publications

[1] Berenguer R., García-Mateos, F.J. Rodríguez-Mirasol, J., Cordero, T. Partículas y materiales carbonosos con propiedades optimizadas, procedimientos para su obtención, y aplicaciones de los mismo.ES2531462B2, 2016

[2] García-Mateos, F.J., Ruiz-Rosas, R., Rosas, J.M., Rodríguez-Mirasol, J., Cordero, T. Controlling the composition, morphology, porosity, and surface chemistry of lignin-based electrospun carbon materials. Front. Mater. 2019; 6:114

[3] García-Mateos, F.J., Berenguer, R., Valero-Romero, M.J., Rodríguez-Mirasol, J., Cordero, T. Phosphorus functionalization for the rapid preparation of highly nanoporous submicron-diameter carbon fibers by electrospinning of lignin solutions. J. Mater. Chem. A 2018; 6(3): 1219-1233

[4] García-Mateos, F.J., Cordero-Lanzac, T., Berenguer, R., Morallón, E., Cazorla-Amorós, D., Rodríguez-Mirasol, J., Cordero, T. Lignin-derived Pt supported carbon (submicron) fiber electrocatalysts for alcohol electro-oxidation. App. Catal. B: Environ 2017; 211 18-30

[5] Berenguer, R., García-Mateos, F.J., Ruiz-Rosas, R., Morallón, E., Cazorla-Amorós, D., Rodríguez-Mirasol, J., Cordero, T. Biomass-derived binderless fibrous carbon electrodes for ultrafast energy storage. Green Chem. 2016; 18(6): 1506-1515

This PhD thesis can be downloaded from www.uma.es

Pt-Sn Electrocatalysts for the ethanol oxidation reaction

Rubén Rizo

rizo@fhi-berlin.mpg.de

Presented in 2017, Instituto Universitario de Materiales y Nanotecnología, Universidad de La Laguna, 38206, La Laguna, Spain.

Supervisors: E. Pastor (Universidad de La Laguna, España) and M.J. Lázaro (Instituto de Carboquímica, CSIC, Spain)

Objectives and Novelty

Electrochemical energy conversion and storage play essential roles in addressing the global energy challenge. In particular, direct ethanol fuel cells (DEFC) represent an attractive alternative to resources based on fossil fuel combustion for portable power generation. Ethanol is an eco-friendly and renewable fuel (naturally available in large quantities from biomass), and its complete oxidation to CO_2 and H_2O would lead to high energy densities. In addition, the easy handling, storage and transportation of liquid fuel, such as ethanol, avoids some of the problems associated with gaseous fuel (e.g. H_2) systems.

Over the past decades, platinum (Pt) has been shown to be the most active pure metal catalyst for the ethanol oxidation reaction (EOR). However, Pt is prone to deactivation by the adsorption of some intermediates (such as CO) and reaction by-products during the different pathways of the reaction. This fact, in combination with the high cost of Pt, has fueled the search for more active and stable EOR electrocatalysts. To achieve this objective, the synthesis of nanoparticle catalysts (with a high surface area to volume ratios), the combination of Pt with other metals and the control of the exposed Pt surface structure, have been extensively studied individually. However, the deliberate and integrated combination of these three approaches is clearly complex.

The most promising bimetallic catalysts for the EOR is Pt-Sn, resulting in a great improvement in the Pt pure catalytic activity. Furthermore, the EOR is a structure-sensitive surface reaction, which makes essential to control the surface morphology of the catalyst, and the catalyst support should be also considered since it can greatly influence the activity of the catalyst toward the EOR.

The present work aimed to outline important progress obtained from the study of the influence of the surface structure as well as the metal composition and catalyst support on the mechanism and electroactivity toward EOR. The knowledge generated in this works allowed the final synthesis of highly-active and stable shape-controlled Pt-Sn nanoparticles, which provides a promising electrocatalyst for DEFCs, in particular, and alcohol-based fuel cells, in general.

Results

In order to study the influence of the carbon support and the Pt-Sn composition on the activity toward EOR and CO oxidation reaction, Pt-Sn catalysts with different Pt-Sn atomic ratios and supported on CNF, Vulcan and oxidized Vulcan, were synthesized and studied in acid and alkaline media in order to design an optimized material with the appropriate composition and carbon support to provide the highest catalytic activity toward EOR. The carbon materials employed were carbon nanofibers (CNF), commercial Vulcan XC-72R and normalized Vulcan XC-72R with nitric and sulfuric acid at room temperature 30 min (Vulcan NSTa0.5). X-ray photoelectron spectroscopy analyses (XPS) indicated that Sn is mostly in an oxidized state and promotes the oxidation of both metals in the catalysts. On the other hand, X-ray diffraction results (XRD) evidenced the presence of SnO_2 along with Pt, finding Pt crystallite sizes in the order of 3–5 nm. The relative quantity of Pt_3Sn_1 crystallite phase in the materials increased with Sn content, having an important effect on the whole catalytic behavior towards CO and EOR.

The addition of Sn shifted the onset potential for adsorbed CO oxidation to more negative values with respect to bare Pt. Instead, the atomic Pt:Sn ratio did not significantly influence the CO oxidation behavior, whereas the carbonaceous support affected the CO tolerance, being CNF the one with the lowest oxidation potential in both acid and alkaline electrolytes. The chemical functionalization of Vulcan did not significantly improve the tolerance toward CO oxidation.

Regarding the EOR, the addition of Sn and, consequently, the content of Pt_3Sn_1 crystallite phase, strongly improved the catalytic activity. Electrochemistry studies showed lower activity for Pt-Sn 1:3 than for the Pt-Sn 1:1 catalyst, but similar stationary currents for both formulations, regardless of the carbon support and electrolyte (Figure 1).

This is an important result considering the low noble metal content of the Pt-Sn 1:3 material. In all cases, the activity of the catalysts toward EOR was higher in alkaline media than in sulfuric acid media.

An effect of carbon support on the Pt-Sn catalytic activity was also found, being CNF the one which showed the highest activities toward CO stripping and EOR. The oxidation treatment of Vulcan was also found to positively influence the EOR activity.

Additionally, not only the reactivity but also the influence of the carbon support and the metal composition on the mechanism toward EOR was studied by employing *in situ* spectroelectrochemical techniques, like *in situ* Fourier transform infrared (*in situ* FTIR) or differential electrochemical mass spectrometry (DEMS). These techniques allowed us to identify adsorbed reaction intermediates and products as well as volatile reaction products during the EOR. In a simplified manner, it is well established that the EOR on Pt occurs via two possible general

pathways. The incomplete oxidation of ethanol does not entail the breaking of the C-C bond and during this pathway, 2 electrons release to form acetaldehyde and 2 more for its further oxidation to acetic acid. On the other hand, the complete oxidation of ethanol can also take place, leading to higher energy densities (12 electrons releases during the process) but also to the breaking of the C-C bond and the formation of C1 poisoning intermediates (CO_{ad}, $CH_{x,ad}$).

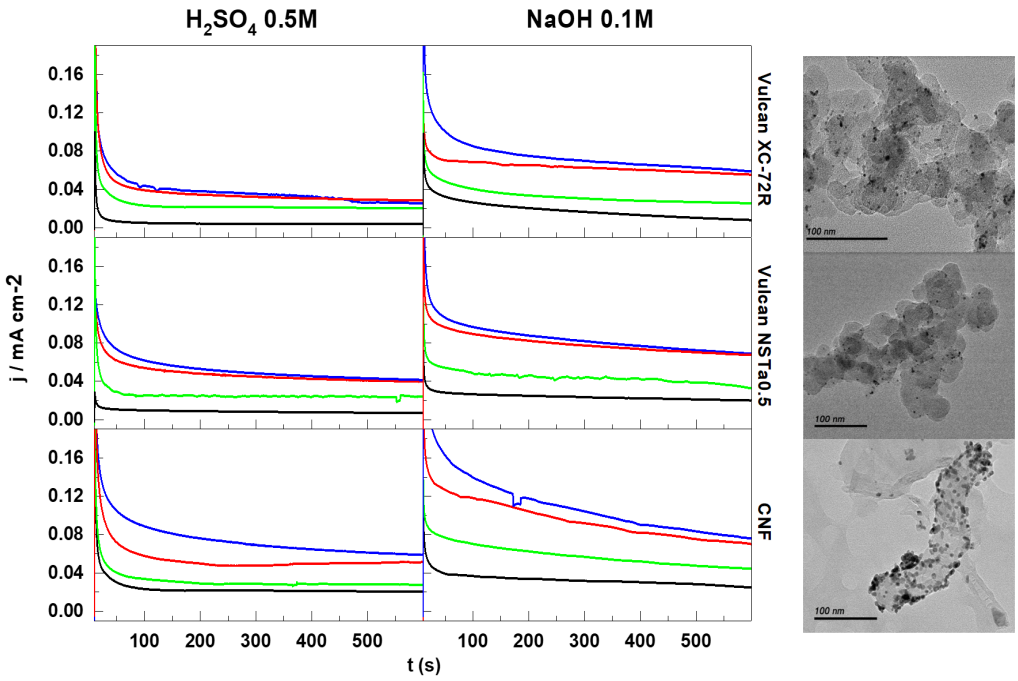

Figure 1. Current-time curves for ethanol 1 M electrooxidation: comparison of Pt-(black solid line), Pt-Sn 3:1 (green solid line), Pt-Sn 1:1 (blue solid line) and Pt-Sn 1:3 (red solid line) recorded at 0.5 V in 0.5 M H_2SO_4 (left) and 0.1 M NaOH (right) at 20 °C. The insets correspond to the TEM images of Pt-Sn 3:1 supported on the respective carbon support.

In the present study, we found that that CNF shows the highest selectivity to acetaldehyde/acetic acid, which means that the enhancement of current density for this catalyst results from obtaining a higher amount of C2 products during the incomplete oxidation of ethanol.

Furthermore, studies about the influence of the composition in the mechanism showed that the C-C scission occurs at low overpotentials and at the same values independently of the Sn loading. Additionally, it was detected that acetic acid and acetaldehyde increases meanwhile CO formation decreases with the Sn loading, indicating that the enhanced catalytic activity toward the EOR is mainly due to the incomplete EOR.

Moreover, fundamental studies of the influence of the surface structure of the catalyst in the activity and mechanism toward the EOR were also carried out. For this purpose, Sn-modified Pt single crystals (Pt basal planes) were employed and enhanced activity, in terms of lower onset potential and a higher oxidation current, was found in the modified electrodes. The results revealed that the optimum Sn coverage depends on the Pt crystallography and the Sn/Pt(110) system is the surface that exhibits the highest activity. Additionally, DEMS experiments showed that on Pt(111) and Pt(110), the presence of Sn enhances the oxidation of ethanol to acetaldehyde. However, the further oxidation of acetaldehyde is sensitive to the Pt surface structure: on Pt(110) there are sites able to break the C−C bond in acetaldehyde to form CO_2, whereas on Pt(111) such sites are not available and acetaldehyde is oxidized further to acetic acid.

All of the knowledge acquired was also finally employed for the synthesis of highly-active cubic Pt-Sn NPs. They possessed a core-shell nanostructure with a Sn-rich shell and Pt-rich core. The electrochemical activity of this material was found to be about three times higher than that obtained with unshaped Pt–Sn nanoparticles and six times higher than that of Pt nanocubes (Figure 2).

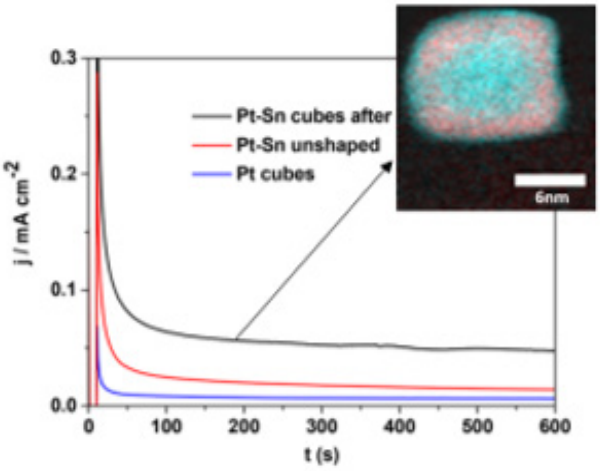

Figure 2. Current transients at 0.50 V of Pt:Sn nanocubes (black), unshaped Pt:Sn NPs (red), and Pt-cubic NPs (blue) in 0.5 M H_2SO_4 + 1 M EtOH solution. The inset corresponds to the STEM-EELS data of the Pt-Sn cubic NPs with Sn in red and Pt in cyan.

In addition, stability tests indicated that the electrocatalyst preserves its morphology and remains well-dispersed on the carbon support after 5000 potential cycles, while a cubic (pure) Pt catalyst exhibited severe agglomeration of the nanoparticles after a similar stability testing protocol. A detailed analysis of the elemental distribution in the nanoparticles by STEM-EELS indicated that Sn dissolves from the outer part of the shell after potential cycling, forming a □0.5 nm Pt skin. This particular atomic composition profile having a Pt-rich core, a Sn-rich subsurface layer, and a Pt-skin surface structure is responsible for the high activity and stability.

CONCLUSIONS

The influence of the composition, surface structure and carbon support of Pt-Sn catalysts on the activity and mechanism toward EOR, was studied. In the presence of Sn and CNF as catalyst support, the incomplete oxidation is more favored but also the oxidation of poisoning intermediates, which results in higher activity and lower onset potential for EOR because of the higher oxidation efficiency via C2 products formation. Regarding surface structure studies, fundamental experiments demonstrated that the presence of Sn improve the electrode activity regardless of the Pt crystallographic orientation but the Sn/Pt(110) surface is the one which showed the highest EOR currents. Finally, guided by the acquired knowledge, highly active and stable shape-controlled Pt-Sn catalysts were synthesized, which can be considered as a promising electrocatalyst for DEFCs, in particular, and alcohol-based fuel cells, in general.

RELATED PUBLICATIONS

[1] Rizo R, Arán-Ais RM, Padgett E., Muller DA, Lázaro MJ, Solla-Gullón J, Feliu JM, Pastor E, Abruña HD, Pt-Richcore/Sn-Richsubsurface/Ptskin Nanocubes As Highly Active and Stable Electrocatalysts for the Ethanol Oxidation Reaction. Journal of the American Chemical Society, 2018; 140, 3791-3797.

[2] Rizo R, Sebastián D, Rodríguez JL, Lázaro MJ, Pastor E, Influence of the nature of the carbon support on the activity of Pt/C catalysts for ethanol and carbon monoxide oxidation. Journal of Catalysis, 2017; 348, 22-28.

[3] Rizo R, Sebastián D, Lázaro, MJ, & Pastor E, On the design of Pt-Sn efficient catalyst for carbon monoxide and ethanol oxidation in acid and alkaline media. Applied Catalysis B: Environmental, 2017; 200, 246-254.

[4] Rizo R, Pastor E, Koper MTM, CO electrooxidation on Sn-modified Pt single crystals in acid media, Journal of Electroanalytical Chemistry, 2017; 800, 32-38.

[5] Rizo R, Lázaro MJ, Pastor E, Koper MTM, Ethanol oxidation on Sn- modified Pt single crystal electrodes: New mechanistic insights by online electrochemical mass spectrometry. ChemElectroChem, 2016; 3, 2196-2201.

[6] Rizo R, Lázaro MJ, Pastor E, Koper MTM, Garcia G, Spectroelectrochemical Study of Carbon Monoxide and Ethanol Oxidation on Pt/C, PtSn(3:1)/C and PtSn(1:1)/C Catalysts. Molecules, 2016; 21, 1225-1237.

[7] Rizo R, García G, Pastor E, Methanol Oxidation on Bimetallic Electrode Surfaces. Reference Module in Chemistry, Molecular Sciences and Chemical Engineering, 2018; 719-729.

Full Thesis can be downloaded from https://riull.ull.es/xmlui/handle/915/16382

Socios protectores del Grupo Español del carbón

Industrial Química del Nalón, S.A.
NalónChem

bonsai
ADVANCED TECHNOLOGIES

ELCOGAS